DEVELOPMENT OF INFRARED REFLECTANCE CHARACTERISTICS OF SURROGATE ROADSIDE OBJECTS

A Thesis

Submitted to the Faculty

of

Purdue University

by

Abir Saha

In Partial Fulfillment of the

Requirements for the Degree

of

Master of Science in Electrical and Computer Engineering

August 2018

Purdue University

Indianapolis, Indiana

THE PURDUE UNIVERSITY GRADUATE SCHOOL
STATEMENT OF COMMITTEE APPROVAL

Dr. Stanley Yung-Ping Chien, Chair

Department of Electrical and Computer Engineering

Dr. Lingxi Li

Department of Electrical and Computer Engineering

Dr. Lin Li

Department of Earth Sciences

Approved by:

Dr. Brian King

Head of the Graduate Program

To my parents, who are currently 8000 miles away, but always in my heart,

and

to my loving wife Maitraye, for being with me through thick and thin. Her love, encouragement and endless support kept me going no matter how difficult things got.

ACKNOWLEDGMENTS

The research for this thesis was done with the patient guidance of Dr. Stanley Chien and Dr. Lin Li.

Throughout the entire research, Dr. Stanley Chien has been a source of support and motivation to me as my thesis advisor. His inquisitive mind and tremendous attention to detail helped me explore new territories while trying to solve any problem. From him, I learned the quality of never giving up. I will forever be thankful to him.

I am equally grateful to Dr. Lin Li for introducing me to the theoretical foundations that drove this research. Whenever I needed directions, he always made himself available to help me. He was kind enough to trust me with a spectrometer from his own lab, which was used for all the experiments described in this thesis. I would also like to thank Dr. Lingxi Li for his kind consent to be a member of my supervising committee. In addition, I want to express my gratitude to Dr. Qiang Yi for his friendly guidance.

I would like to thank Dan Shen, Jun Lin and Wensen Niu, my colleagues and friends at Transportation Active Safety Institute (TASI) for their tremendous help and helpful suggestions.

Last but not least, I am grateful to my parents, brother and wife, who have been my source of support and joy throughout this journey. I will also fondly remember the happy days and nights with Indy Gang, my group of Bangladeshi friends here in Indianapolis, who have become my family away from home and will always remain so.

TABLE OF CONTENTS

Page

LIST OF TABLES viii

LIST OF FIGURES ix

ABBREVIATIONS xvii

ABSTRACT xviii

1 INTRODUCTION 1

1.1 Motivation 1

1.2 Related Work 3

1.3 Problem Statement and Contributions 4

2 BACKGROUND 6

2.1 Operation of LIDAR 6

2.2 Reflectance 7

2.3 Measurement Instruments 9

2.4 Measurement Procedure 14

2.5 Selection of Roadside Objects 15

3 SPECIFICATION OF REPRESENTATIVE INFRARED REFLECTANCE OF SURROGATE ROADSIDE OBJECTS 16

3.1 Relevant Definitions 16

3.2 Approaches for Reflectance Measurement 19

3.2.1 Approach 1: Outdoor Perpendicular Measurement 20

3.2.2 Approach 2: Indoor Measurement 21

3.2.3 Approach 3: Outdoor Measurement for Verifying the Indoor Results 23

3.3 Specification of Suggested Infrared Reflectance of Surrogate Concrete Skin 23

Page

3.3.1 Concrete Reflectance Measurement using Approach 1 (Outdoor Perpendicular Measurement) . . . 24
3.3.2 Concrete Reflectance Measurement using Approach 2 (Indoor Measurement from Different Angles) . . . 29
3.3.3 Specification of Suggested IR Reflectance of Concrete Surrogate Skin for Different Angles . . . 34
3.4 Specification of Suggested Infrared Reflectance of Surrogate Metal Guardrail Skin . . . 40
3.4.1 I-beam Reflectance Measurement using Approach 1 (Outdoor Perpendicular Measurement) . . . 41
3.4.2 I-beam Reflectance Measurement using Approach 2 (Indoor Measurement from Different Angles) . . . 47
3.4.3 Approach 3: Outdoor Measurement of I-beam to Verify the Accuracy and Consistency of Indoor Results . . . 52
3.4.4 Specification of Suggested IR Reflectance of Metal Guardrail Surrogate Skin for Different Angles . . . 53
3.5 Specification of Required Infrared Reflectance of Surrogate Grass . . . 59
3.5.1 Grass Reflectance Measurement using Approach 1 (Outdoor Perpendicular Measurement) . . . 59
3.5.2 Grass Reflectance Measurement using Approach 2 (Indoor Measurement from Different Angles) . . . 65
3.5.3 Specification of Suggested IR Reflectance of Surrogate Grass for Different Angles . . . 69
3.5.4 Specification of Suggested IR Reflectance of Dirt for Different Angles . . . 75
3.6 Summary . . . 81
4 MAKING SURROGATE OBJECTS WITH DESIRED INFRARED REFLECTANCE . . . 82
4.1 Surrogate Objects . . . 82
4.2 Surrogate Concrete Skin with Desired Infrared Reflectance . . . 83
4.2.1 Finalized Design of the Concrete Surrogate Skin . . . 84
4.2.2 IR Reflectance Performance of the Concrete Surrogate Skin . . . 85

Page

4.3 Surrogate Metal Guardrail Skin with Desired Infrared Reflectance . . . 89
4.3.1 Finalized Design of the Metal Guardrail Surrogate Skin 90
4.3.2 IR Reflectance Performance of the Surrogate Metal Guardrail Skin 90
4.4 Surrogate Grass with Desired Infrared Reflectance 95
4.4.1 Iterative approach for making the surrogate grass 96
4.4.2 Finalized Surrogate Grass Samples 98
4.4.3 IR Reflectance Performance of the Surrogate Grass Samples . . 99
4.4.4 Finalized Dirt Colored Surrogate Grass 104
4.4.5 IR Reflectance Performance of Dirt Colored Surrogate Grass . 104
5 CONCLUSION AND FUTURE WORK 110
5.1 Conclusion 110
5.2 Future Work 110
REFERENCES 112

LIST OF TABLES

Table Page

2.1 Most common types of roadside objects (found by a road/roadside study project by TASI) 15

LIST OF FIGURES

Figure Page

2.1 Geometry describing the Bidirectional Reflection Distribution Factor . . . 8

2.2 Example of specular and diffuse reflections (courtesy of [23]) 9

2.3 ASD FieldSpec Pro Spectrometer (left), the included optical fiber probe (middle), and 1° field-of-view reducer accessory (right) 11

2.4 The White Reference Panel (99% Spectralon) 13

2.5 ASD ProLamp Light Source (left) and the radiance of the lamp measured using 99% Spectralon white reference panel (right) 13

3.1 The green line indicates the normal line for (a) horizontal surface and (b) vertical surface 17

3.2 Measurement angle for (a) horizontal surface and (b) vertical surface . . . 17

3.3 Illumination angle for (a) horizontal surface and (b) vertical surface 18

3.4 Geometry of phase angle 19

3.5 Approach 1 (outdoor perpendicular measurement), 0° measurement angle, no control over illumination angle (60° in this case) 20

3.6 Approach 2 (Indoor measurement), measurement angle = illumination angle = 0° , phase angle = 20°. 21

3.7 Approach 2 (Indoor measurement), measurement angle = illumination angle = 70° , phase angle = 20°. 22

3.8 Top view of approach 2 (Indoor measurement), measurement angle = illumination angle = 0° , phase angle = 20°. 22

3.9 Approach 3 (outdoor measurement to verify the indoor results), measurement angle = illumination angle = 60° , phase angle = 20°. 24

3.10 Four samples of old curb 25

3.11 Three samples of new curb 25

3.12 Old divider sample no. 1. Samples 2-6 are of similar appearance 25

3.13 New concrete divider 26

Figure Page

3.14 Comparison of new and old concrete curb samples (0° measurement angle, 27.8°-45.5° illumination angle, 10° phase angle) 26

3.15 Inner surface without coating (left) and outer surface with coating (right) of a new curb 27

3.16 Comparison of new and old concrete divider samples (0° measurement angle, 19°-38.5° illumination angle, 10° phase angle) 28

3.17 Concrete block no. 1- indoor measurement - 0° measurement angle (left) vs 70° measurement angle (right); illumination angle same as measurement angle; phase angle = 20°. 29

3.18 Concrete Wall being measured in an indoor setup (measurement angle = illumination angle = 70°), phase angle = 20°. 30

3.19 Two concrete dividers (measured using indoor setup after sunset) 30

3.20 Reflectance of concrete block No. 1- indoor measurement from different measurement angles (for all cases, illumination angle = measurement angle); 20° phase angle 31

3.21 Reflectance of concrete block No. 2- indoor measurement from different measurement angles (for all cases, illumination angle = measurement angle); 20° phase angle 32

3.22 Reflectance of concrete wall indoor measurement from different measurement angles (for all cases, illumination angle = measurement angle); 20° phase angle 32

3.23 IR reflectance spectra of concrete divider-1 for 0°-70° measurement angles (illumination angle equal to corresponding measurement angle, 20° phase angle) 33

3.24 IR reflectance spectra of concrete divider-2 for 0°-70° measurement angles (illumination angle equal to corresponding measurement angle, 20° phase angle) 34

3.25 Reflectance curves of all concrete samples for the same angle grouped in the same plot 35

3.26 Suggested IR reflectance range of surrogate concrete skin for 0° LIDAR view angle 36

3.27 Suggested IR reflectance range of surrogate concrete skin for 10° LIDAR view angle 37

3.28 Suggested IR reflectance range of surrogate concrete skin for 20° LIDAR view angle 37

Figure Page

3.29 Suggested IR reflectance range of surrogate concrete skin for 30° LIDAR view angle 38

3.30 Suggested IR reflectance range of surrogate concrete skin for 40° LIDAR view angle 38

3.31 Suggested IR reflectance range of surrogate concrete skin for 50° LIDAR view angle 39

3.32 Suggested IR reflectance range of surrogate concrete skin for 60° LIDAR view angle 39

3.33 Suggested IR reflectance range of surrogate concrete skin for 70° LIDAR view angle 40

3.34 Metal Guardrail. The horizontal bar is W-beam, the vertical support bars are I-beams 41

3.35 Appearance of I-beam samples of different ages 42

3.36 I-beam kept in horizontal orientation. Measurement angle is 0°. Illumination angle is 17.5°-19.7° 43

3.37 Measurement from multiple parts of I-beam kept horizontally. 0° measurement angle, 17.5°-19.7° illumination angle, 0° phase angle 43

3.38 Mirrorlike reflection of sun on I-beam surface (0° measurement angle and 17.5° illumination angle) 44

3.39 Absence of high specular reflection from probe's point of view (0° measurement angle, 64.7° illumination angle) 45

3.40 Measurement from multiple parts of I-beam kept vertically. 0° measurement angle, 48.9°-64.7° illumination angle, 0° phase angle 45

3.41 Reflectance of I-beams of different age. 0° measurement angle, 48°-70° illumination angle, and 0° phase angle 46

3.42 I-beam - indoor measurement - 0° measurement angle (left) vs 70° measurement angle (right); illumination angle same as measurement angle, 20° phase angle 48

3.43 New I-beam sample – indoor measurement from different measurement angles (for all cases, illumination angle = measurement angle); 20° phase angle 49

3.44 I-beam measured indoor - multiple attempts to measure I-beam at 0° measurement angle and 0° illumination angle (20° phase angle) 50

Figure Page

3.45 I-beam measured indoor - multiple attempts to measure I-beam at 10° measurement angle and 10° illumination angle (20° phase angle) 51

3.46 I-beam measured indoor - multiple attempts to measure I-beam at 20° measurement angle and 20° illumination angle (20° phase angle) 51

3.47 I-beam, Indoor vs. outdoor measurement (30° measurement angle, 30° illumination angle, 20° phase angle) 52

3.48 Three reflectance measurements from different parts of the I-beam for each angle 54

3.49 Suggested IR reflectance range of surrogate concrete skin for 0° LIDAR view angle 55

3.50 Suggested IR reflectance range of surrogate concrete skin for 10° LIDAR view angle 55

3.51 Suggested IR reflectance range of surrogate concrete skin for 20° LIDAR view angle 56

3.52 Suggested IR reflectance range of surrogate concrete skin for 30° LIDAR view angle 56

3.53 Suggested IR reflectance range of surrogate concrete skin for 40° LIDAR view angle 57

3.54 Suggested IR reflectance range of surrogate concrete skin for 50° LIDAR view angle 57

3.55 Suggested IR reflectance range of surrogate concrete skin for 60° LIDAR view angle 58

3.56 Suggested IR reflectance range of surrogate concrete skin for 70° LIDAR view angle 58

3.57 Pure green grass: short (left), medium (middle) and long (right) 60

3.58 Mixed grass (green majority): short (left) and medium (right) 60

3.59 Mixed grass (yellow majority): short (left) and medium (right) 61

3.60 Pure yellow grass 61

3.61 Reflectance comparison of pure green grass samples of different lengths. 0° measurement angle, 52°-60° illumination angle, 10° phase angle 62

3.62 Reflectance comparison of mixed color grass samples of different lengths. (0° measurement angle, 52°-60° illumination angle, 10° phase angle) 63

Figure Page

3.63 Reflectance of grass of different colors (0° measurement angle, 52°-60° illumination angle, 10° phase angle) 64

3.64 (from left to right) Indoor grass sod-1,indoor grass sod-2, outdoor green grass, and dead grass sod 65

3.65 Measurement of grass sod in indoor setup: 0° measurement angle (left) and 70° measurement angle (right), illumination angle same as measurement angle. 20° phase angle 66

3.66 Reflectance of grass sod-1 at different measurement angles, illumination angle same as measurement angle, 20° phase angle 67

3.67 Reflectance of grass sod-1 at different measurement angles, illumination angle same as measurement angle, 20° phase angle 67

3.68 Reflectance of outdoor green grass at different measurement angles, illumination angle same as measurement angle, 20° phase angle 68

3.69 Reflectance of dead grass sod at different measurement angles, illumination angle same as corresponding angle, 20° phase angle 68

3.70 All grass measurements for the same angle grouped together in the same figure 70

3.71 Suggested infrared reflectance range of surrogate grass for 0° LIDAR view angle 71

3.72 Suggested infrared reflectance range of surrogate grass for 10° LIDAR view angle 72

3.73 Suggested infrared reflectance range of surrogate grass for 20° LIDAR view angle 72

3.74 Suggested infrared reflectance range of surrogate grass for 30° LIDAR view angle 73

3.75 Suggested infrared reflectance range of surrogate grass for 40° LIDAR view angle 73

3.76 Suggested infrared reflectance range of surrogate grass for 50° LIDAR view angle 74

3.77 Suggested infrared reflectance range of surrogate grass for 60° LIDAR view angle 74

3.78 Suggested infrared reflectance range of surrogate grass for 70° LIDAR view angle 75

3.79 Dirt sample 76

Figure Page

3.80 Reflectance of dirt sample at different measurement angles, illumination angle same as corresponding measurement angle, 20° phase angle 76

3.81 Suggested infrared reflectance range of surrogate dirt for 0° LIDAR view angle 77

3.82 Suggested infrared reflectance range of surrogate dirt for 10° LIDAR view angle 78

3.83 Suggested infrared reflectance range of surrogate dirt for 20° LIDAR view angle 78

3.84 Suggested infrared reflectance range of surrogate dirt for 30° LIDAR view angle 79

3.85 Suggested infrared reflectance range of surrogate dirt for 40° LIDAR view angle 79

3.86 Suggested infrared reflectance range of surrogate dirt for 50° LIDAR view angle 80

3.87 Suggested infrared reflectance range of surrogate dirt for 60° LIDAR view angle 80

3.88 Suggested infrared reflectance range of surrogate dirt for 70° LIDAR view angle 81

4.1 Surrogate concrete divider (frame is covered by surrogate concrete skin) . . 84

4.2 Reflectance of concrete surrogate skin compared with the suggested range (0° measurement angle, 0° illumination angle, 20° phase angle) 85

4.3 Reflectance of concrete surrogate skin compared with the suggested range (10° measurement angle, 10° illumination angle, 20° phase angle) 86

4.4 Reflectance of concrete surrogate skin compared with the suggested range (20° measurement angle, 20° illumination angle, 20° phase angle) 86

4.5 Reflectance of concrete surrogate skin compared with the suggested range (30° measurement angle, 30° illumination angle, 20° phase angle) 87

4.6 Reflectance of concrete surrogate skin compared with the suggested range (40° measurement angle, 40° illumination angle, 20° phase angle) 87

4.7 Reflectance of concrete surrogate skin compared with the suggested range (50° measurement angle, 50° illumination angle, 20° phase angle) 88

4.8 Reflectance of concrete surrogate skin compared with the suggested range (60° measurement angle, 60° illumination angle, 20° phase angle) 88

Figure Page

4.9 Reflectance of concrete surrogate skin compared with the suggested range (70° measurement angle, 70° illumination angle, 20° phase angle) 89

4.10 Surrogate Metal Guardrail. The skin has been mounted on both surrogate W-beam frame and surrogate I-beam frame 90

4.11 Reflectance of surrogate metal guardrail skin compared with the suggested range (0° measurement angle, 0° illumination angle, 20° phase angle) . . . 91

4.12 Reflectance of surrogate metal guardrail skin compared with the suggested range (10° measurement angle, 10° illumination angle, 20° phase angle) . . 92

4.13 Reflectance of surrogate metal guardrail skin compared with the suggested range (20° measurement angle, 20° illumination angle, 20° phase angle) . . 92

4.14 Reflectance of surrogate metal guardrail skin compared with the suggested range (30° measurement angle, 30° illumination angle, 20° phase angle) . . 93

4.15 Reflectance of surrogate metal guardrail skin compared with the suggested range (40° measurement angle, 40° illumination angle, 20° phase angle) . . 93

4.16 Reflectance of surrogate metal guardrail skin compared with the suggested range (50° measurement angle, 50° illumination angle, 20° phase angle) . . 94

4.17 Reflectance of surrogate metal guardrail skin compared with the suggested range (60° measurement angle, 60° illumination angle, 20° phase angle) . . 94

4.18 Reflectance of surrogate metal guardrail skin compared with the suggested range (70° measurement angle, 70° illumination angle, 20° phase angle) . . 95

4.19 Leaning directions of artificial turf with respect to measurement probe . . 97

4.20 Reflectance of low density turf measured from three viewing orientations and compared to the suggested IR reflectance of surrogate grass for 0°, 20°, 40° and 70° measurement angles. Illumination angle equal to measurement angle, 20° phase angle 98

4.21 Four color shades of surrogate grass: (from left to right) light green, medium green, light yellow and darker yellow 99

4.22 Reflectance of all surrogate grass samples compared to the suggested range (0° measurement angle, 0° illumination angle, 20° phase angle) 100

4.23 Reflectance of all surrogate grass samples compared to the suggested range (10° measurement angle, 10° illumination angle, 20° phase angle) 100

4.24 Reflectance of all surrogate grass samples compared to the suggested range (20° measurement angle, 20° illumination angle, 20° phase angle) 101

Figure Page

4.25 Reflectance of all surrogate grass samples compared to the suggested range (30° measurement angle, 30° illumination angle, 20° phase angle) 101

4.26 Reflectance of all surrogate grass samples compared to the suggested range (40° measurement angle, 40° illumination angle, 20° phase angle) 102

4.27 Reflectance of all surrogate grass samples compared to the suggested range (50° measurement angle, 50° illumination angle, 20° phase angle) 102

4.28 Reflectance of all surrogate grass samples compared to the suggested range (60° measurement angle, 60° illumination angle, 20° phase angle) 103

4.29 Reflectance of all surrogate grass samples compared to the suggested range (70° measurement angle, 70° illumination angle, 20° phase angle) 103

4.30 Dirt colored surrogate grass 104

4.31 Reflectance of dirt colored surrogate grass compared to the suggested reflectance of dirt (0° measurement angle, 0° illumination angle, 20° phase angle) 105

4.32 Reflectance of dirt colored surrogate grass compared to the suggested reflectance of dirt (10° measurement angle, 10° illumination angle, 20° phase angle) 106

4.33 Reflectance of dirt colored surrogate grass compared to the suggested reflectance of dirt (20° measurement angle, 20° illumination angle, 20° phase angle) 106

4.34 Reflectance of dirt colored surrogate grass compared to the suggested reflectance of dirt (30° measurement angle, 30° illumination angle, 20° phase angle) 107

4.35 Reflectance of dirt colored surrogate grass compared to the suggested reflectance of dirt (40° measurement angle, 40° illumination angle, 20° phase angle) 107

4.36 Reflectance of dirt colored surrogate grass compared to the suggested reflectance of dirt (50° measurement angle, 50° illumination angle, 20° phase angle) 108

4.37 Reflectance of dirt colored surrogate grass compared to the suggested reflectance of dirt (60° measurement angle, 60° illumination angle, 20° phase angle) 108

4.38 Reflectance of dirt colored surrogate grass compared to the suggested reflectance of dirt (70° measurement angle, 70° illumination angle, 20° phase angle) 109

ABBREVIATIONS

IR	Infrared
LIDAR	Light Detection and Ranging
LDW	Lane Departure Warning
LKA	Lane Keeping Assist
RDW	Road Departure Warning
RKA	Road Keeping Assist

ABSTRACT

Saha, Abir. M.S.E.C.E., Purdue University, August 2018. Development of Infrared Reflectance Characteristics of Surrogate Roadside Objects. Major Professor: Stanley Y.P. Chien.

An important topic in autonomous vehicle related research in recent times is road departure warning (RDW) and road keeping assistance (RKA). RDW or RKA should be able to recognize and avoid roadside objects. Standard tests are needed to evaluate the performance of RDW and RKA feature of cars from different manufacturers. To avoid damage to the cars under test and the test environment during testing, there is a need of soft, durable and reusable surrogate targets representing various real roadside objects such as curb, concrete divider and metal guardrail. These surrogate objects should have representative characteristics of real roadside objects from the point of view of various commonly used object detection sensors on the vehicles such as camera, radar and LIDAR. Transportation Active Safety Institute (TASI) at Indian University-Purdue University Indianapolis (IUPUI) is in the process of developing surrogate concrete divider, curb metal guardrail and grass that should be recognized as real roadside objects by LIDAR sensors, can be crashed without damage to the test vehicle and can be reused even after multiple crashes. The first step is to understand what the representative roadside objects should look like from the point of view of LIDAR units using laser of various wavelengths, and the next step is to design surrogate objects that successfully emulate the properties of the real roadside objects. Reflectance of an object is an important property for LIDAR detection. This thesis describes an approach for the determination of infrared reflectance property of concrete, metal guardrail and grass for different LIDAR view angles. Various samples of each of these roadside objects were evaluated. Based on these measurements, the

suggested reflectance of surrogate roadside objects in the common LIDAR wavelength range of 800-1100 nm is specified. Finally, the design of surrogate roadside objects that satisfy these requirements is described, and the infrared reflectance of these surrogate objects are compared to the suggested reflectance bounds for different LIDAR view angles.

1. INTRODUCTION

1.1 Motivation

Vehicle road departure is a major cause of vehicle related accidents and fatalities. According to National Highway Traffic Safety Administration (NHTSA), nearly 55% of all single vehicle crashes in the US are due to road departure incidents, and 36% of these road departure crashes resulted in injuries and fatalities [1–3]. A vehicle road departure accident is defined as an incident where a vehicle crosses the road edge, and strikes roadside objects, or roll over or collide head-on with vehicles coming from the opposite direction [4, 5]. To aid the prevention of roadway departure accidents, production models coming from many car manufacturers incorporate active safety features such as Lane Departure Warning (LDW) and Lane Keeping Assist (LKA). These existing technologies do not perform well in the absence of clear lane markings. Since many roads in the US either have no lane markings at all or have very poorly visible lane markings, it is important to pursue technologies that do not simply rely on lane markings to recognize road departure incidents. To this end, a new generation of active safety features called Road Departure Warning (RDW) and Road Keeping Assist (RKA) have seen significant research in recent times [6, 7]. RDW and RKA systems will work in the absence of clear lane markings and will instead observe roadside objects to determine whether a road departure incident is occurring.

Whenever a new active safety feature is introduced, it is essential to have standard testing equipment and procedures to evaluate the performance of such a feature quantitatively. Although such evaluation standards exist for LKA [8], to author's knowledge, no such standard testing scheme is available for evaluating the performance of RKA and RDW systems yet. Transportation Active Safety Institute (TASI) at Indiana University-Purdue University Indianapolis (IUPUI) is currently collaborat-

ing with Toyota Collaborative Safety Research Center (CSRC) to develop standard testing methods, scenarios and equipment for evaluating vehicle road departure and mitigation systems. One of the most important tasks for this project is to develop surrogate roadside objects (such as concrete divider, curb, metal guardrail and grass) for the test track. These surrogate objects should have representative characteristics of real roadside objects to different automotive sensors (such as camera, radar and LIDAR), but should also be soft and reusable, so that they can be crashed multiple times without causing damage to the test track, the vehicles being tested and the surrogate objects themselves.

LIDAR (Light Detection and Ranging) is currently one of the most reliable sensors that can be used in vehicle active safety systems. LIDAR is a remote sensing technology that makes use of laser pulses to determine the distance of a target. LIDAR units used in vehicles use a rotating laser beam that continuously sends pulses to its surroundings. Each LIDAR unit typically uses laser of only one wavelength, but the wavelength varies from one unit to another depending on the manufacturer. Most automotive LIDARs use near infrared wavelengths between 800 nm and 1100 nm [9]. Based on the time needed from sending the laser pulses to receiving the return laser pulses, these vehicular LIDAR units create accurate 3D mapping of its surrounding area.

In addition to collecting 3-dimensional distance data called 'point cloud', LIDAR also collects intensity values for each point in the point cloud. LIDAR intensity for any wavelength depends on the reflectance of the target object [10, 11]. Hence, to develop a surrogate object that looks like an actual object to LIDAR, it should not only have the same shape and color but also have the same IR reflectance property as the real object. Besides, LIDAR may see a roadside object from different angles. LIDARs send laser beams that will be incident on the roadside objects at different angles, and the return beams will be received at roughly the same angle as the angle of incidence (i.e., incidence angle is equal to view angle).

Therefore, it is very important to study the near infrared reflectance of concrete dividers, curbs, metal guardrails, and grass from different viewing angles by ensuring that angle of incidence is equal to the viewing angle. Based on these measurements, it is necessary to suggest infrared reflectance range for the surrogate objects and design surrogate skins that satisfy this requirement.

1.2 Related Work

Measurement of reflectance has seen significant attention, especially in the remote sensing arena. Two types of reflectance measurement are most popular: directional-hemispherical reflectance and bidirectional reflectance [12]. Directional-hemispherical reflectance is usually measured in a laboratory where the source is a collimated directional beam, and light is captured from all possible view angles using an integrating sphere. On the other hand, bidirectional reflectance is determined by measuring the incident energy and reflected energy from a set of incident and view angles [13]. Most imaging spectrometers can measure the bidirectional reflectance across a range of wavelengths both indoors and outdoors.

Herold et al. [14] studied the bidirectional reflectance of different urban objects such as roof tiles, asphalt, and concrete under sun within two hours of solar noon. Similar studies were done in [15] and [16]. Infrared reflectance properties of green vegetation were studied by Campbell [17], Danson [18] and Slaton et al. [19], while similar study regarding senescing i.e. yellowing vegetation was done by Adams et al. [20]. For all these literatures, the reflectance measurement was done from one view angle (from perpendicular position) and a limited range of light incident angles (during solar noon).

Honkavaara et al. [21] studied the effect of different incidence and view angles on the reflectance of concrete for visible green wavelengths. However, further analysis for the near infrared wavelength for concrete, grass and galvanized zinc is necessary for accurately specifying the required reflectance range for roadside objects, specifically by always keeping direction of incidence same as direction of viewing.

1.3 Problem Statement and Contributions

The objective of this thesis is to specify the representative near infrared (800-1100 nm) reflectance of concrete curb, divider, metal guardrail and grass for different viewing angles of LIDAR in the United States of America, and to prepare surrogate objects that satisfy these suggested reflectance requirements. To this end, this thesis makes the following contributions:

- It specifies the procedure to measure the reflectance of an object from different angles.
- Based on the measurement of real samples, the suggested IR reflectance for different LIDAR view angles and 800-1100nm wavelengths are specified for surrogate concrete, metal guardrail and grass.
- Based on the specified IR reflectance requirements, the process of developing surrogate concrete skin, metal guardrail skin and artificial grass is described. The performance of these surrogate objects is compared to the suggested IR reflectance for different angles.

The rest of this thesis is organized as follows. Section 2 gives relevant background on LIDAR operation, reflectance and the associated measurement tools. Section 3 describes measurement methods, measures different samples of concrete, metal guardrail and grass, and specifies the suggested IR reflectance of surrogate objects for each of

these objects. Section 4 describes the development of surrogate objects and compares their performance to the suggested reflectance specified in Section 3. Finally, Section 5 gives conclusion and future work.

2. BACKGROUND

2.1 Operation of LIDAR

LIDAR intensity is a measure of the power of reflected laser pulse, which is dependent on the transmitted power, viewing geometry, atmospheric and target characteristics, and other parameters specific to the system. Received power of LIDAR is generally specified by the LIDAR range equation. The basic form of LIDAR range equation is given below [22]:

$$P_R = P_T \times \frac{\eta}{\pi^2 R^4} \times \frac{A_{rec}}{Div_{trans}} \times \frac{\rho A_{target}}{Div_{ref}} \tag{2.1}$$

Here, P_R is received power, P_T is transmitted power, η is quantum efficiency of the receiver, R represents the range to the target, A_{rec} is the area of the receiver, A_{target} is the area of the target, Div_{trans} is the laser beam divergence before reflection, Div_{ref} is the laser beam divergence after reflection, and finally, ρ is the target reflectance. The range of the target can be calculated by multiplying the speed of light by the sum of time required by laser pulse to travel from source to target and time required by the reflected pulse to reach the receiver from target and then dividing the product by 2. This simplified equation ignores atmospheric effects and only takes sensor characteristics and target behavior into account. Other forms of the LIDAR range equation are also present in literature that takes environmental factors into account [9]. One such form is given below:

$$P_R = \frac{P_T D_r^2 \eta_{atm} \eta_{sys} \rho}{4R^2} \cos \alpha_i \tag{2.2}$$

Here, η_{atm} is atmospheric transmission factor, η_{sys} is system transmission factor, D_r is the receiver aperture diameter, and α_i is the angle of incidence. This equation assumes that the target surface is purely Lambertian, i.e. the surface seems equally bright from every viewing direction.

If the range is considered an independent variable and the other parameters are constant, then it is easy to notice that the received power is heavily dependent on the reflectance of the target surface. Therefore, to make surrogate objects that can mimic real roadside objects, it is very important for the surrogate objects to match the reflectance properties of real objects.

2.2 Reflectance

In general terms, reflectance at a given optical wavelength is defined as the ratio of radiant flux reflected by a surface and radiant flux incident on the surface. Reflectance is a directional property and is highly dependent on surface characteristics and viewing geometry. Reflectance of a surface is fully described by Bidirectional Reflectance Distribution Factor (BRDF). The term 'bidirectional' denotes that this factor is a function of directions of both incident and reflected light. BRDF can be described by the following equation:

$$BRDF : f(\theta_i, \phi_i, \theta_r, \phi_r : \lambda) = \frac{L_{surface}(\theta_r, \phi_r)}{E_{surface}(\theta_i, \phi_i)} \tag{2.3}$$

Here, θ_r is the viewing zenith angle, ϕ_r is the viewing azimuth angle, λ is the wavelength of incident light (in nm), θ_i is the incident zenith angle, ϕ_i is the incident azimuth angle, $L_{surface}$ is the radiance of surface in the direction of viewing, and $E_{surface}$ is the irradiance at surface in the direction of incident light. The geometry is shown in Fig. 2.1. The zenith angles are conventionally measured with respect to the normal line (z-axis in the figure).

BRDF is a measure of shininess/glossiness of a surface, i.e., how the surface reflects light in different directions. Reflection can be of two types: specular and diffuse.

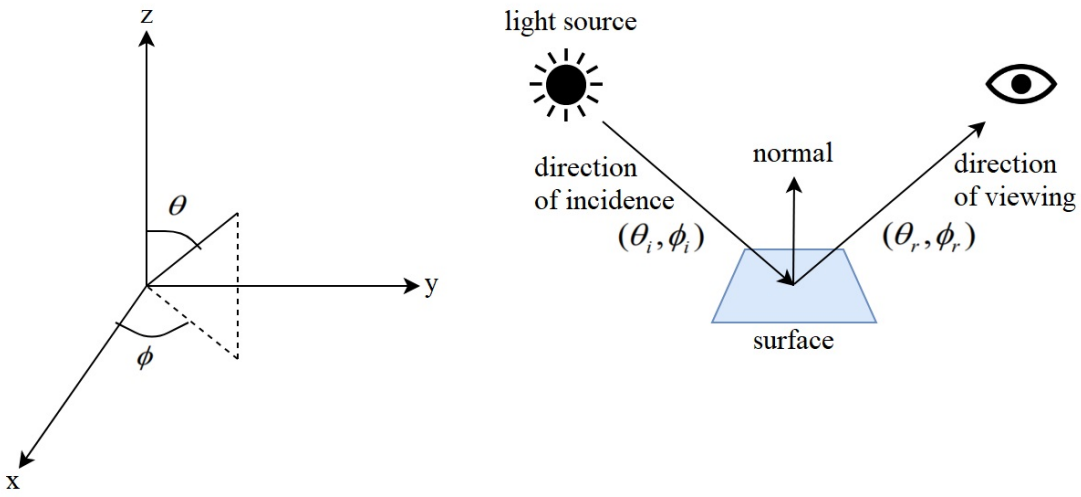

Fig. 2.1: Geometry describing the Bidirectional Reflection Distribution Factor

Specular reflection: In case of specular reflection, light energy is completely reflected towards one direction. For example: mirrors and shiny metals exhibit mostly specular reflection, because most of the light reflected by them follows the angle of reflection (BRDF will be high if viewed from that direction), and very little amount of energy is reflected towards other directions (very low BRDF in those directions). The more a surface is specular, the more shiny or glossy it is.

Diffuse reflection: In case of diffuse reflection, light is uniformly reflected towards every direction (i.e. BRDF will be uniform for all viewing directions). Matte surfaces exhibit mostly diffuse reflection. Pure diffuse reflectors (i.e. reflectors which reflect all incident light in a diffuse manner) are called Lambertian reflectors.

Most real objects we come across exhibit a combination of both types of reflections. Different kind of reflection is shown in Fig. 2.2. As LIDAR units have both the light source (laser) and detector (receiver) in the same casing, it is intuitive to assume that angles of incidence and viewing angles are roughly same.

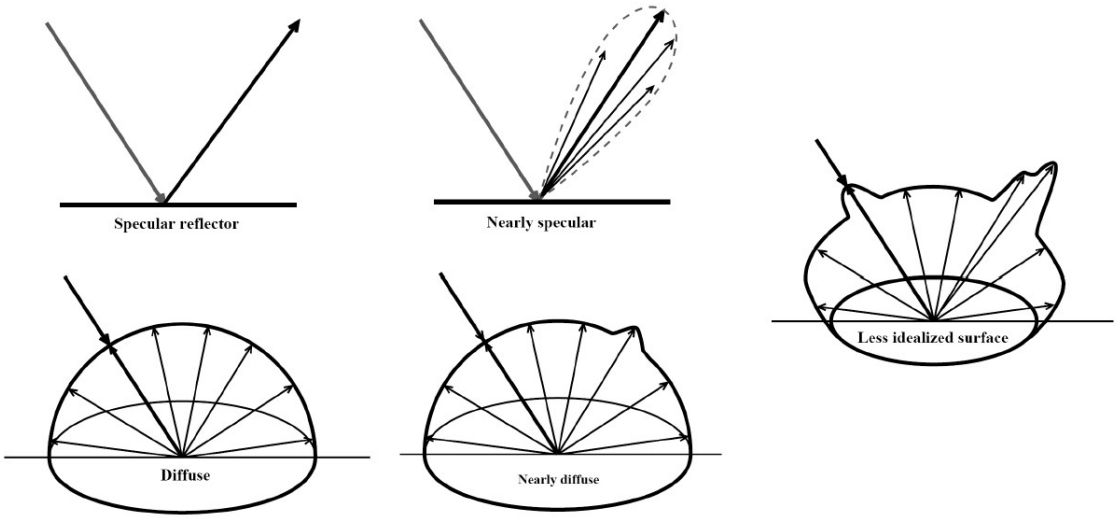

Fig. 2.2: Example of specular and diffuse reflections (courtesy of [23])

2.3 Measurement Instruments

Although the purpose of this thesis is to design surrogate objects for that can mimic LIDAR measurements of real roadside objects, it is not suitable to use LIDARs for reflectance measurement. The first reason is that each LIDAR sensor has its own parameters and configurations that are often not made public by the manufacturer. Besides, there are atmospheric parameters that are often hard to model. Without the knowledge of such parameters, it is often impossible to accurately measure the reflectance. Secondly, each LIDAR only uses laser of a single wavelength. Since we are interested in covering a relatively large wavelength range (800-1100 nm), use of a LIDAR for our measurement is not suitable.

Spectroradiometers, or spectrometers are viable commercially available instruments suited to this specific task. Spectrometers can do radiometric measurements in a wide range of wavelengths. The spectrometer used for this thesis, ASD FieldSpec Pro, has a range of 350-2500 nm [24]. Spectrometers measure the reflectance of a surface with respect to a reference panel with known reflectance characteristics. . In

simple terms, reflectance is the ratio of reflected light and incident light. The reference panel with known reflectance characteristics act as a measure of the incident light.

Spectrometers are often portable, making them well-suited for both outdoor and indoor measurements. For outdoor measurements, the sun acts as a light source. However, it is very difficult to achieve the desired light direction because: (i) the movement of sun cannot be controlled and is time dependent, and (ii) depending on the season and geographic location of experiment, some sun angles are not achievable at all. Indoor measurement can take care of this limitation. In this case, a standard indoor light source is used. Both the illumination direction and measurement direction can be customized to suit the requirements.

For the scope of this thesis, the following three components were used for reflectance measurement:

1. ASD FieldSpec Pro Spectroradiometer by Analytical Spectral Devices, Inc. (Model: FSP 350-2500P)
2. 99% Spectralon White Reference Panel by Labsphere Inc.
3. ASD ProLamp indoor light source (350-2500 nm).

ASD FieldSpec Pro Spectroradiometer

The ASD FieldSpec Pro full range Spectroradiometer (spectrometer in short) is a field spectrometer that allows spectral measuring and viewing in real time, enabling the user to readily measure radiance and reflectance spectra of materials. This spectrometer is manufactured by Analytical Spectral Devices, Inc. (ASD). This spectrometer operates in the 350-2500 nm spectral region and consists of three separate detectors that perform reflectance measurement in VNIR (350-1050 nm), SWIR1 (900-1850 nm) and SWIR2 (1700-2500 nm) regions respectively. The VNIR detector has a sampling interval of 1.4 nm and a spectral resolution of 3 nm, while each of the

SWIR detectors has sampling interval of 2 nm and spectral resolution of 10-12 nm depending on the scanning angle. Fig. 2.3 shows ASD FieldSpec Pro spectrometer and the optical fiber probe through which it collects light information.

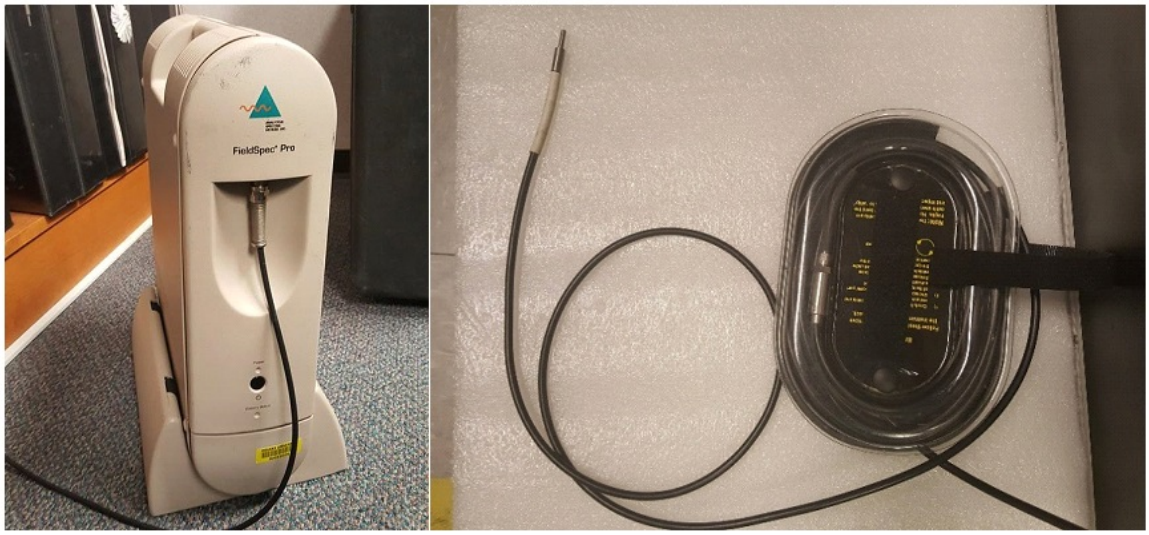

Fig. 2.3: ASD FieldSpec Pro Spectrometer (left), the included optical fiber probe (middle), and 1° field-of-view reducer accessory (right)

FieldSpec Pro makes use of a probe made of a fiber optics bundle to collect light information. The bare optical fiber has a 25° field of view (FOV); but an FOV reducer was used to bring down the field of view to 1°. The FOV reducer accessory is useful for measuring reflectance of narrow objects like I-beam. Light is collected by the fiber optics and then fed to a holographic diffraction grating. The grating separates the wavelength components of the light and feeds it to the detectors for measurement. Incident photons are converted to electrons, and during readout, a 16-bit analog to digital converter converts the photoelectric current from each detector to a voltage and digitizes the voltage. The digital data is sent to a controlling computer using a wire, which connects to the computer through an enhanced parallel port.

Data acquisition and examination is done using proprietary software provided by ASD named 'RS3' and 'ViewSpec Pro'. Using RS3 software, it is possible to see and record real-time measurement data. The recorded data can later be seen and exported in suitable formats using the ViewSpec Pro software. Both software are pre-installed on the IBM ThinkPad X31 Laptop that came with the spectrometer.

White Reference Panel

In addition to measurement taken from the unknown material, a measurement taken from a reference surface with known characteristics is also necessary to neutralize the effect of characteristics of incident light. If the light source is stable, and the illumination geometry is identical for both the unknown and reference material (i.e., during measurement, both the unknown material and the reference material are in similar orientation with respect to the light source and probe, and lighting stays similar throughout), the characteristics of the light source can be eliminated when the ratio of these two measurements is taken to calculate the reflectance of unknown material.

In short, reflectance is computed using measurements from both the sample material and a reference material with known reflectance properties. A reference panel with nearly 100% reflectance throughout the whole wavelength range is called a white reference standard or white reference panel. The reference panel used for this work is a 99% Spectralon white reference panel manufactured by Labsphere Inc. (shown in Fig. 2.4), which exhibits near-perfect reflectance properties to ensure reflectance data collection with great accuracy.

ASD ProLamp Light Source

The ASD ProLamp (shown in Fig. 2.5) is a 14.5V-50W Lamp. It can be mounted on a tripod and provides light over a 350 - 2500 nm wavelength range. This makes indoor reflectance measurement very convenient.

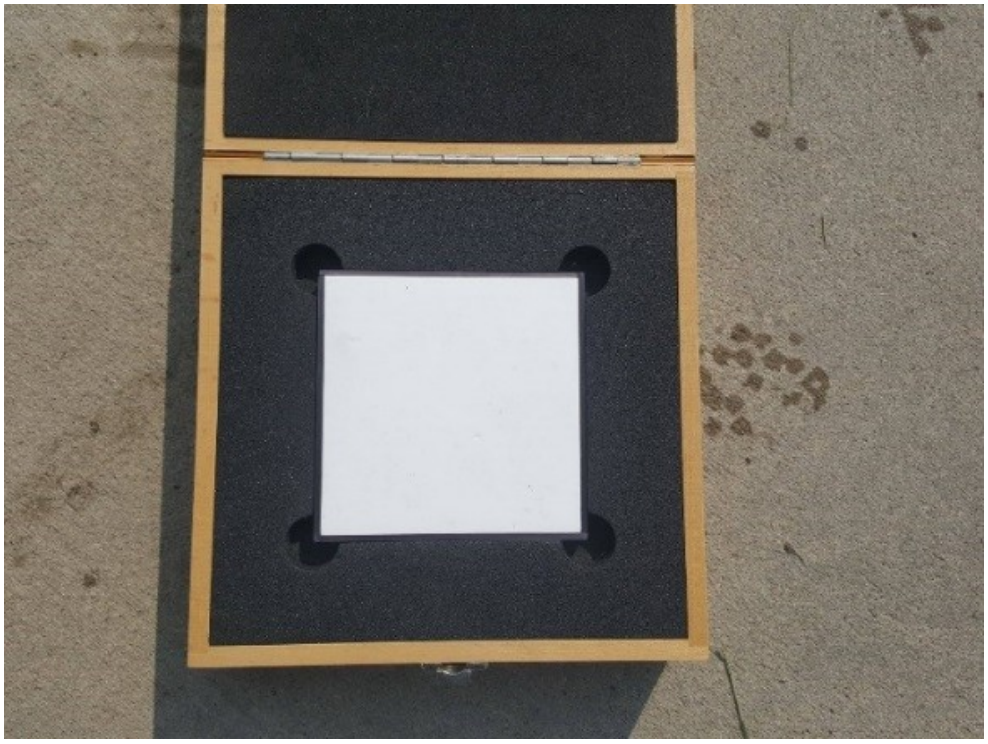

Fig. 2.4: The White Reference Panel (99% Spectralon)

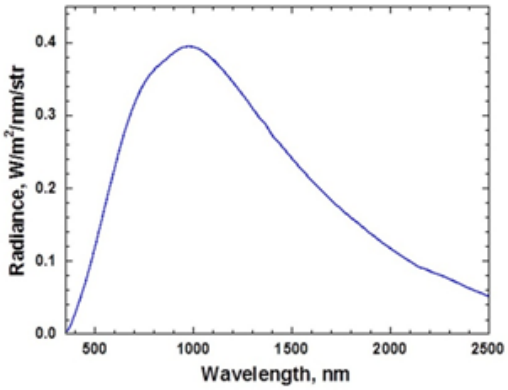

Fig. 2.5: ASD ProLamp Light Source (left) and the radiance of the lamp measured using 99% Spectralon white reference panel (right)

2.4 Measurement Procedure

A general procedure used in this work for both indoor and outdoor measurement of reflectance is described below. More details and figures will be given in later sections.

1. The laptop and the spectrometer are turned on at the test site. Spectrometer must be warmed up for a 30-minute period before use. The 'RS3' software is opened.

2. A suitable sample site for taking measurement is selected (for example, a fixed portion of road). For movable samples, the sample is fixed in a desired angle using angle calculator. The white reference plate is kept on top of that site. The probe is fixed at a desired angle. In case of indoor measurement, the light source is also fixed at a desired angle and distance.

3. The instrument is optimized by selecting "Control → Optimize instrument settings" in the software.

4. Using the ruler and angle calculator, the distance and angle between the optical fiber probe and the sample are found out. The probe is pointed at the white reference panel.

5. In the software, the following option is selected: "Control → Take white reference measurement". After this measurement, the subsequent measurements would return reflectance values.

6. The white reference plate is removed from the site. The optical fiber probe is pointed towards the target material at the same geometric orientation used in case of the white reference panel. The real-time reflectance spectrum of the material can be seen on the software interface.

7. On the software, "Control → Spectrum save" is selected. A suitable file name is selected and 'Number of files to save' is assigned a value of 10. Spectrum collection is started by clicking "Begin save". This will take 10 readings of reflectance over the entire spectra.

8. Post-processing is done using 'ViewSpec Pro' software. The average of these 10 readings are taken and the average reflectance spectra is generated. It can be exported as figure or CSV.

2.5 Selection of Roadside Objects

During a road/roadside study project in 2016, TASI sampled 24,735 locations to find the most common types of roadside objects. The results are shown in Table 2.1. It is evident from the table that the most common types of roadside objects are grass, concrete curb, metal guardrail and concrete divider. Therefore, this thesis is interested in making surrogate objects replicating concrete, metal guardrail and grass.

Table 2.1: Most common types of roadside objects (found by a road/roadside study project by TASI)

Road edge/boundary	**Number of locations**	**%Locations in US roads**
Grass	13544	54.75%
Concrete curb	3965	16.03%
Metal guardrail	2148	8.68%
Concrete divider	1031	4.17%
Gravel	774	3.13%
Traffic barrel or cones	70	0.28%
Others	3203	12.95%
Total	24735	100%

3. SPECIFICATION OF REPRESENTATIVE INFRARED REFLECTANCE OF SURROGATE ROADSIDE OBJECTS

In this section, the representative Infrared (IR) reflectance of three types of surrogate objects (metal guardrail, concrete and grass) for different LIDAR view angles are specified. To achieve this, multiple real samples of each type of objects are tested both outdoor and indoor, and their reflectance for the required angles are measured. Based on the measurement data, the upper and lower bounds of reflectance curve for each angle are suggested for each object.

The contents of this section are organized as follows. Section 3.1 describes some definitions related to the measurement method used in this thesis. Section 3.2 briefly describes the three measurement approaches used in this thesis and their objectives. Section 3.3 describes in detail the measurement of real metal guardrails and specifies the suggested IR reflectance range of surrogate metal guardrail skin for 0-70° LIDAR viewing angles. Section 3.4 describes the measurement of real concrete samples and specifies the suggested IR reflectance range of surrogate concrete skin for 0-70° LIDAR viewing angles. Finally, Section 3.5 describes the measurement of various grass samples and specifies the suggested IR reflectance range of surrogate grass for 0-70° LIDAR viewing angles.

3.1 Relevant Definitions

Normal line: Normal line is a line that is perpendicular to the surface plane being measured. The green dashed line in Fig. 3.1 denotes normal line. When measuring a horizontal surface, the normal line is vertical (Fig. 3.1a). On the other hand, when measuring a vertical surface, the normal line is horizontal (Fig. 3.1b).

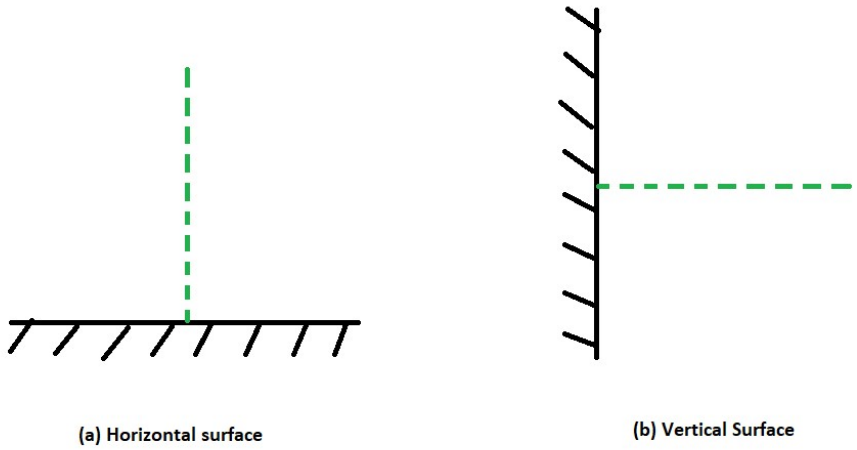

Fig. 3.1: The green line indicates the normal line for (a) horizontal surface and (b) vertical surface

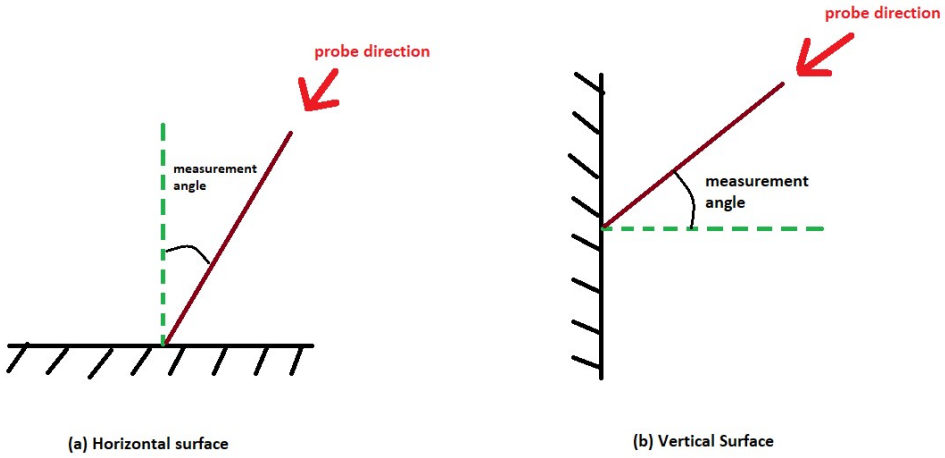

Fig. 3.2: Measurement angle for (a) horizontal surface and (b) vertical surface

Measurement angle (or probe angle): Measurement angle (or probe angle) is the angle between the normal line and probe direction is defined as measurement angle (Fig. 3.2). This is equivalent to the viewing zenith angle described in Section 2.2. 0° measurement angle means that the probe direction is perpendicular to the surface,

and 90° measurement angle means that the probe direction is parallel to the surface plane. When probe is nearly horizontal (0°-20° measurement angles), we define such angles as near-horizontal measurement angles.

Illumination angle: Illumination angle is the angle between the normal line and the light direction (Fig. 3.3). This is equivalent to the incidence zenith angle described in Section 2.2. 0° illumination angle means that light falls perpendicularly on the surface, and 90° illumination angle means that light emitted by the source is parallel to the surface plane.

In case of outdoor measurements where sun is the light source, if the surface being measured is vertical (Fig. 3.3b), then the normal line is horizontal. Therefore, the illumination angle will be equal to sun elevation angle (i.e., the angle between sunlight direction and horizontal plane). If the surface being measured is horizontal (Fig. 3.3a), then the normal line is vertical. Therefore, in this case, sun illumination angle = 90° - sun elevation angle.

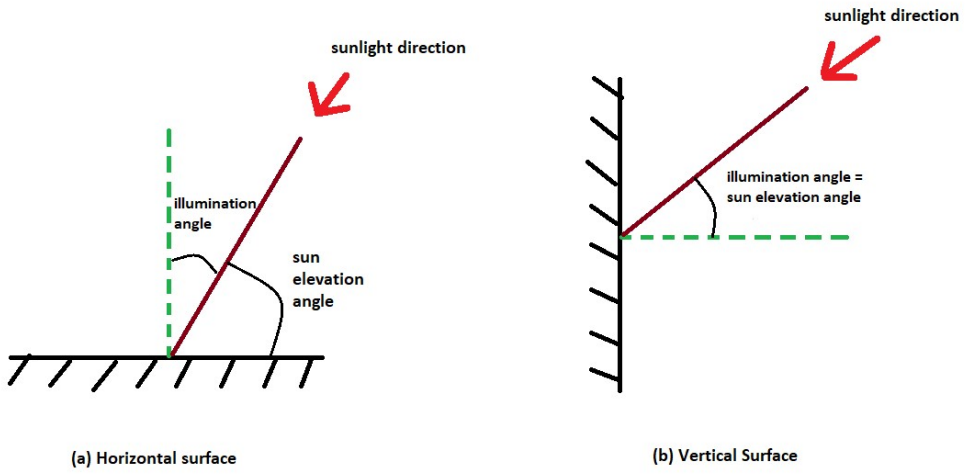

Fig. 3.3: Illumination angle for (a) horizontal surface and (b) vertical surface

Phase angle: Phase angle is the angle between the vertical plane of light direction and the vertical plane of probe direction (i.e. 0° phase angle = probe and light source are in the same vertical plane). This angle is equal to the difference of incidence azimuth angle and viewing azimuth angle described in Section 2.2. The geometry of phase angle is shown in Fig. 3.4.

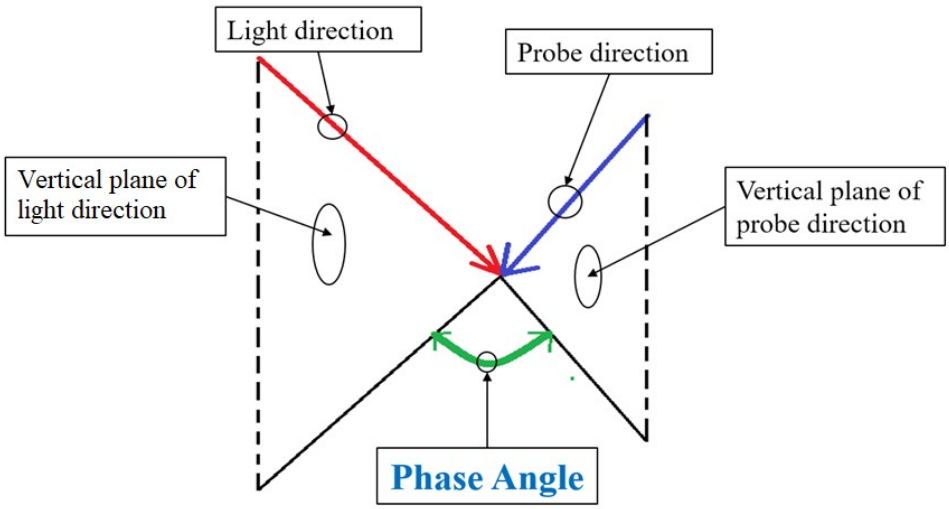

Fig. 3.4: Geometry of phase angle

LIDAR operation conditions: LIDAR sends and receives light in the same direction. Therefore, to mimic LIDAR conditions during reflectance measurement, the illumination angle should be equal to measurement angle for all measurements, and the phase angle should ideally be 0°. However, due to equipment limitations, keeping the phase angle exactly 0° results in uneven illumination or severe shadowing on the surface being measured. Therefore, for most measurements, a small 10°-20° phase angle was kept.

3.2 Approaches for Reflectance Measurement

In general, three approaches were adopted to study multiple samples of metal guardrail, concrete and grass. Their objectives are briefly described below:

3.2.1 Approach 1: Outdoor Perpendicular Measurement

These measurements were done outdoors with sun as the illumination source. For these measurements, the probe was always kept perpendicular to the surface being examined, i.e., the measurement angle was 0° (see Fig. 3.5). Illumination angles were variable (between 48°-70°) depending on the measurement time during the day. For comparison between similar objects, efforts were made to keep illumination angle within similar range.

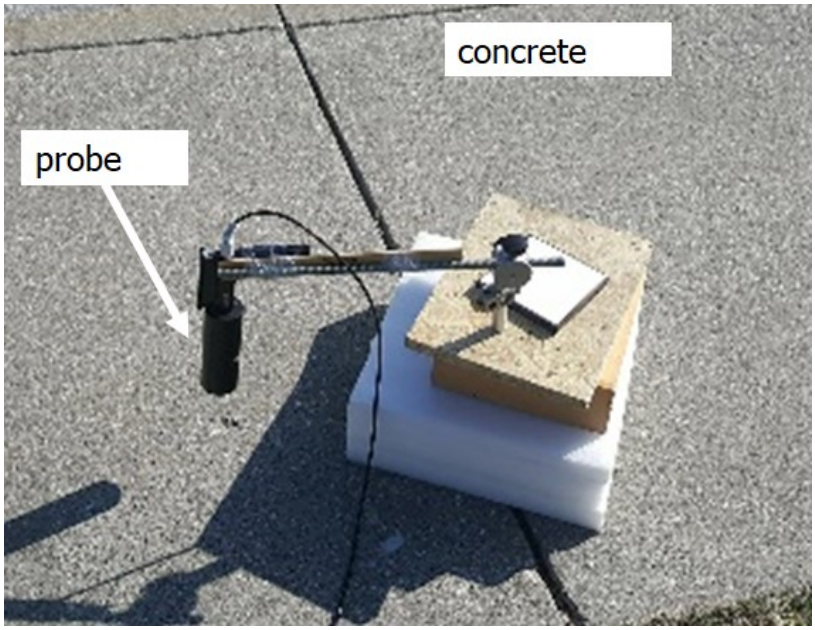

Fig. 3.5: Approach 1 (outdoor perpendicular measurement), 0° measurement angle, no control over illumination angle (60° in this case)

This approach gave the flexibility to measure a large number of samples, because all roadside objects are available in plentiful outdoors. We were able to compare the reflectance properties of different samples of the same roadside object. However, since the illumination angle was not controllable, it was difficult to mimic LIDAR operation conditions; in other words, finding the moments where illumination angle equal was to measurement angle requires significant effort, and certain angles are not achievable depending on geographic locations and time of year.

3.2.2 Approach 2: Indoor Measurement

These measurements were done indoors with the ASD ProLamp as the artificial light source. Sample position, light position and probe position – all three were adjustable, which enabled precise control over measurement angle and illumination angle. Measurement angles were varied from 0° to 70° (in 10° increments), and in each case, the illumination angle was kept equal to measurement angle. A small 10°-20° phase angle was kept. Therefore, mimicking LIDAR operation conditions was possible using this setup. Fig. 3.6 and Fig. 3.7 shows example setups for 0° and 70° measurement angles respectively. Fig. 3.8 gives a top view of the measurement setup and shows the probe, light source and phase angle in detail. These pictures were taken with other light sources on to ensure clear photos. It should be noted that all other light sources except the ASD ProLamp shall be turned off during measurement, to eliminate noise.

Fig. 3.6: Approach 2 (Indoor measurement), measurement angle = illumination angle = 0° , phase angle = 20°.

Fig. 3.7: Approach 2 (Indoor measurement), measurement angle = illumination angle = 70° , phase angle = 20°.

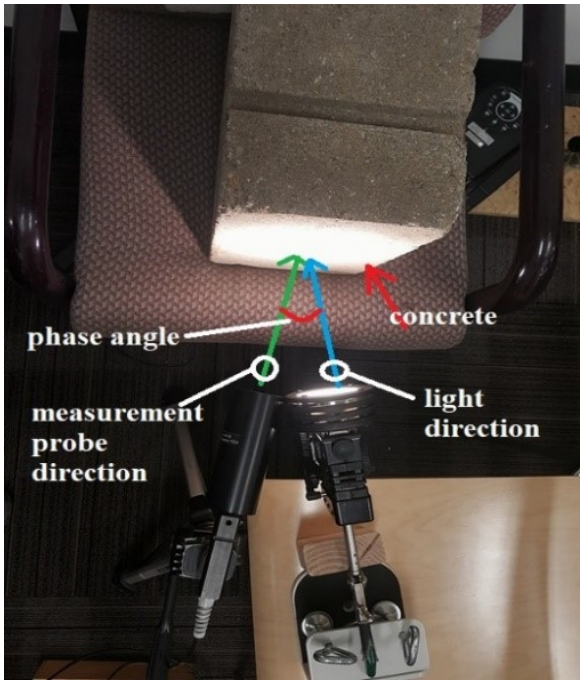

Fig. 3.8: Top view of approach 2 (Indoor measurement), measurement angle = illumination angle = 0° , phase angle = 20°.

This approach was the most important approach, because the IR reflectance requirements of surrogate objects for different angles were specified by measuring real samples using this approach.

The limitation was that sometimes it was not possible to bring all desired roadside samples in an indoor setup.

3.2.3 Approach 3: Outdoor Measurement for Verifying the Indoor Results

Although getting desired sun positions was very difficult, it was possible to get a few conditions when the illumination angle became equal to measurement angle. This was done by using the web application 'Suncalc' [25] to track sun movement and find the exact timings of these desired illumination angles with respect to Indianapolis, the test site for this thesis. For these illumination angles, some measurements were taken by keeping the measurement angle equal to the illumination angle for each type of roadside object, and phase angle was kept 10°-20° to avoid shadowing of the surface being measured. These data were later compared with indoor measurements done with the exact same measurement angle and illumination angle to verify the accuracy of indoor measurement. Fig. 3.9 shows an example of measurement done using approach 3.

3.3 Specification of Suggested Infrared Reflectance of Surrogate Concrete Skin

Both concrete dividers and curbs are made using the same material: Portland cement. Therefore, we suspected that their IR reflectance to be the similar. To verify this and to find the representative IR reflectance of curb and concrete divider, the reflectance of multiple real concrete samples (curbs, dividers, blocks and wall) was

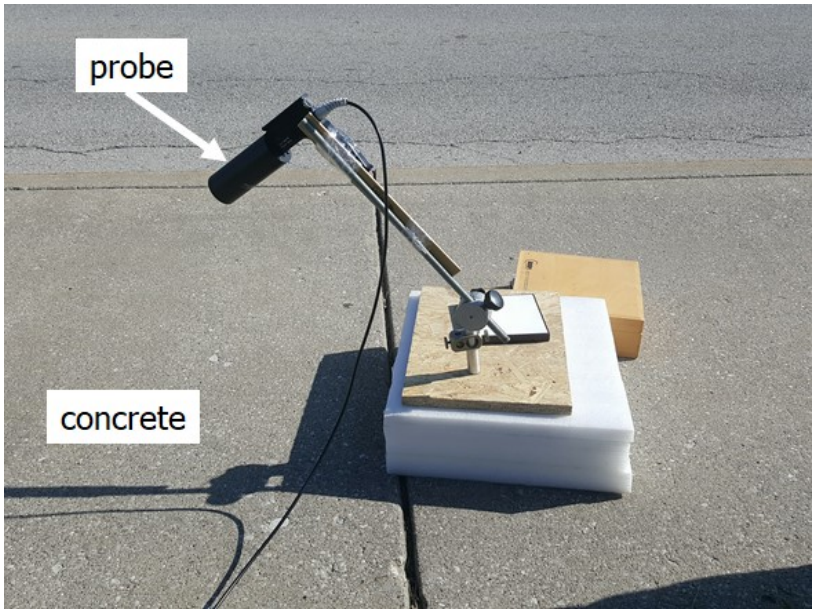

Fig. 3.9: Approach 3 (outdoor measurement to verify the indoor results), measurement angle = illumination angle = 60° , phase angle = 20°.

measured using the three approaches described in Section 3.2. Based on these measurements, the suggested IR reflectance of concrete surrogate skin for 0°-70° LIDAR view angles are specified.

3.3.1 Concrete Reflectance Measurement using Approach 1 (Outdoor Perpendicular Measurement)

For this task, the reflectance of several concrete curb and divider samples was measured from 0° measurement angle. Since sun is the outdoor light source, the illumination angle could not be controlled. Since the LIDAR operation conditions could not be mimicked for this measurement, this approach was taken to simply compare different concrete samples in same condition.

The following samples were examined:

- 4 samples of old curbs (Fig. 3.10).
- 3 samples of new curbs, constructed 1 week before measurement (Fig. 3.11).

Fig. 3.10: Four samples of old curb

Fig. 3.11: Three samples of new curb

Fig. 3.12: Old divider sample no. 1. Samples 2-6 are of similar appearance

- 5 samples of old dividers (Fig. 3.12).
- 1 sample of newer divider (Fig. 3.13).

Fig. 3.13: New concrete divider

From the figures, it is apparent that the older concrete looks somewhat yellowish and less bright, while the newer concrete samples look white and brighter.

Measurement Results

New curb versus old curb: With 0° measurement angle, 27.8°-45.5° illumination angle and 0° phase angle, the IR reflectance of four old curbs and three new curbs were measured, and their reflectance spectra are compared in Fig. 3.14.

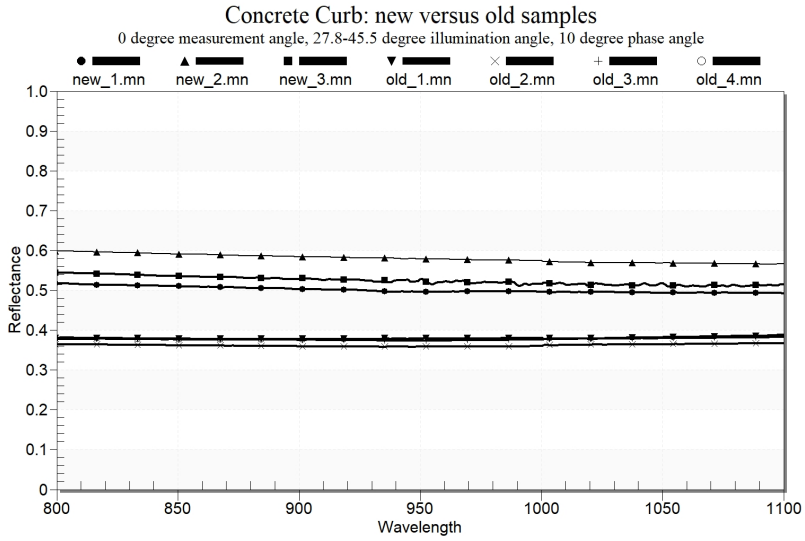

Fig. 3.14: Comparison of new and old concrete curb samples (0° measurement angle, 27.8°-45.5° illumination angle, 10° phase angle)

There is a significant difference in reflectance between the old curb samples and the new curb samples; new curb reflectance seems to be much higher. Upon examination, it was found that during the construction of the new curbs, curing compounds are often used. For example, a white-pigmented curing compound named 'SEALTIGHT 1600-WHITE' was applied to the outer visible surface of one of the curbs measured during this experiment. After application,it creates a reflective coat and ensures optimized retention of water. The white pigment reflects the sun's rays, and this results in a overall higher reflectance for the new curbs.

Fig. 3.15 shows the outside (visible) and inside (non-visible) part of a newly constructed curb. The outside surface has a reflective coating and is white in color, but the inside surface does not have the coating and is yellowish.

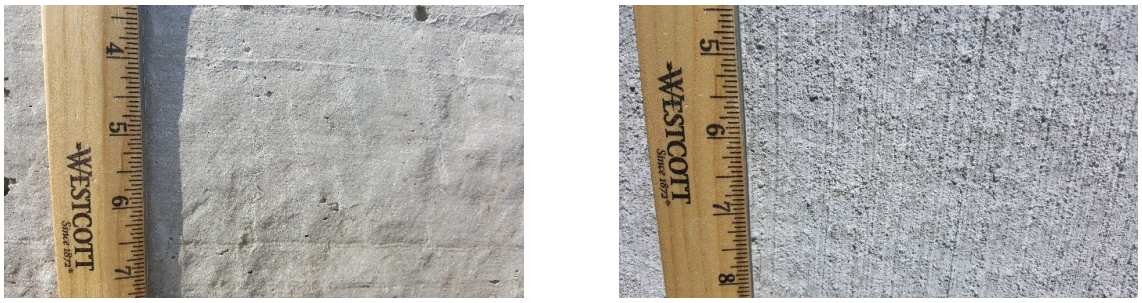

Fig. 3.15: Inner surface without coating (left) and outer surface with coating (right) of a new curb

New divider versus old divider: With 0° measurement angle and 27.8°-45.5° illumination angle, the reflectance spectra of new and old dividers are compared in Fig. 3.16. The phenomenon is the same as that of curbs: the new divider shows higher reflectance than the old ones.

Remarks

1. The IR reflectance of concrete curb and concrete divider are similar.

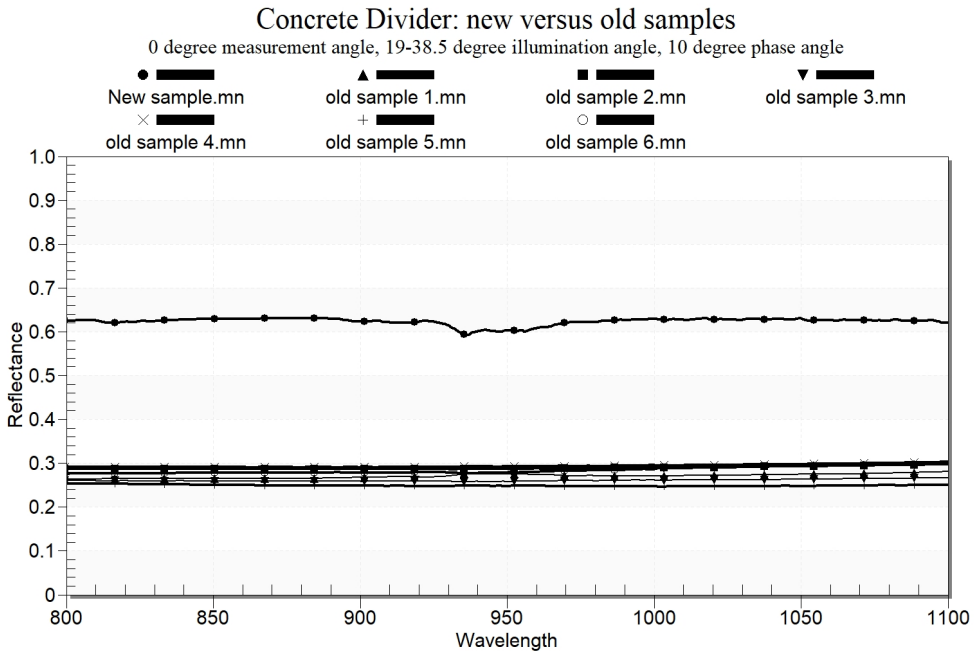

Fig. 3.16: Comparison of new and old concrete divider samples (0° measurement angle, 19°-38.5° illumination angle, 10° phase angle)

2. It is apparent that from the reflectance measurement using approach 1 (0° measurement angle) that older concrete samples without coating have lower overall reflectance than the newer concrete samples with coating. Since coatings will disappear with time, the representative concrete IR reflectance should be the same as of the old concrete.

The limitation of this measurement is that the desired illumination angles for simulating LIDAR operation conditions (measurement angle and illumination angle should be same) takes great effort to achieve. Therefore, it is not a good way to specify the IR reflectance requirements using outdoor measurement under Sunlight. Indoor measurement with approach 2 takes care of this limitation.

3.3.2 Concrete Reflectance Measurement using Approach 2 (Indoor Measurement from Different Angles)

Indoor measurement setup made it possible to simulate LIDAR operation conditions. Measurement angle was varied from 0° to 70° (in 10° increments every time), and for each case, illumination angle was kept equal to the corresponding measurement angle. 20° phase angle was kept in order to ensure even illumination of the surface being measured.

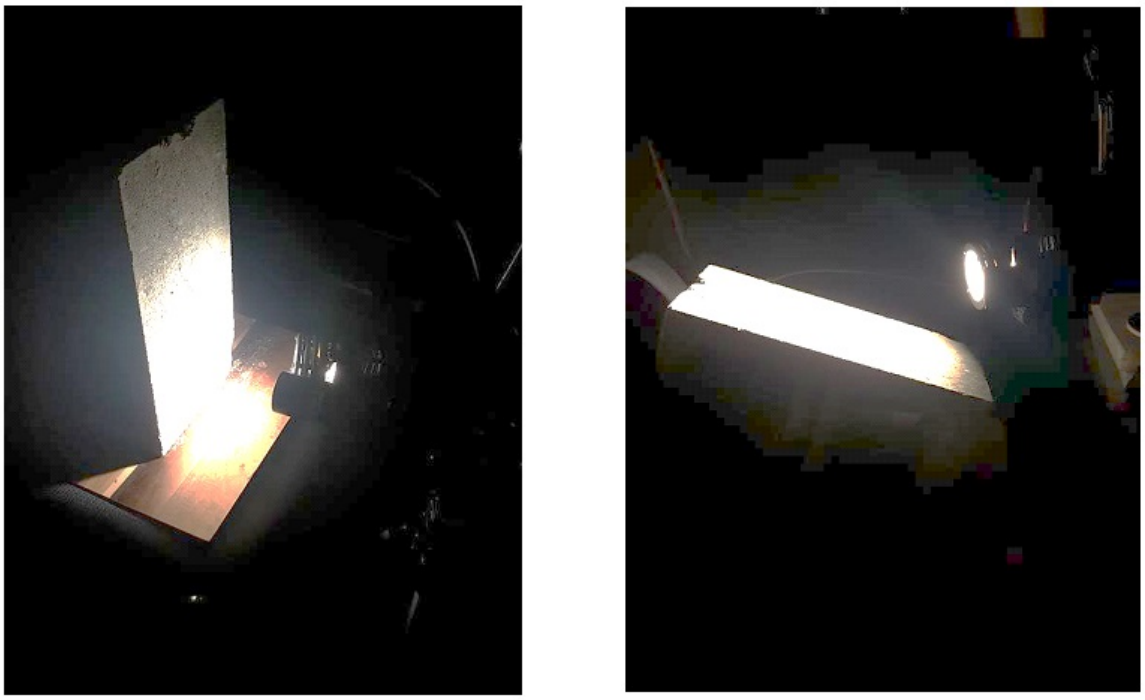

Fig. 3.17: Concrete block no. 1- indoor measurement - 0° measurement angle (left) vs 70° measurement angle (right); illumination angle same as measurement angle; phase angle = 20°.

As mentioned before, the representative concrete should match the old concrete without coating. Therefore, two concrete blocks without coating that have similar appearance to old curbs were obtained. Fig. 3.17 shows the measurement of concrete block -1; the same setup was used to measure the concrete block-2. In addition, a concrete wall of a building was also measured (Fig. 3.18). Finally, two concrete dividers

were also measured at dark night using the indoor measurement setup (Fig. 3.19). In total, five samples were evaluated using indoor measurement setup: two concrete blocks, one concrete wall and two concrete dividers.

Fig. 3.18: Concrete Wall being measured in an indoor setup (measurement angle = illumination angle = 70°), phase angle = 20°.

Fig. 3.19: Two concrete dividers (measured using indoor setup after sunset)

Measurement Results

Fig. 3.20 shows the reflectance curves of concrete block-1 for 0-70° measurement angles (illumination angle same as measurement angle, which simulates LIDAR operation conditions). It is noticeable that reflectance is lowest for 0° measurement angle. As the angle increases, reflectance also increases. For 70° measurement angle, reflectance is the highest.

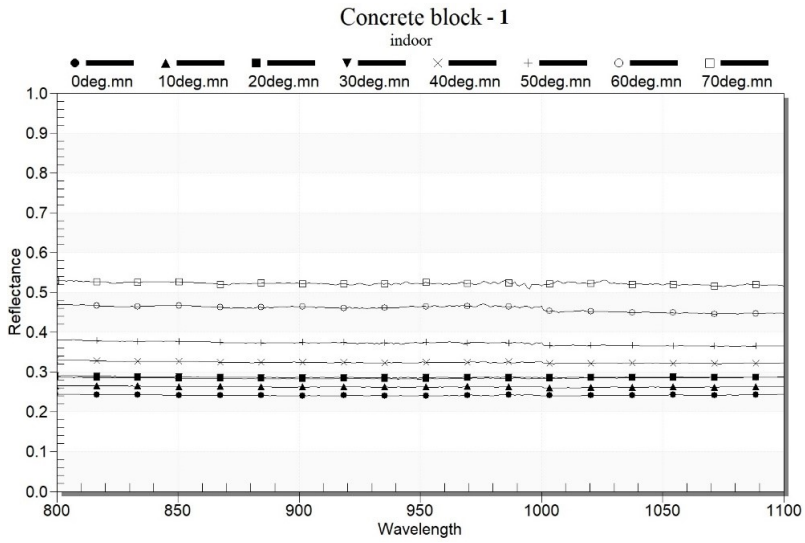

Fig. 3.20: Reflectance of concrete block No. 1- indoor measurement from different measurement angles (for all cases, illumination angle = measurement angle); 20° phase angle

Fig. 3.21 and Fig. 3.22 shows reflectance at different angles for Concrete block-2 and concrete wall respectively. Same pattern can be seen here, reflectance increases as the measurement angle increases.

In addition, the reflectance of two old concrete dividers was measured using the indoor probe-light setup. These concrete dividers were found in a parking lot near Indianapolis International Airport. Although the concrete dividers were outdoors, they were measured after sunset to mimic indoor conditions (no sunlight, only the ASD Pro Lamp was used as light source). For each concrete divider, the reflectance

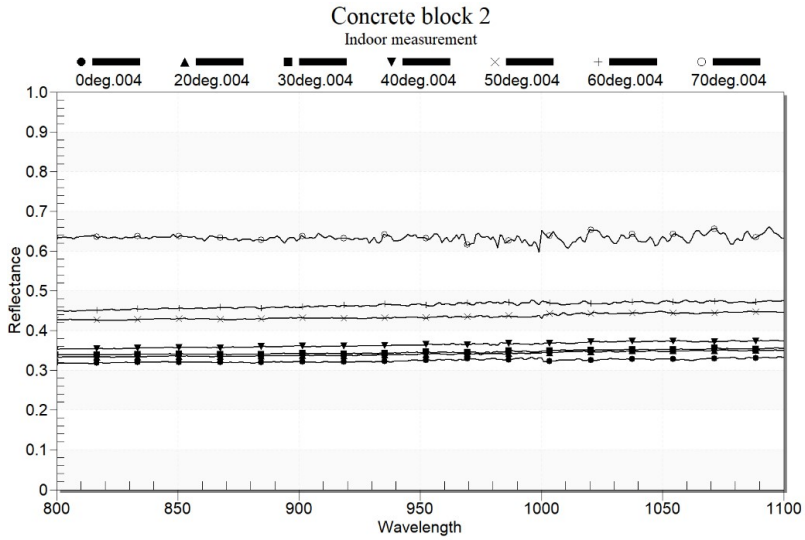

Fig. 3.21: Reflectance of concrete block No. 2- indoor measurement from different measurement angles (for all cases, illumination angle = measurement angle); 20° phase angle

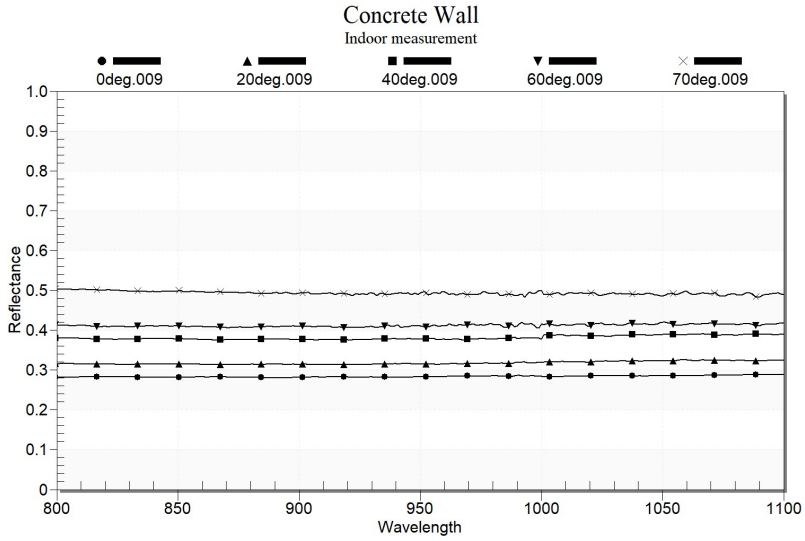

Fig. 3.22: Reflectance of concrete wall indoor measurement from different measurement angles (for all cases, illumination angle = measurement angle); 20° phase angle

for 0°-70° measurement angles was measured (in 10° increments each time), and for each case, illumination angle was kept equal to measurement angle to mimic LIDAR operation conditions.

The reflectance of these two concrete dividers for different measurement angles are shown in Figs. 3.23 and 3.24. These concrete dividers also show similar reflectance properties like concrete blocks and concrete wall measured before, i.e., reflectance increases as the measurement angle increases, and the values are also similar.

Remarks

Indoor measurement makes it possible to simulate LIDAR operation conditions, and therefore, it was possible to quantify the reflectance of concrete at different LIDAR view angles by measuring five concrete samples. Based on these measurements, the suggested IR reflectance of surrogate concrete for different LIDAR view angles will be specified in Section 3.3.3.

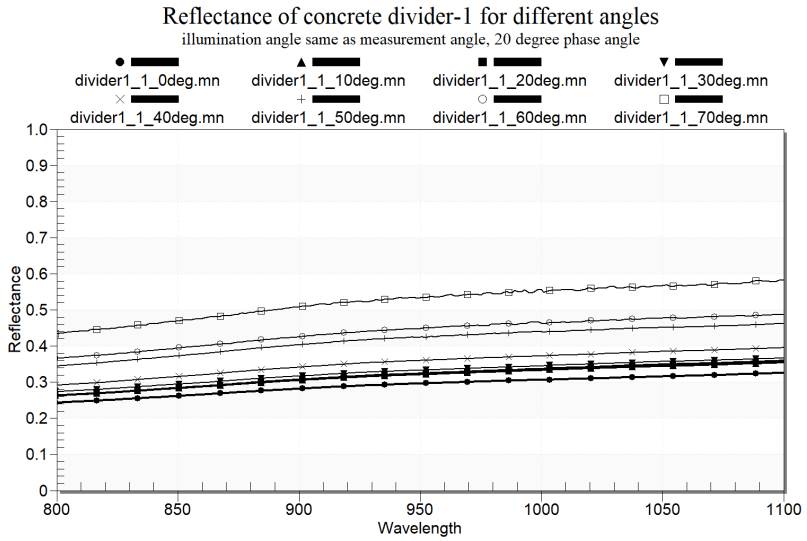

Fig. 3.23: IR reflectance spectra of concrete divider-1 for 0°-70° measurement angles (illumination angle equal to corresponding measurement angle, 20° phase angle)

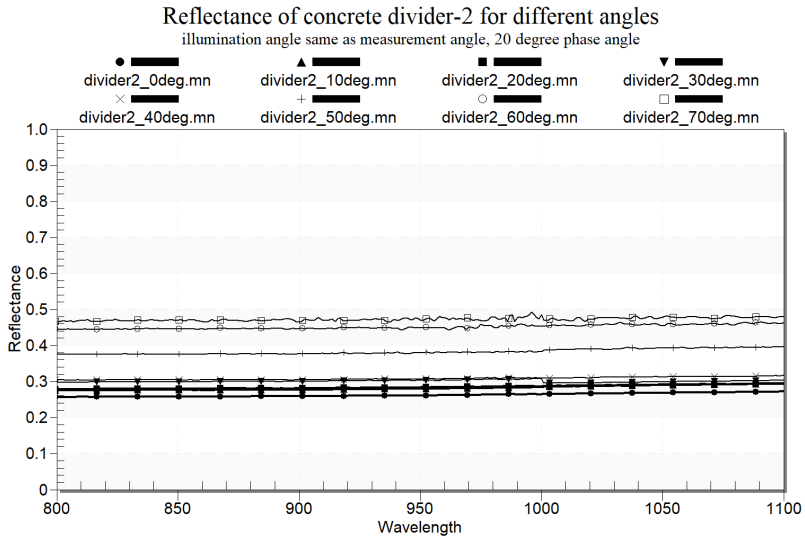

Fig. 3.24: IR reflectance spectra of concrete divider-2 for 0°-70° measurement angles (illumination angle equal to corresponding measurement angle, 20° phase angle)

3.3.3 Specification of Suggested IR Reflectance of Concrete Surrogate Skin for Different Angles

The indoor measurement of five concrete samples described in Section 3.3.2 simulates LIDAR operation conditions. All five concrete samples show similar reflectance properties. To generate the suggested reflectance of surrogate concrete skin for a particular angle, at first the reflectance curves of these five concrete samples for that angle are taken into account. In Fig. 3.25, the reflectance curves of all samples for the same angle are grouped in the same plot.

From Fig. 3.25, it is very easy to see that for each angle, reflectance of concrete samples varies within some range. Then, for each angle, the reflectance data of all available samples are processed to find the lowest and highest reflectance value observed for each wavelength. After this step, two sets of data are obtained for each angle - one contains the minimum observed reflectance values for all wavelengths, and the other contains the maximum observed reflectance values for all wavelengths. These two sets of data give the range of observed concrete reflectance for each angle.

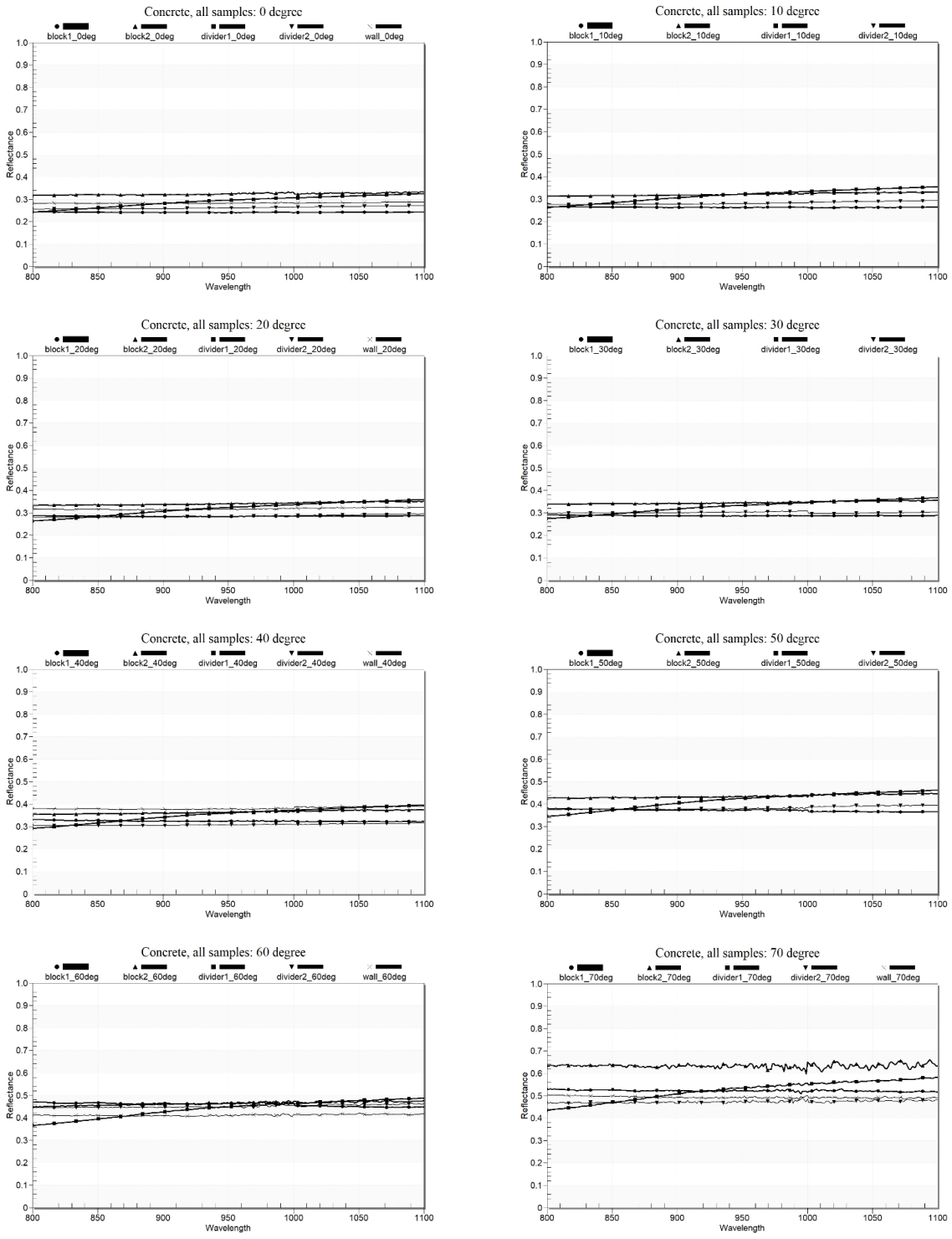

Fig. 3.25: Reflectance curves of all concrete samples for the same angle grouped in the same plot

Finally, a tolerance of ±0.05 is given to the range of observed concrete reflectance, because such a small variation of reflectance is very common within different samples and even within the same sample. Therefore, 0.05 is added to the set of maximum observed reflectance values, while 0.05 is subtracted from the set of minimum observed reflectance values. This gives the suggested upper and lower bounds for the IR reflectance of surrogate concrete skin for each angle. Fig. 3.26 through Fig. 3.33 show the suggested IR reflectance of surrogate concrete skin for 0°-70° angles.

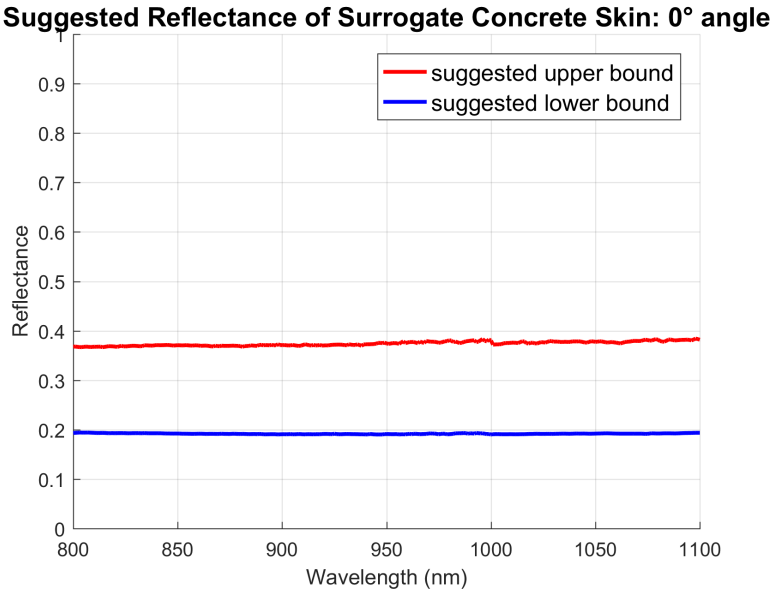

Fig. 3.26: Suggested IR reflectance range of surrogate concrete skin for 0° LIDAR view angle

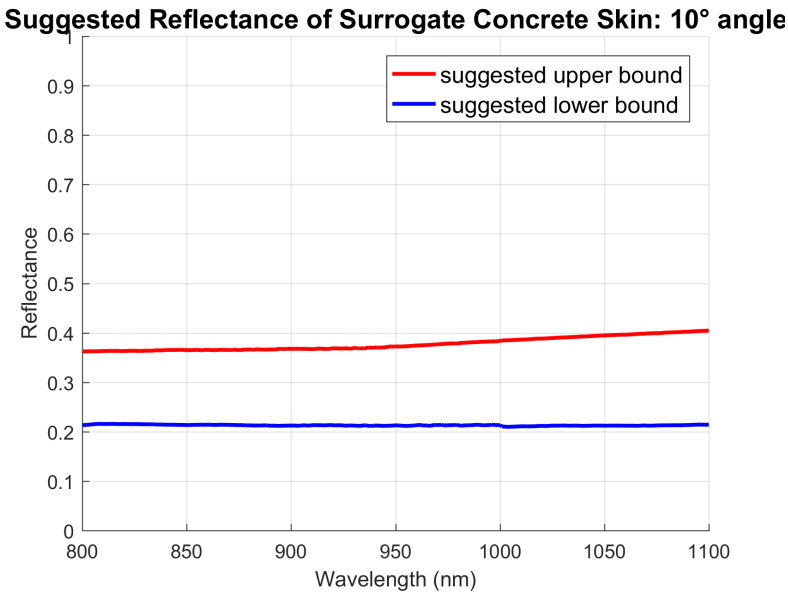

Fig. 3.27: Suggested IR reflectance range of surrogate concrete skin for 10° LIDAR view angle

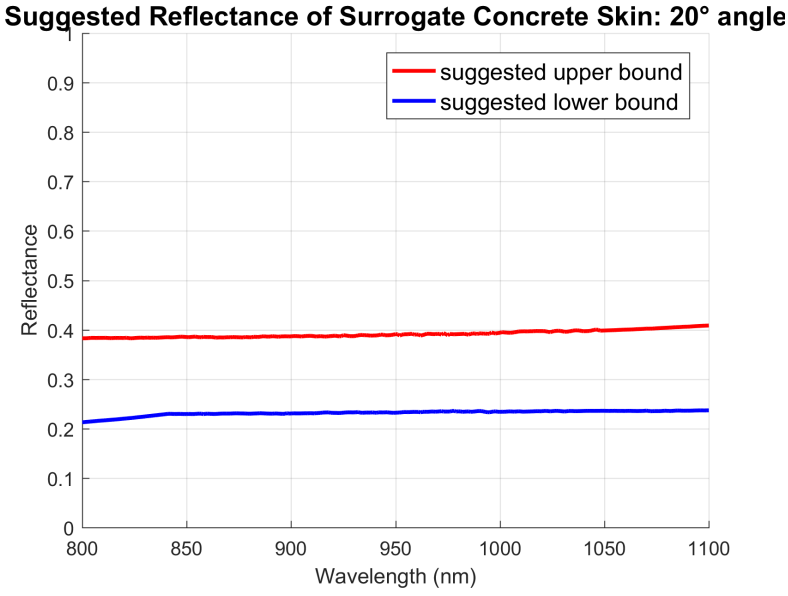

Fig. 3.28: Suggested IR reflectance range of surrogate concrete skin for 20° LIDAR view angle

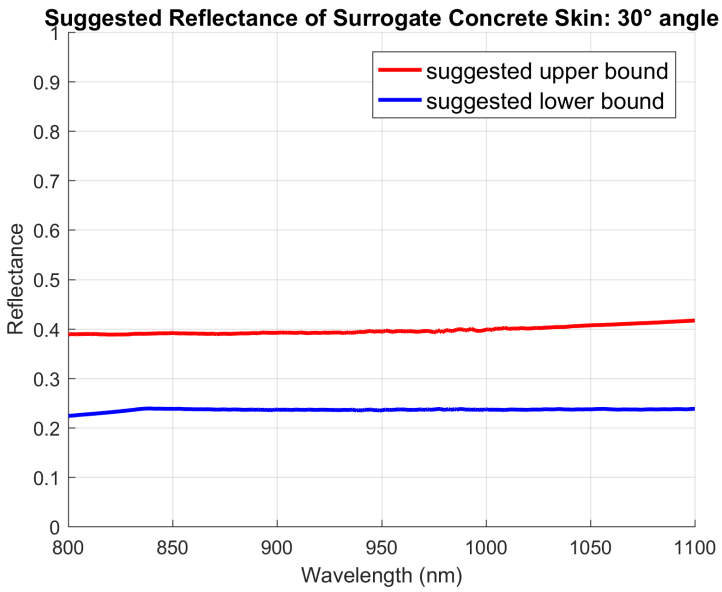

Fig. 3.29: Suggested IR reflectance range of surrogate concrete skin for 30° LIDAR view angle

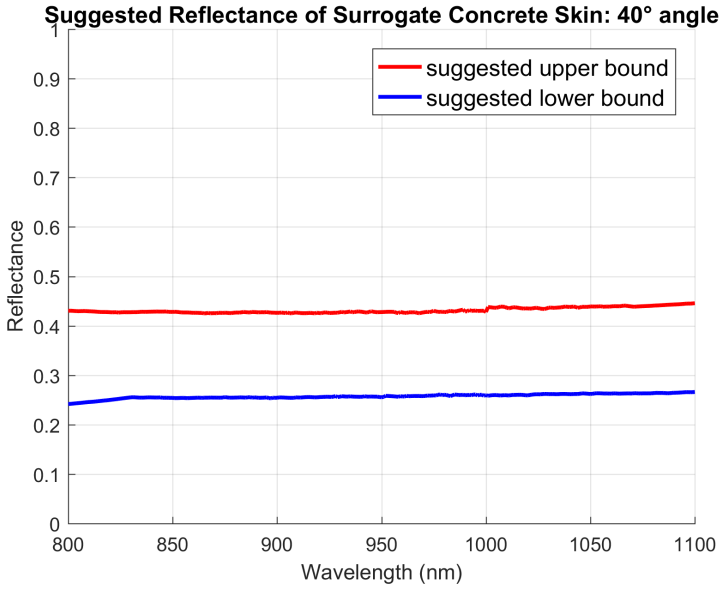

Fig. 3.30: Suggested IR reflectance range of surrogate concrete skin for 40° LIDAR view angle

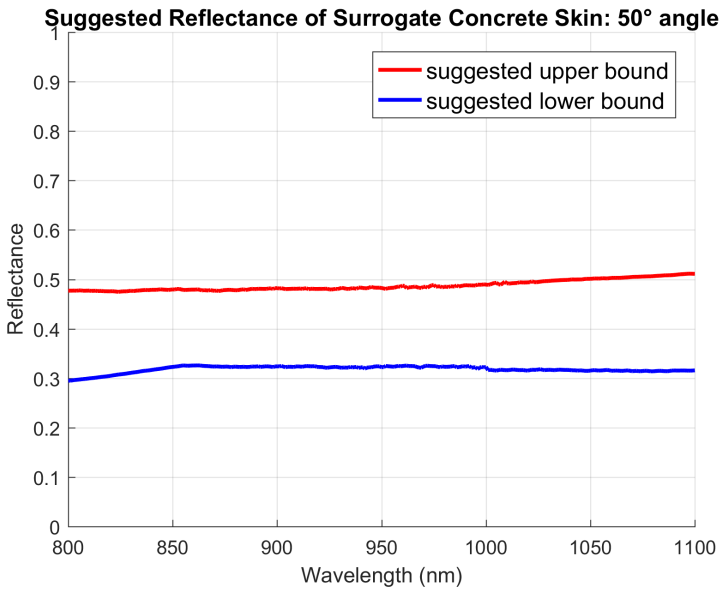

Fig. 3.31: Suggested IR reflectance range of surrogate concrete skin for 50° LIDAR view angle

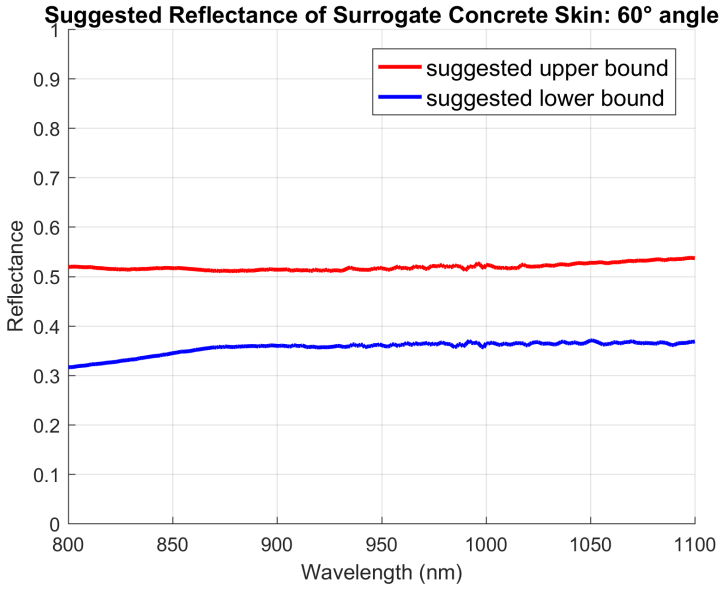

Fig. 3.32: Suggested IR reflectance range of surrogate concrete skin for 60° LIDAR view angle

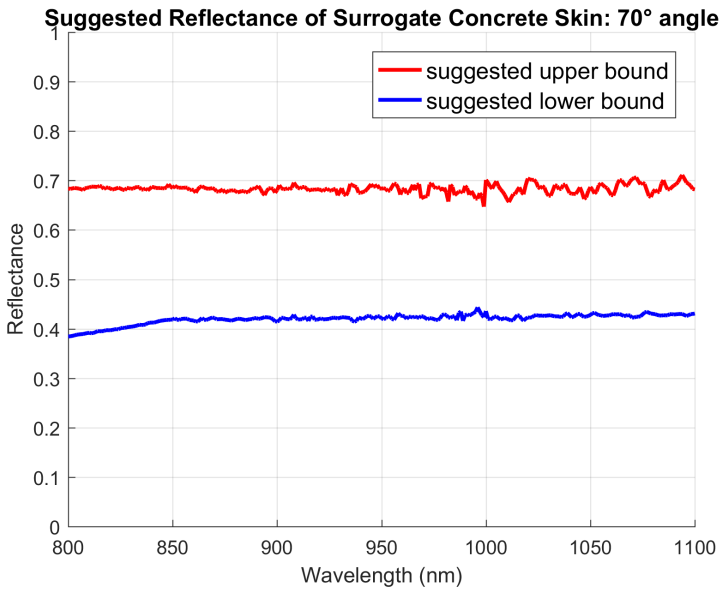

Fig. 3.33: Suggested IR reflectance range of surrogate concrete skin for 70° LIDAR view angle

3.4 Specification of Suggested Infrared Reflectance of Surrogate Metal Guardrail Skin

Metal Guardrail (Fig. 3.34) consists of two major parts: the vertical I-beam and horizontal W-beam. The cross section of W-beam is w-shaped, while the cross section of I-beam is I-shaped. The lack of flat surfaces of W-beam make it difficult to measure reflectance without errors. I-beams on the other hand have flat surfaces, which are suitable for reflectance measurement using spectrometer. Therefore, all IR reflectance specifications were made based on measurement of I-beam reflectance. Both I-beam and W-beam are made of galvanized steel and zinc is on outer surface. Therefore, one surrogate skin will be enough to represent both W-beam and I-beam.

To find the representative IR reflectance of surrogate metal guardrail, the reflectance of multiple real I-beam samples was measured using three approaches described in Section 3.2. Based on these measurements, the suggested IR reflectance of surrogate metal guardrail skin for 0°-70° LIDAR view angles are specified.

Fig. 3.34: Metal Guardrail. The horizontal bar is W-beam, the vertical support bars are I-beams

3.4.1 I-beam Reflectance Measurement using Approach 1 (Outdoor Perpendicular Measurement)

In this section, reflectance is measured by testing multiple I-beam samples of different age for 0° measurement angle. The illumination angle varied for different measurements at different times of days, because in case of outdoor measurement, sun light angle changes over time of day, and therefore these measurements cannot simulate LIDAR operation conditions. These measurements are done to observe the highly specular nature of reflection coming from the glossy metallic surface of I-beam.

The following samples were examined (Fig. 3.35):

- New I-beam: 1 sample, purchased, movable.
- ∼3 years old: 2 samples, fixed, near Whitestown, IN.
- ∼10 years old: 1 sample, fixed, near Whitestown, IN.
- Very old (unknown age): 1 sample, fixed, in a parking lot near St. Clair and Senate, Indianapolis, IN.

Fig. 3.35: Appearance of I-beam samples of different ages

Measurement results

I-beam measurement with illumination angle close to measurement angle: In this case, the new I-beam was placed on the ground horizontally, and measurement was taken at multiple parts of this I-beam at 0° measurement angle. The illumination angle was 17.5°-19.7°. The setup is shown in Fig. 3.36, and results are shown in Fig. 3.37.

In this setup, the perpendicular probe was able to see the direct reflection of sun on the glossy I-beam surface. As described in Section 2, this is a phenomenon of specular (or mirrorlike) reflection. Fig. 3.38 shows the high specular reflection from I-beam surface for 0° measurement angle and 17.5° illumination angle. This resulted in very high reflectance values. Another interesting thing to see here is that the reflectance curves for multiple points of this same I-beam showed a lot of variation in a large range. This happens because some parts of the I-beam were very shiny, while other parts were less shiny due to heavy scratches. The less shiny parts exhibited much lower reflectance curves.

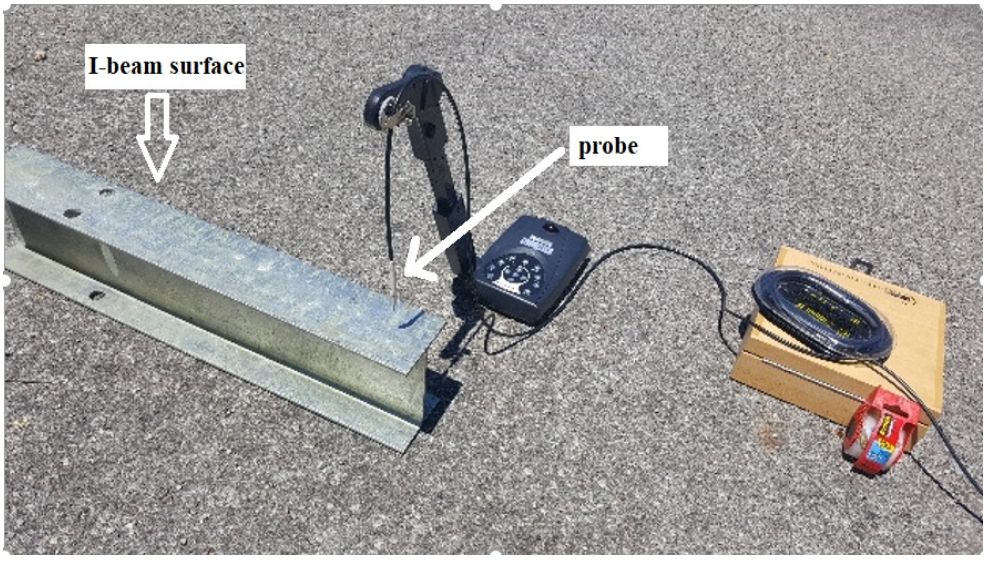

Fig. 3.36: I-beam kept in horizontal orientation. Measurement angle is 0°. Illumination angle is 17.5°-19.7°

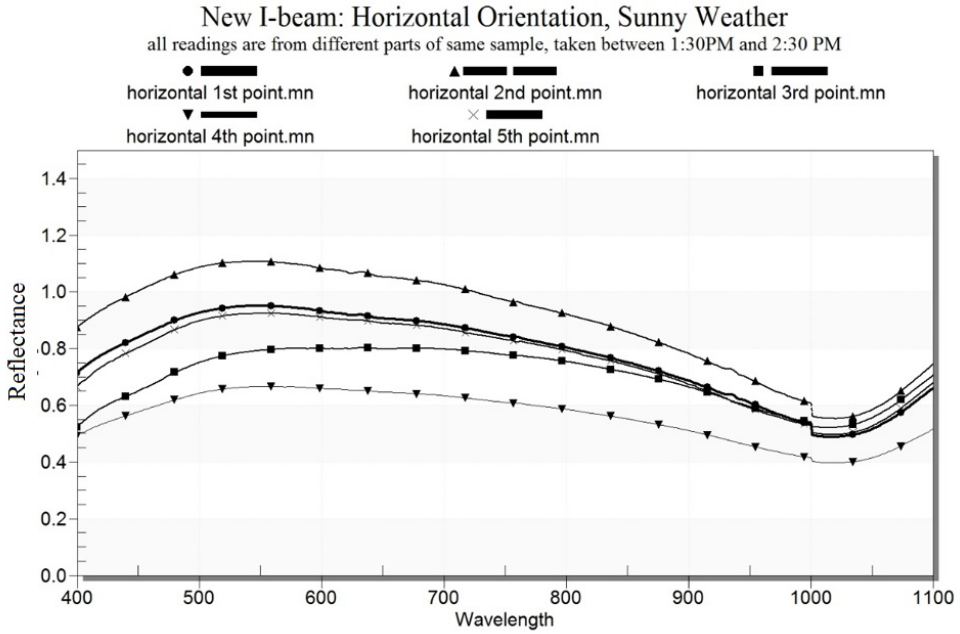

Fig. 3.37: Measurement from multiple parts of I-beam kept horizontally. 0° measurement angle, 17.5°-19.7° illumination angle, 0° phase angle

Fig. 3.38: Mirrorlike reflection of sun on I-beam surface (0° measurement angle and 17.5° illumination angle)

New I-beam – reflectance during absence of specular reflection: In this case, the I-beam was set-up in a vertical orientation (as on the roadside). The probe was kept perpendicular to the I-beam surface (i.e., parallel to ground) at 0° measurement angle. Illumination angle was 48.9°-64.7°, phase angle was 0°. In such a setup, from the probe's point of view, there was no specular (mirror-like) reflection of sun visible, as can be seen in Fig. 3.39. In this setup, measurements were taken from multiple parts of the I-beam. The results are shown in Fig. 3.40. In the absence of specular reflection, the reflectance curves have much lower values, and the values are very close for measurements from different parts of the I-beam.

This experiment allows room for some intuitive assumption. In LIDAR operation conditions (measurement angle same as illumination angle), LIDAR will not see specular reflection for I-beam surfaces for higher measurement angles (such as 40°-70°). Therefore, it is intuitive to assume that in these angles for LIDAR operation conditions, reflectance will be low. This will later be experimentally verified in Section 3.4.2.

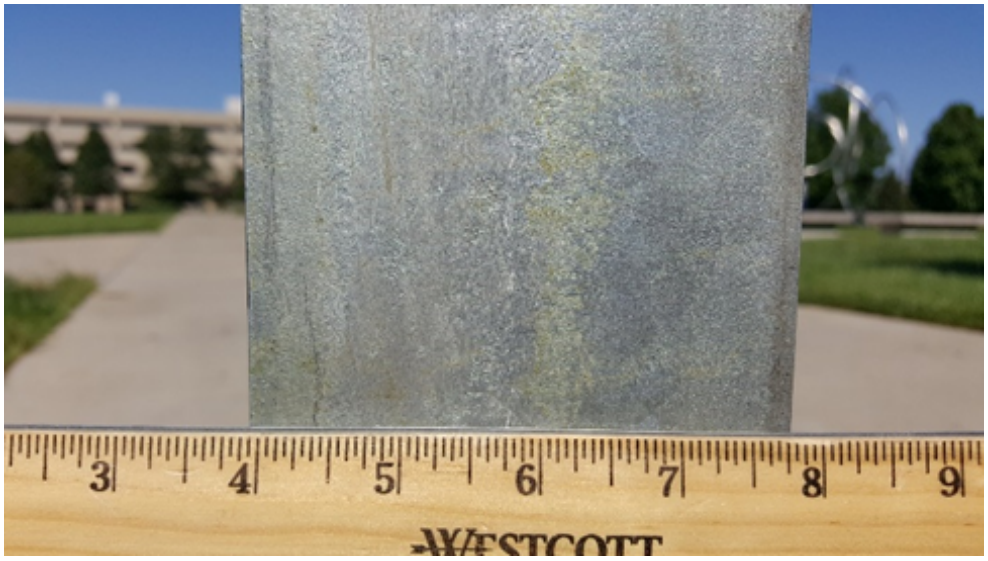

Fig. 3.39: Absence of high specular reflection from probe's point of view (0° measurement angle, 64.7° illumination angle)

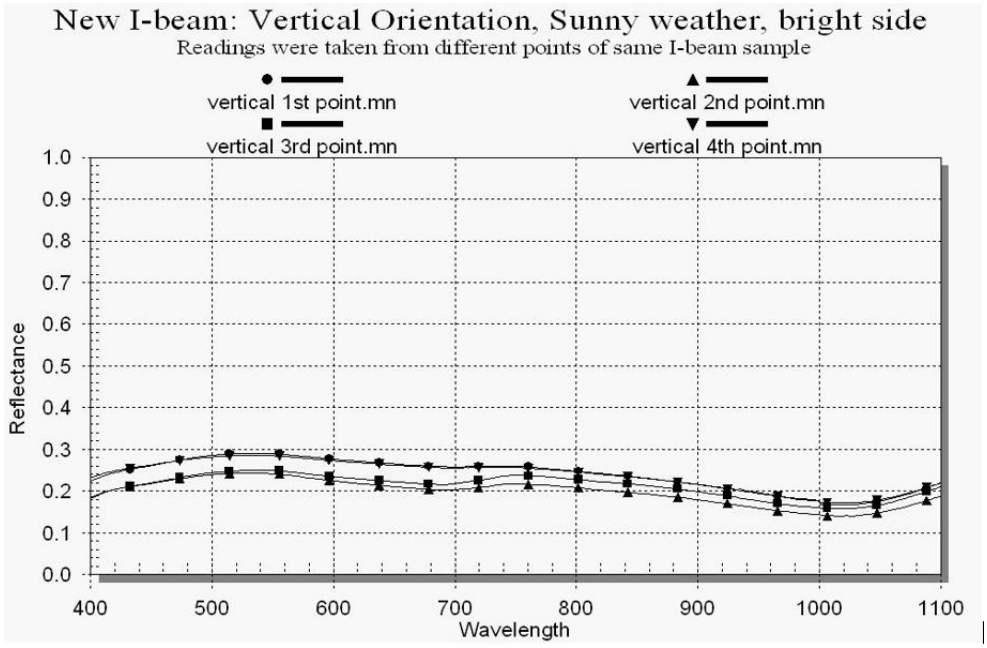

Fig. 3.40: Measurement from multiple parts of I-beam kept vertically. 0° measurement angle, 48.9°-64.7° illumination angle, 0° phase angle

I-beams of different age – reflectance in the absence of specular reflection: In this case, all I-beam samples of different age were kept in vertical orientation, and measurement was done with 0° measurement angle, 48°-70° illumination angle, and 0 phase angle. In such a setup, from the probe's point of view, there was no specular (mirror-like) reflection of sun visible. The results are shown in Fig. 3.41. It is apparent that in the absence of specular reflection, I-beams of different age shows nearly same reflectance.

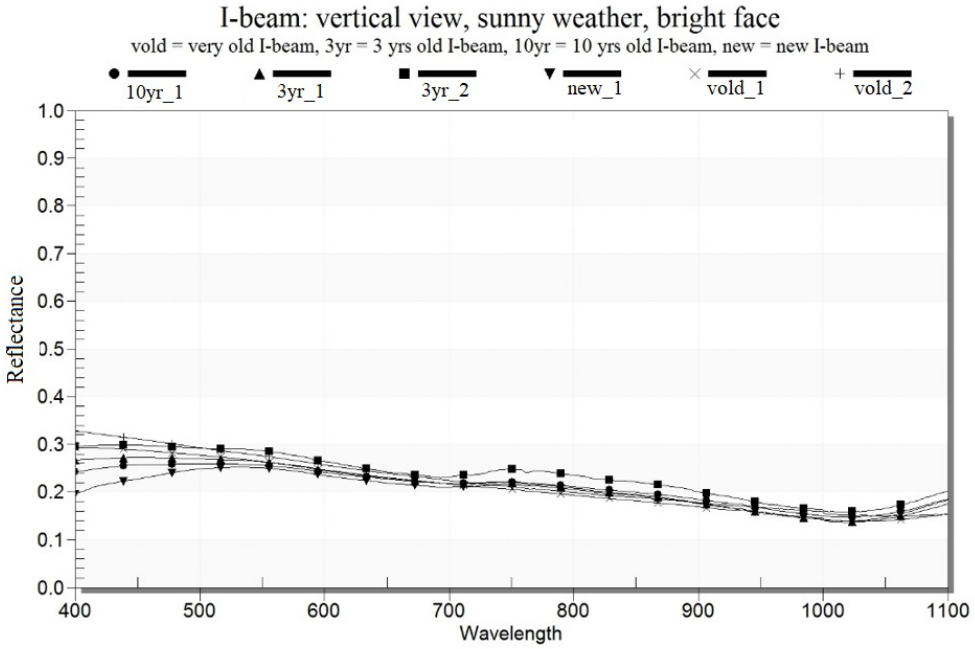

Fig. 3.41: Reflectance of I-beams of different age. 0° measurement angle, 48°-70° illumination angle, and 0° phase angle

This is an important observation, in the sense that for LIDAR operation conditions (measurement angle same as illumination angle) there will not be specular reflection for higher LIDAR view angles (such as 40°-70°), therefore it stands to reason that the age of I-beam will have very minimal effect on reflectance for these angles. As a

result, it will be enough to measure only the new I-beam sample in an indoor setup, since the old I-beams samples real roadside guardrails and were unmovable, and it would not be possible to measure them indoor anyway.

Remarks

The measurement of I-beam samples using approach 1 gives useful insights:

- Specular reflection has a big effect on the reflectance of I-beam.
- The age of I-beams will not affect reflectance in the absence of specular reflection.

However, the limitation of this approach is that the desired illumination angles for simulating LIDAR operation conditions (measurement angle and illumination angle should be same) could not be achieved. Indoor measurement with approach 2 takes care of this limitation.

3.4.2 I-beam Reflectance Measurement using Approach 2 (Indoor Measurement from Different Angles)

Indoor measurement setup made it possible to simulate LIDAR operation conditions. Measurement angle was varied from 0° to 70° (in 10° increments every time), and for each case, illumination angle was kept equal to the corresponding measurement angle. 20° phase angle was kept in order to ensure even illumination of the surface being measured. Fig. 3.42 shows the setup to measure the reflectance of I-beam indoors.

The only sample available for measuring indoors was the new I-beam purchased. Since various samples measured outdoors show very close result for non-specular case, measuring one sample indoors should be sufficient. The I-beam was placed vertically (perpendicular to ground) in front of the probe-light setup (which was facing the I-beam surface perpendicularly) and a measurement was taken. This gave

Fig. 3.42: I-beam - indoor measurement - 0° measurement angle (left) vs 70° measurement angle (right); illumination angle same as measurement angle, 20° phase angle

the reflectance for 0° measurement angle. After each reading, the light-probe setup was kept still, but the I-beam was inclined 10° each time, and measurement was performed. After repeating this process multiple times, the reflectance curves for 0°, 10°, 20°, 30°, 40°, 50°, 60°, and 70° measurement angles were obtained, and in every case, the illumination angle is equal to the corresponding measurement angle.

Measurement results

Angle varied from 0°-70°: The results are shown in Fig. 3.43. Here, the reflectance is highest (0.55-0.72) when both the measurement angle and the illumination angle are 0°. As the measurement and illumination angles increase, the reflectance decreases. This is expected behavior, because, at 0° angle, the light source and probe

are both facing the I-beam surface directly, and therefore the probe can see specular (mirror-like) reflection of the light source. As the angle increases, specular reflectance decreases significantly. Reflectance becomes very low at 70° measurement angle.

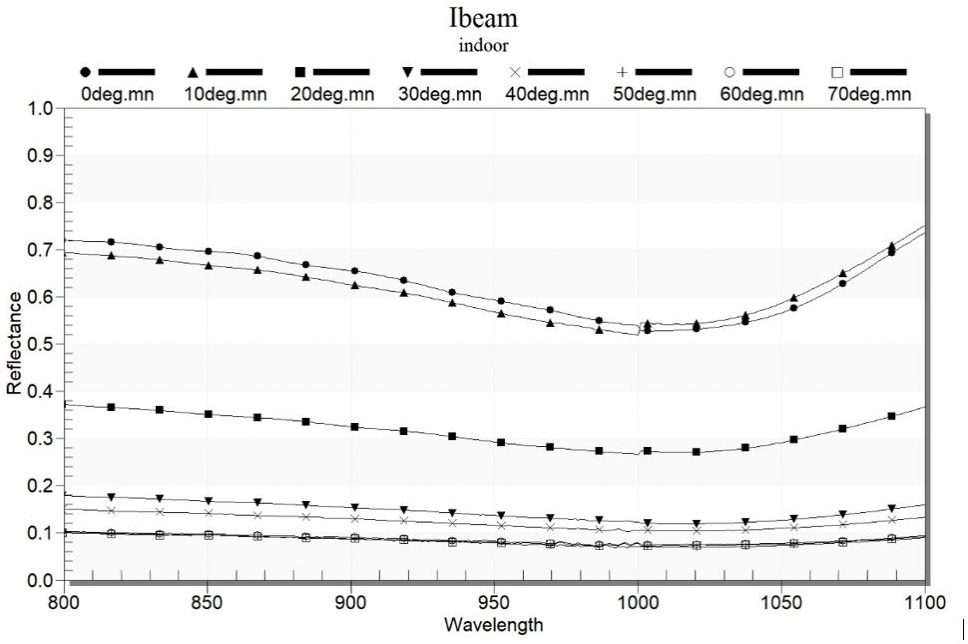

Fig. 3.43: New I-beam sample – indoor measurement from different measurement angles (for all cases, illumination angle = measurement angle); 20° phase angle

Multiple measurements for each measurement angle: For the measurements in Fig. 3.43, there is only one measurement for each angle. Previously, during outdoor measurement using approach 1 (Section 3.4.1), it was seen that when the probe can see mirror-like reflection of light source, reflectance varied significantly for multiple measurements. Therefore, reflectance varied between different measurements for the same angle. Since the I-beam does not look completely homogeneous, some part of it was shinier while other parts were less shiny. This creates drastic changes in the 0° or 10° measurement angle reflectance. Therefore, to specify a range, three measurements were taken for each angle. Fig. 3.44 shows three measurements done at 0 measurement angle. As expected, there is a large variation of reflectance for 0 measurement angle.

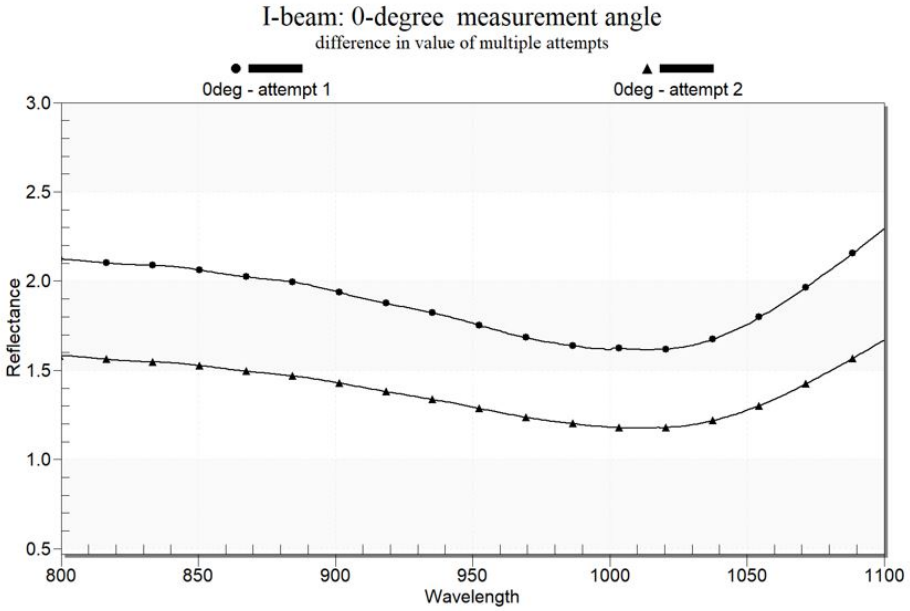

Fig. 3.44: I-beam measured indoor - multiple attempts to measure I-beam at 0° measurement angle and 0° illumination angle (20° phase angle)

Fig. 3.45 and 3.46 shows three measurements done in case of 10° and 20° measurement angles respectively. For 10°, the variation is still high. But the variation becomes much lower for 20° measurement angle.

Multiple measurements were also done for higher angles (30°-70°). But the variation for multiple measurements became very low for these angles. The plots for each angle will be shown in Section 3.4.4 below.

Remarks

Indoor measurement makes it possible to simulate LIDAR operation conditions, and therefore, it was possible to quantify the reflectance of I-beam at different LIDAR view angles by measuring one indoor sample at multiple points. Using the multiple indoor measurements of real I-beam for all angles, the suggested IR reflectance of surrogate metal guardrail skin will be specified in Section 3.4.4.

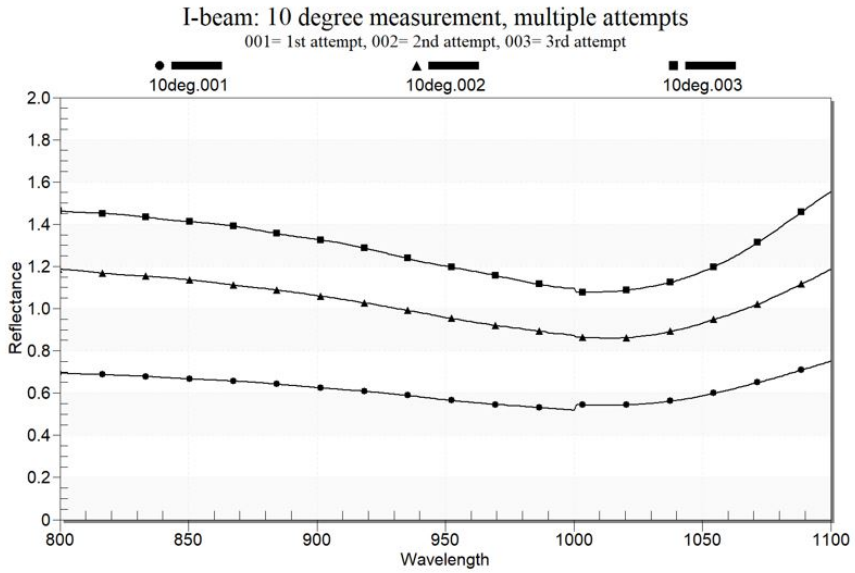

Fig. 3.45: I-beam measured indoor - multiple attempts to measure I-beam at 10° measurement angle and 10° illumination angle (20° phase angle)

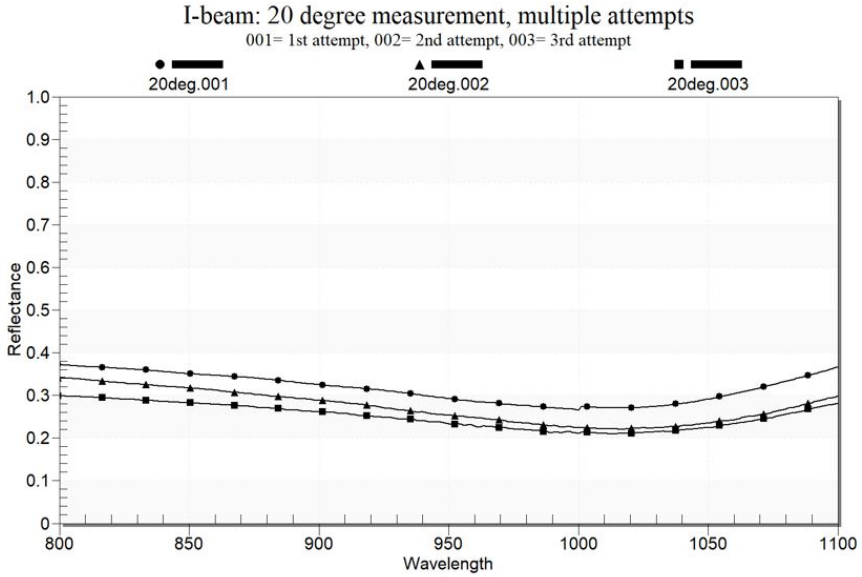

Fig. 3.46: I-beam measured indoor - multiple attempts to measure I-beam at 20° measurement angle and 20° illumination angle (20° phase angle)

3.4.3 Approach 3: Outdoor Measurement of I-beam to Verify the Accuracy and Consistency of Indoor Results

It is necessary to verify some results obtained from indoor measurement by comparing them with outdoor I-beam measurements in identical measurement and illumination angles. It is challenging to get the desired illumination angle outdoors, because certain sun angles may be unavailable due to geographic location and relative position of the place of experiment with respect to the sun. However, by tracking sun angle and time of day, it was possible to obtain a suitable time of day for outdoor setup when measurement angle = illumination angle = 30°. This result was compared to the result of I-beam in indoor setup with the exact same measurement angle and illumination angle. The comparison is shown in Fig. 3.47. It is apparent that both indoor and outdoor result of I-beam give very close values.

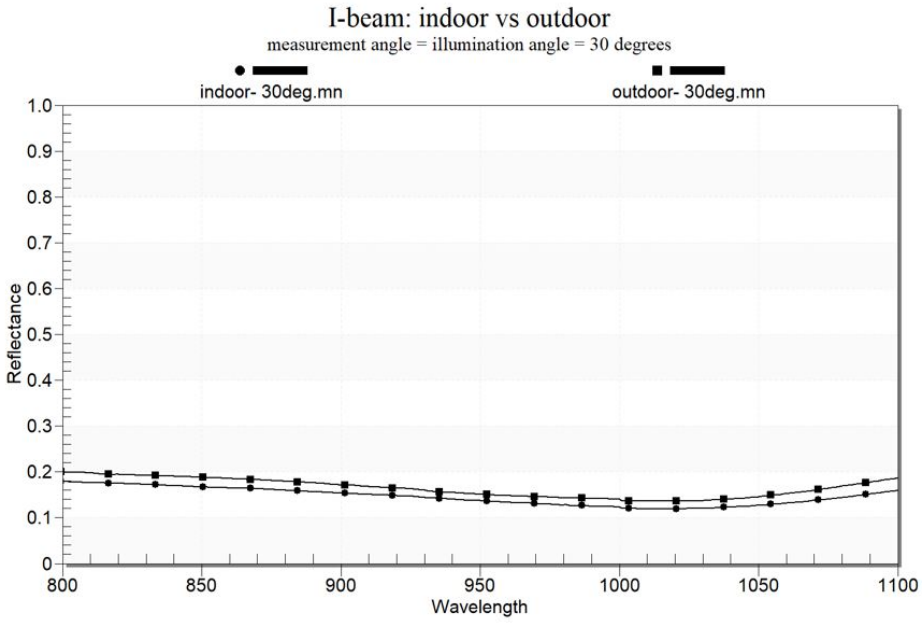

Fig. 3.47: I-beam, Indoor vs. outdoor measurement (30° measurement angle, 30° illumination angle, 20° phase angle)

3.4.4 Specification of Suggested IR Reflectance of Metal Guardrail Surrogate Skin for Different Angles

The indoor measurement of the I-beam sample described in Section 3.4.2 simulates LIDAR operation conditions.

To generate the suggested reflectance range of surrogate I-beam for a particular angle, three measurements from different parts of the I-beam sample are taken for that angle. In Fig. 3.48, for each angle, three measurements taken from different parts of the I-beam sample are grouped together.

From Fig. 3.48, it is easy to see that for each angle, reflectance of I-beam varies within some range. Then, for each angle, the reflectance data of all readings for the same angle are processed to find the lowest and highest reflectance value observed for each wavelength. After this step, two sets of data are obtained for each angle – one contains the minimum observed reflectance values for all wavelengths, and the other contains the maximum observed reflectance values for all wavelengths. These two sets of data give the range of observed metal guardrail reflectance for each angle.

Finally, a tolerance of ± 0.02 is given to the range of observed metal guardrail reflectance, because such a small variation of reflectance is very common within different I-beam samples and even within the same sample. Therefore, 0.02 is added to the set of maximum observed reflectance values, while 0.02 is subtracted from the set of minimum observed reflectance values. This gives the suggested upper and lower bounds for the IR reflectance of surrogate metal guardrail skin for each angle. Figs. 3.49 through 3.56 show the suggested IR reflectance of surrogate metal guardrail skin for 0°-70° angles.

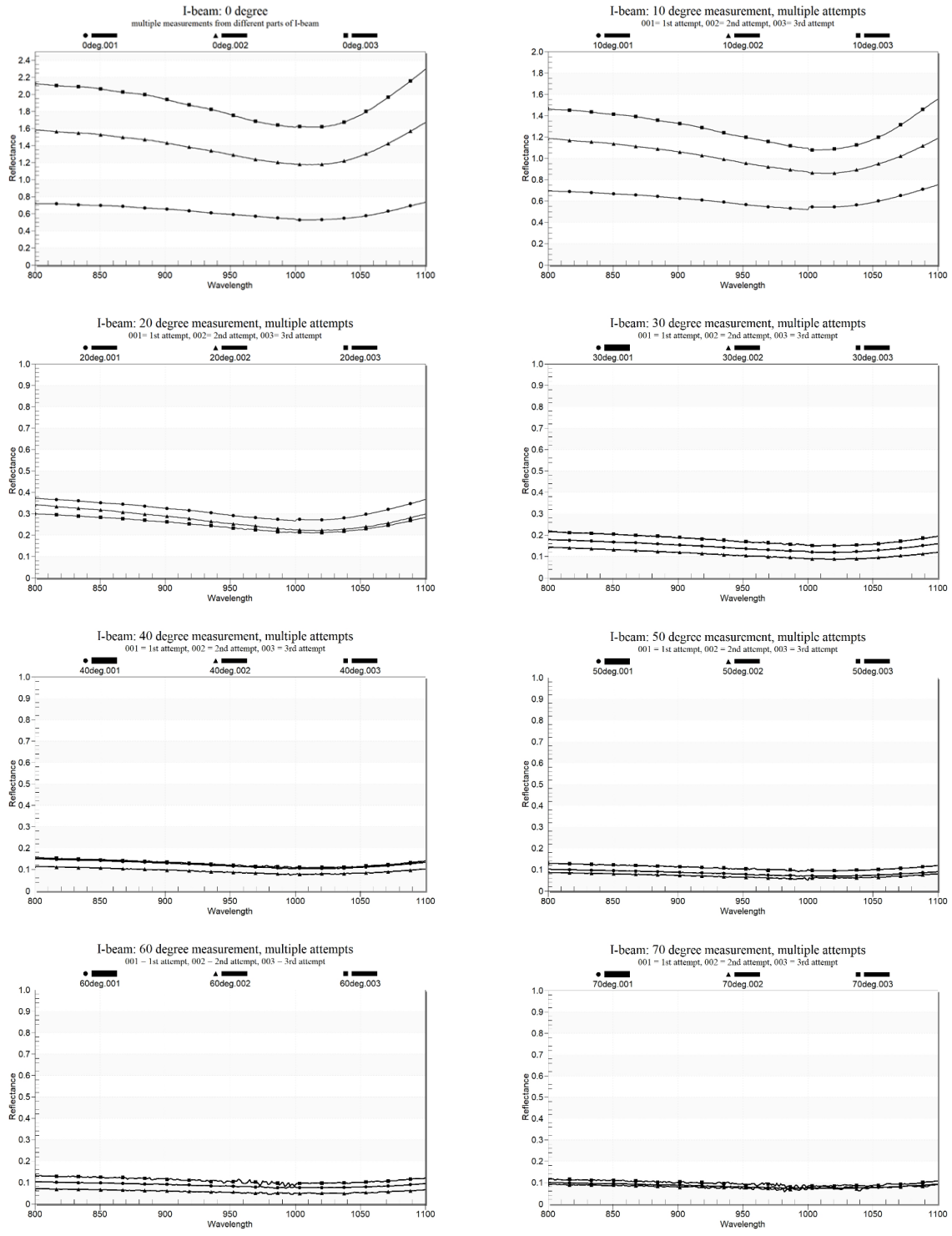

Fig. 3.48: Three reflectance measurements from different parts of the I-beam for each angle

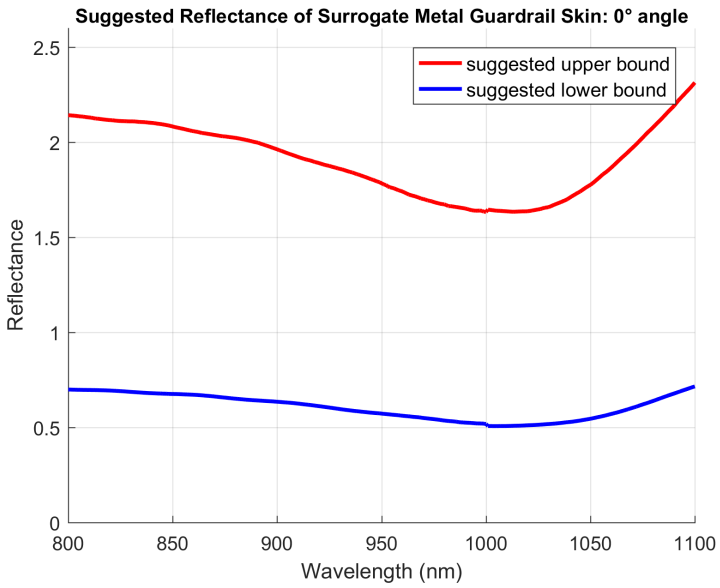

Fig. 3.49: Suggested IR reflectance range of surrogate concrete skin for 0° LIDAR view angle

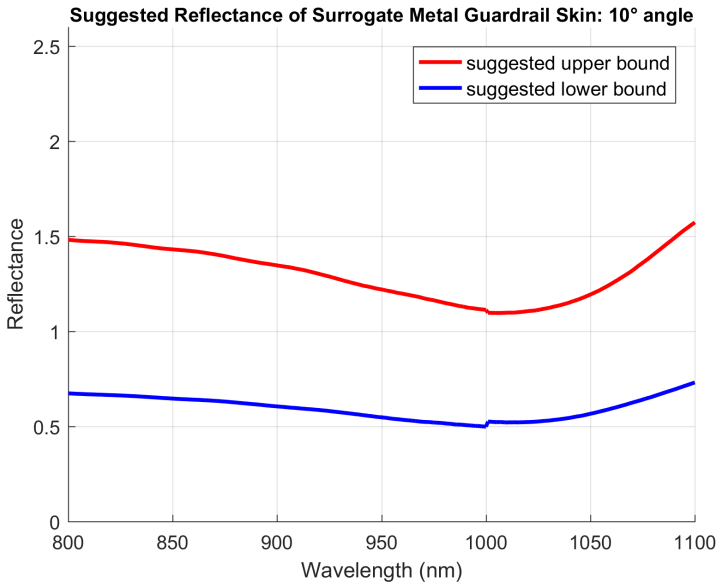

Fig. 3.50: Suggested IR reflectance range of surrogate concrete skin for 10° LIDAR view angle

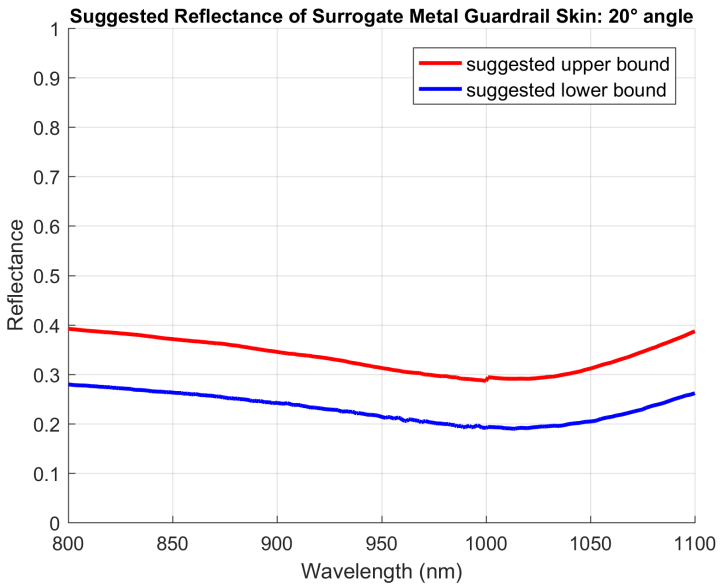

Fig. 3.51: Suggested IR reflectance range of surrogate concrete skin for 20° LIDAR view angle

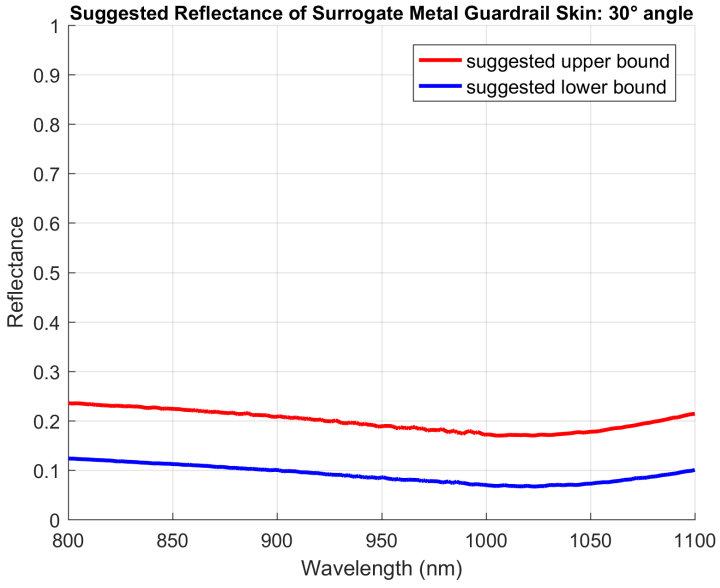

Fig. 3.52: Suggested IR reflectance range of surrogate concrete skin for 30° LIDAR view angle

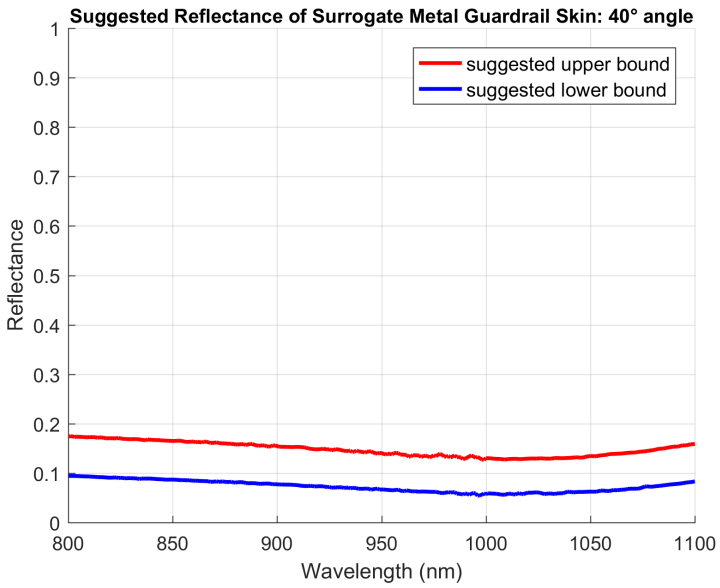

Fig. 3.53: Suggested IR reflectance range of surrogate concrete skin for 40° LIDAR view angle

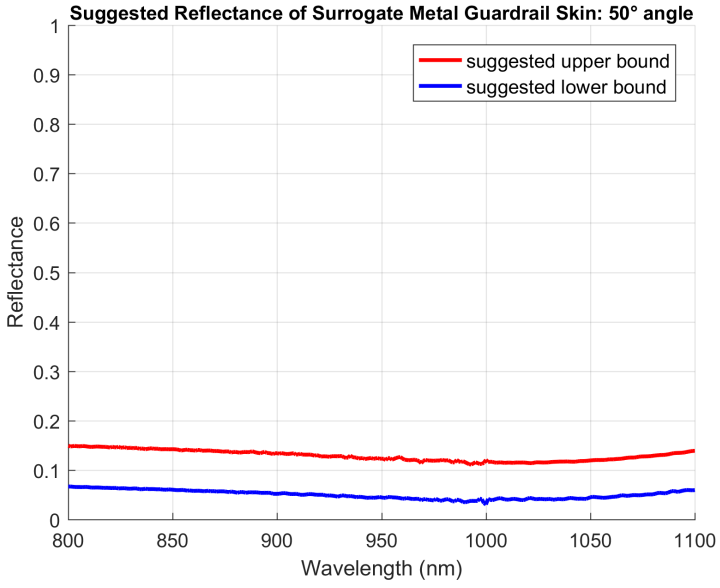

Fig. 3.54: Suggested IR reflectance range of surrogate concrete skin for 50° LIDAR view angle

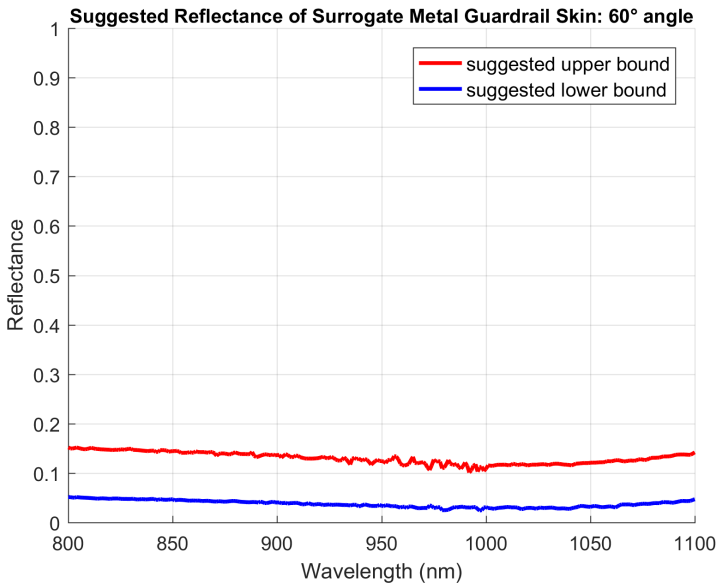

Fig. 3.55: Suggested IR reflectance range of surrogate concrete skin for 60° LIDAR view angle

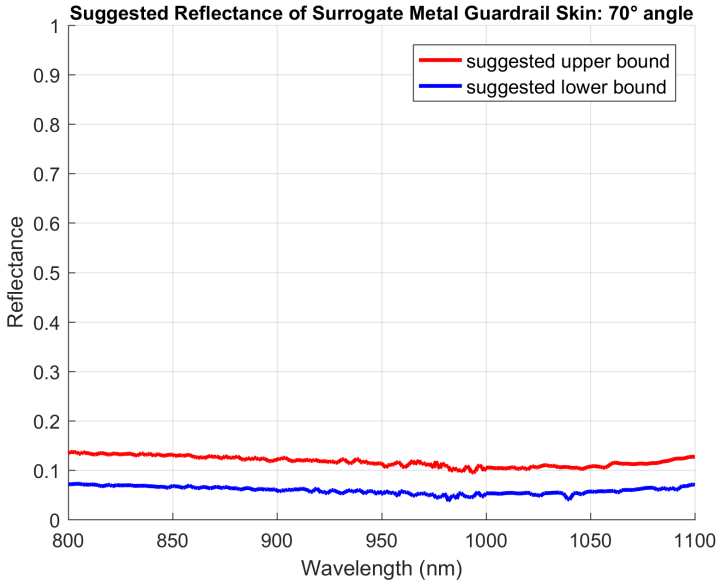

Fig. 3.56: Suggested IR reflectance range of surrogate concrete skin for 70° LIDAR view angle

3.5 Specification of Required Infrared Reflectance of Surrogate Grass

Grass is a tricky object for reflectance measurement, in the sense that there is great variation in both color and length, and also because grass blades lean towards random directions. In this section, the reflectance of multiple samples of grass is examined both outdoors and indoors. Outdoor measurements are done using approach 1 (0° measurement angle only) to compare the reflectance of grass of different color and different lengths. Then, samples of grass were measured using indoor setup by mimicking LIDAR operation conditions (measurement angle same as illumination angle) to specify the suggested IR reflectance of surrogate grass for different angles. Additionally, since dirt patches are very common among grass, a dirt sample was also measured to suggest reflectance bounds of dirt for different angles.

3.5.1 Grass Reflectance Measurement using Approach 1 (Outdoor Perpendicular Measurement)

In this subsection, reflectance is measured by testing multiple grass samples for 0° measurement angle. The illumination angle varied for different measurements at different times of days. Due to geographic location of the test site and its position relative to the sun, getting suitable sun angles is very time consuming, and some sun angles are not available at all. Therefore, these measurements cannot simulate LIDAR operation conditions for all angles. These measurements are done to observe the effect of length and color of grass.

To understand the effect of color and height of the grass to their IR reflectance, the grass color was classified into four categories: pure green, mixed color (green majority), mixed color (yellow majority), and pure yellow; the grass height was classified into three categories: short (2-5 inches), medium (6-10 inches), and long (longer than 10 inches). Following samples were tested (the short names of these samples are given inside parentheses):

- Pure green, short length: 4 samples (g_s1, g_s2, g_s3, g_s4).

- Pure green, medium length: 1 sample (g_m1).
- Pure green, long length: 3 samples (g_l1, g_l2, g_l3).
- Mixed color (green majority), short length: 1 sample (mixg_s1).
- Mixed color (green majority), medium length: 1 sample (mixg_m1).
- Mixed color (yellow majority), short length: 1 sample (mixy_s1).
- Mixed color (yellow majority), medium length: 1 sample (mixy_m1).
- Pure yellow, short length: 1 sample (y_s1).

Sample photos of each type of grass are given in Fig. 3.57 through 3.60.

Fig. 3.57: Pure green grass: short (left), medium (middle) and long (right)

Fig. 3.58: Mixed grass (green majority): short (left) and medium (right)

Fig. 3.59: Mixed grass (yellow majority): short (left) and medium (right)

Fig. 3.60: Pure yellow grass

Measurement Results

Pure green grass of different lengths: Different samples of pure green grass (short, medium and long) were tested by pointing the probe perpendicularly towards the grass surface (i.e. 0° measurement angle). The illumination angle was between 52°-60°. Reflectance may vary at different points of the same grass sample due to differences in grass orientation (grass blades lean towards random directions at different parts of same sample) and color texture. Therefore, in some cases, multiple readings were taken at different parts of same sample.

The reflectance curves of these readings are shown in Fig. 3.61. From the curves, it is easy to see that reflectance of pure green grass varies even for the same sample when measurement is done at different parts. However, the key thing to note here is that pure green grass samples of all lengths have reflectance that vary within the same range and have the same shape.

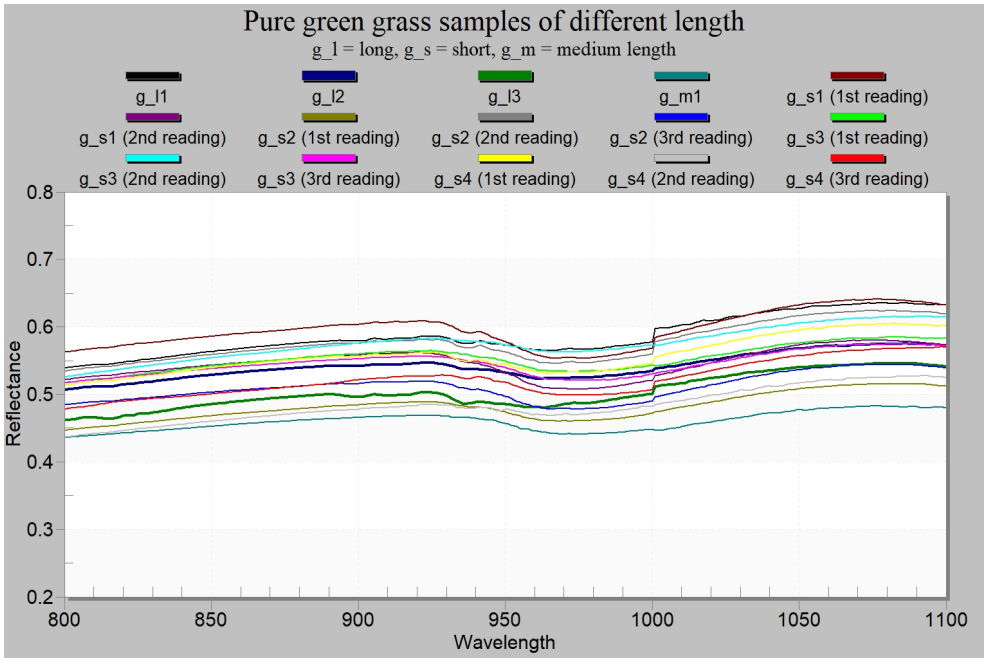

Fig. 3.61: Reflectance comparison of pure green grass samples of different lengths. 0° measurement angle, 52°-60° illumination angle, 10° phase angle

Mixed color grass of different lengths: In Fig. 3.62, reflectance of the four mixed colored grass samples are compared using approach-1 (0° measurement angle, 52-60° illumination angle). All four samples give similar reflectance in the 800-1100 nm wavelength region. Two samples were short and the other two samples were of medium length, but the length did not affect the reflectance. Therefore, we conclude that the length of the grass does not have effect on its IR reflectance.

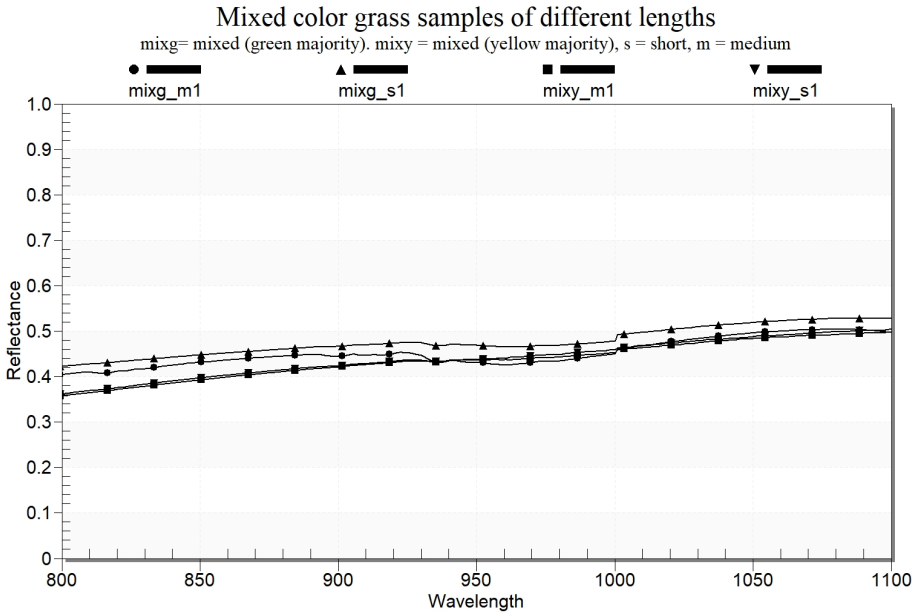

Fig. 3.62: Reflectance comparison of mixed color grass samples of different lengths. (0° measurement angle, 52°-60° illumination angle, 10° phase angle)

Comparison of grass of different colors: In Fig. 3.63, reflectance curves of grass of different colors are compared (each curve corresponds to one sample of each color; 0° measurement angle, 52°-60° illumination angle). In general, for the 800-1100 nm near infrared wavelength range, under similar measurement setups, green grass shows highest reflectance. Mixed color grass shows lower reflectance than green grass. Yellow grass has lowest reflectance. Therefore, infrared reflectance decreases

as grass gradually starts to die. This happens because internal cell structure of green vegetation results in high scattering of near infrared light, and these scattering decreases as cells die in yellow vegetation [20].

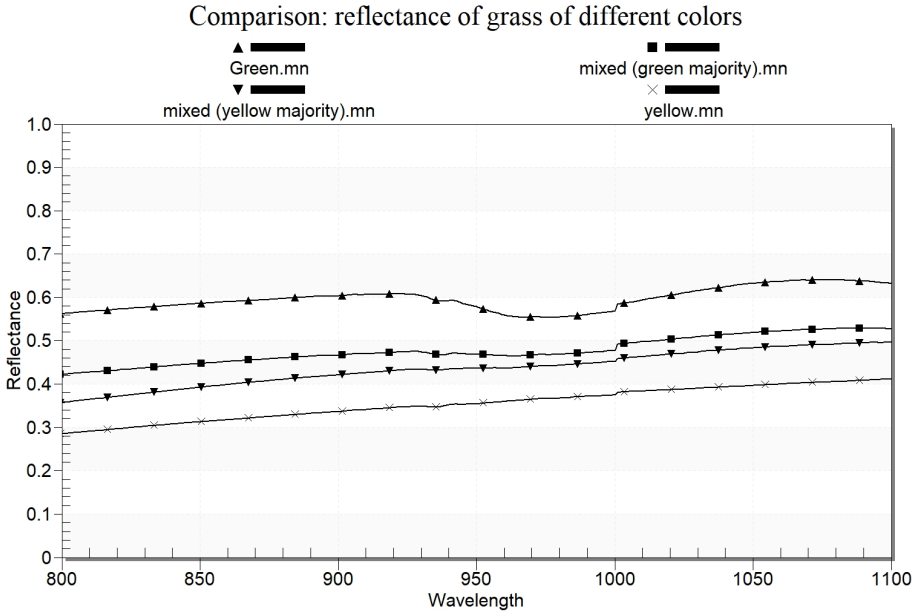

Fig. 3.63: Reflectance of grass of different colors (0° measurement angle, 52°-60° illumination angle, 10° phase angle)

Remarks

In this section, reflectance of grass with different color and length was measured from 0° measurement angle (i.e., perpendicular to grass surface). From these initial measurements, we gained some useful insights. For perpendicular measurement (0° measurement angle), as grass color turned from green to yellow, reflectance decreased. Moreover, the height does not influence IR reflectance if the color of the grass is the same.

The limitation of this measurement is that the desired same measurement angle and illumination angle for simulating LIDAR operation conditions could not be achieved, since it is difficult to follow the sunlight to achieve same measurement angle and illumination angle. For this reason, indoor measurement in approach 2 was adopted.

3.5.2 Grass Reflectance Measurement using Approach 2 (Indoor Measurement from Different Angles)

Indoor measurement setup made it possible to simulate LIDAR operation conditions-measurement angle was varied from 0° to 70° (in 10° increments every time), and for each case, illumination angle was kept equal to the corresponding measurement angle. 20° phase angle was kept in order to ensure even illumination of the surface being measured.

The following four samples of grass were measured using the indoor setup:

- **Indoor grass sod-1:** a grass sod grown indoors (green-yellow mixed color).
- **Indoor grass sod-2:** a grass sod grown indoors (green-yellow mixed color).
- **Outdoor green grass:** Green grass found in front of Taylor Courtyard at IUPUI (green color). Although this sample was found outdoors, it was measured using the same indoor setup after sunset.
- **Dead grass sod:** a grass sod with dead grass.

All four samples are shown in Fig. 3.64. The measurement setups for 0° measurement angle and 70° measurement angle are shown in Fig. 3.65.

Fig. 3.64: (from left to right) Indoor grass sod-1,indoor grass sod-2, outdoor green grass, and dead grass sod

Fig. 3.65: Measurement of grass sod in indoor setup: 0° measurement angle (left) and 70° measurement angle (right), illumination angle same as measurement angle. 20° phase angle

Measurement Results

Grass sod-1: Fig. 3.66 shows the measured reflectance of grass sod-1 at different measurement angles (illumination angle always equal to corresponding measurement angle, 20° phase angle). In general, grass reflectance increases as measurement angle increases.

Grass sod-2: The reflectance properties and values for grass sod -2 are similar to those of grass sod-1 (Fig. 3.67).

Outdoor green grass: To verify if the results obtained from the measurement of two grass sods are consistent, an outdoor sample of green grass was measured using the same indoor setup. Although the grass was found outdoors, it was measured after sunset to mimic indoor conditions. The reflectance was measured for 0-70° measurement angles (in 10° increments each time), and for each case, illumination angle was kept equal to measurement angle to mimic LIDAR operation conditions.

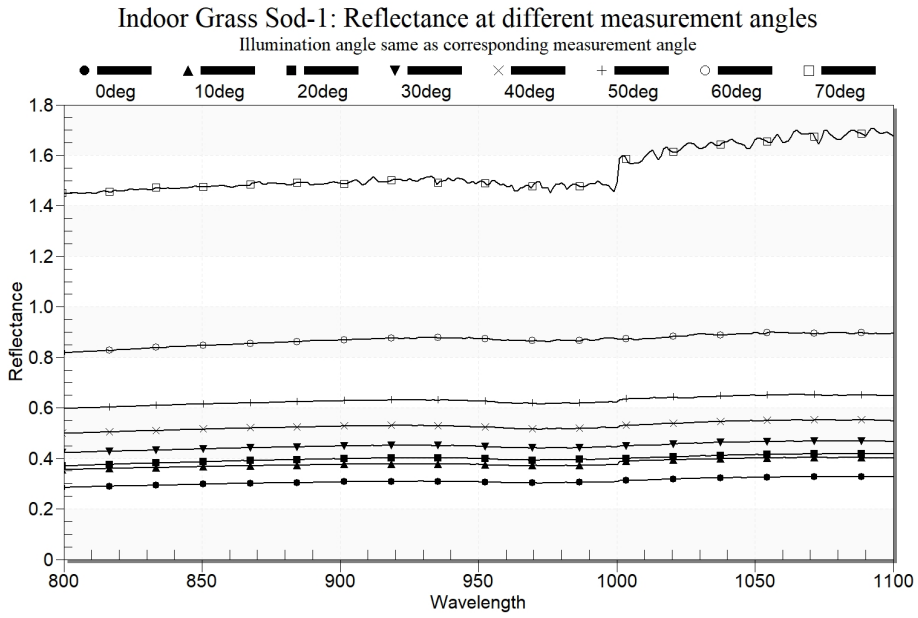

Fig. 3.66: Reflectance of grass sod-1 at different measurement angles, illumination angle same as measurement angle, 20° phase angle

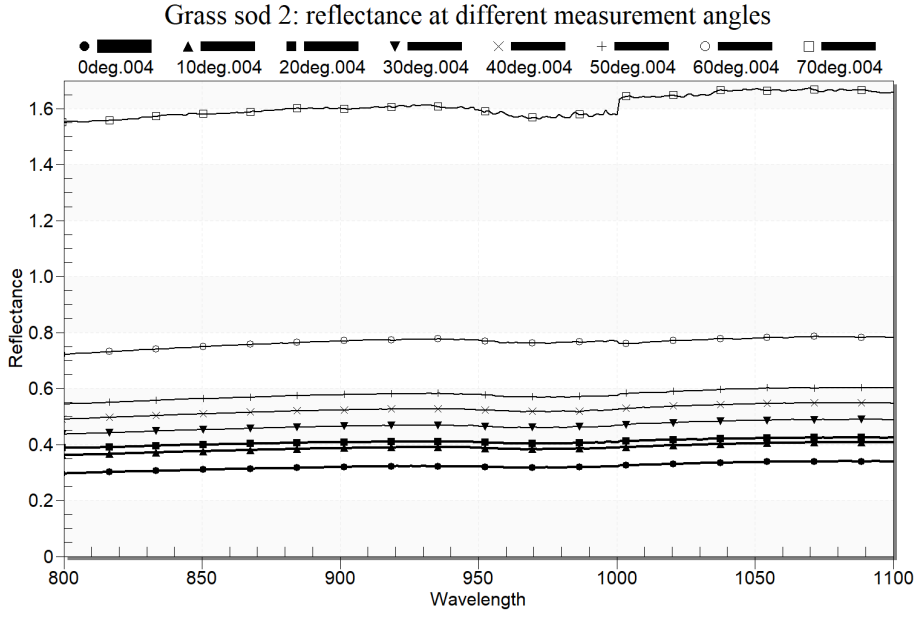

Fig. 3.67: Reflectance of grass sod-1 at different measurement angles, illumination angle same as measurement angle, 20° phase angle

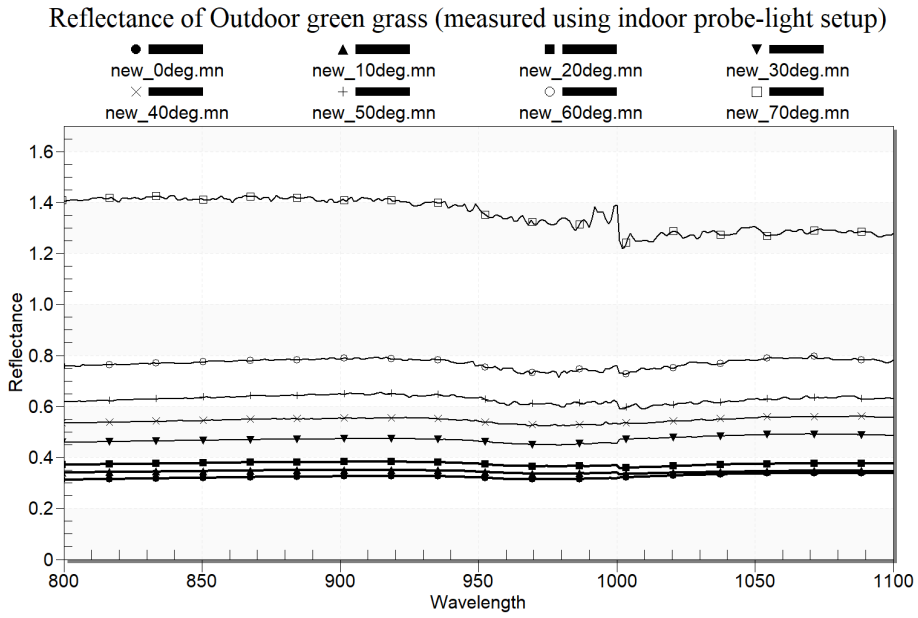

Fig. 3.68: Reflectance of outdoor green grass at different measurement angles, illumination angle same as measurement angle, 20° phase angle

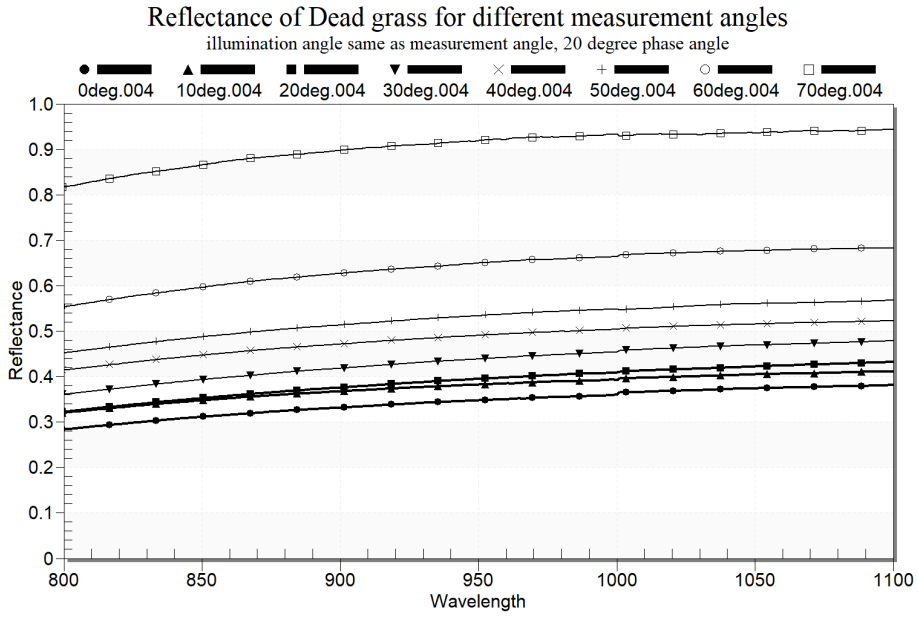

Fig. 3.69: Reflectance of dead grass sod at different measurement angles, illumination angle same as corresponding angle, 20° phase angle

Fig. 3.68 shows the reflectance of outdoor green grass measured using the indoor setup for 0-70° measurement angles. Here the same results are seen - grass reflectance increases as the measurement angle increases. The reflectance values are also very similar to the indoor grass sods 1 and 2.

Dead grass sod: Fig. 3.69 shows the reflectance of dead grass sod for 0-70° measurement angles (illumination angle same as corresponding measurement angle, 20° phase angle). For 0-30° angles, the reflectance of dead grass is very similar to the grass sods 1 and 2 (mixed color) and outdoor green grass we measured. For 40° and higher angles, the reflectance of dead grass is lower than the mixed color and green grass samples.

Remarks

Indoor measurement makes it possible to simulate LIDAR operation conditions, and therefore, it was possible to quantify the reflectance of grass at different LIDAR view angles by measuring four mixed color grass samples. It was seen that reflectance of grass increases as measurement angle increases.

Using the multiple indoor measurements of grass for all angles, the suggested IR reflectance for surrogate grass will be specified in Section 3.5.3.

3.5.3 Specification of Suggested IR Reflectance of Surrogate Grass for Different Angles

Measurement of four grass samples using the indoor setup described in Section 3.5.2 simulates LIDAR operation conditions. Due to variation in grass colors and random leaning directions of grass blades, grass reflectance for the same measurement angle can vary. To specify the suggested IR reflectance of surrogate grass for each angle, multiple measurements from different grass samples are necessary. Therefore, for each angle, 2-5 readings are taken from each grass sample (for each angle, about 11-15 measurements are taken in total from all grass samples). In Fig. 3.70, all measurements for the same angle are grouped together in the same figure.

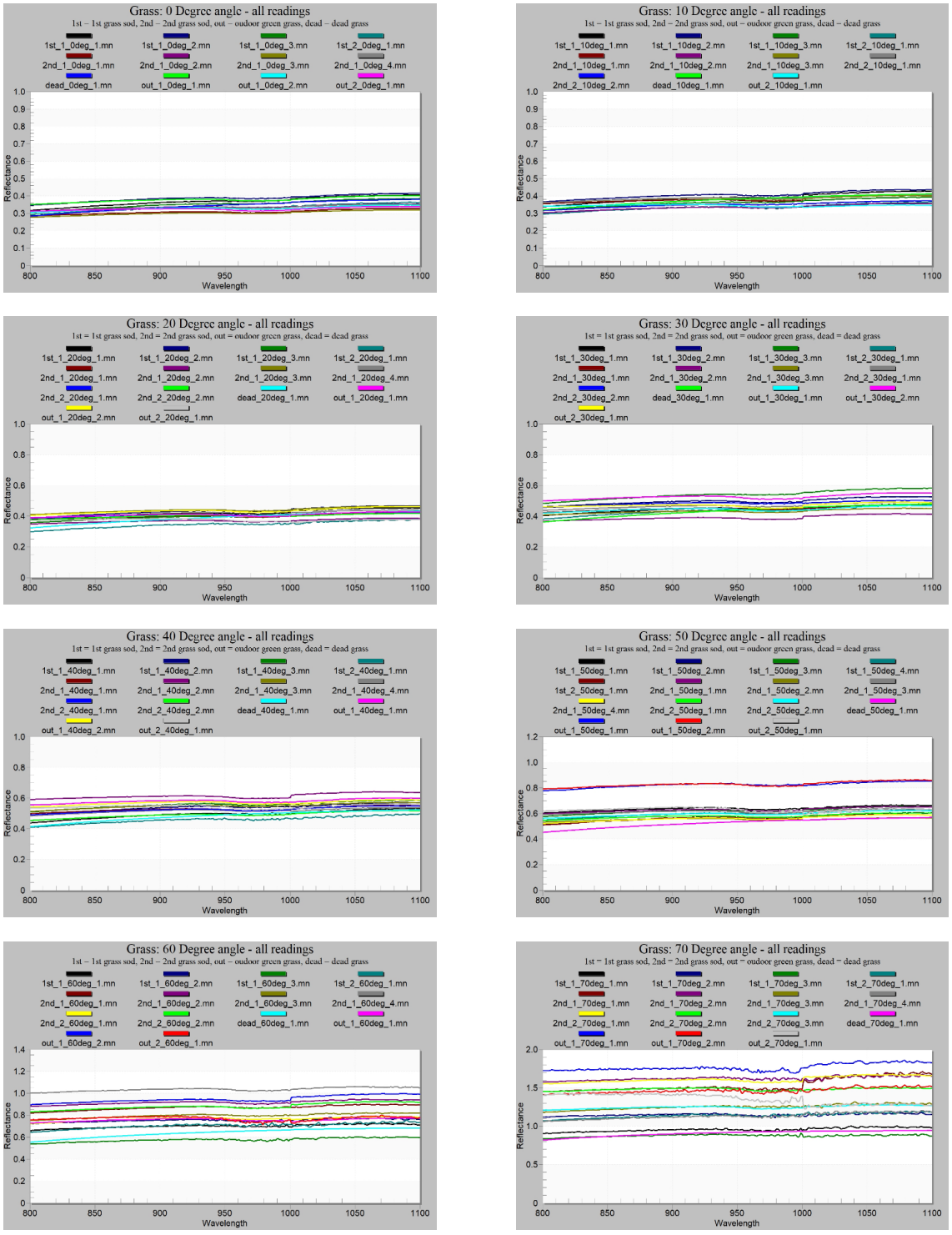

Fig. 3.70: All grass measurements for the same angle grouped together in the same figure

Fig. 3.70 shows that for each angle, reflectance of grass samples varies within some range. Then, for each angle, the reflectance data of all available samples are processed to find the lowest and highest reflectance value observed for each wavelength. After this step, two sets of data are obtained for each angle – one contains the minimum observed reflectance values for all wavelengths, and the other contains the maximum observed reflectance values for all wavelengths. These two sets of data give the range of observed grass reflectance for each angle.

Finally, a tolerance of ±0.05 is given to the range of observed grass reflectance, because such a small variation of reflectance is very common within different grass samples and even within the same sample. Therefore, 0.05 is added to the set of maximum observed reflectance values, while 0.05 is subtracted from the set of minimum observed reflectance values. This gives the suggested upper and lower bounds for the IR reflectance of surrogate grass for each angle. Figs. 3.71 through 3.78 show the suggested IR reflectance of surrogate grass for 0°-70° angles.

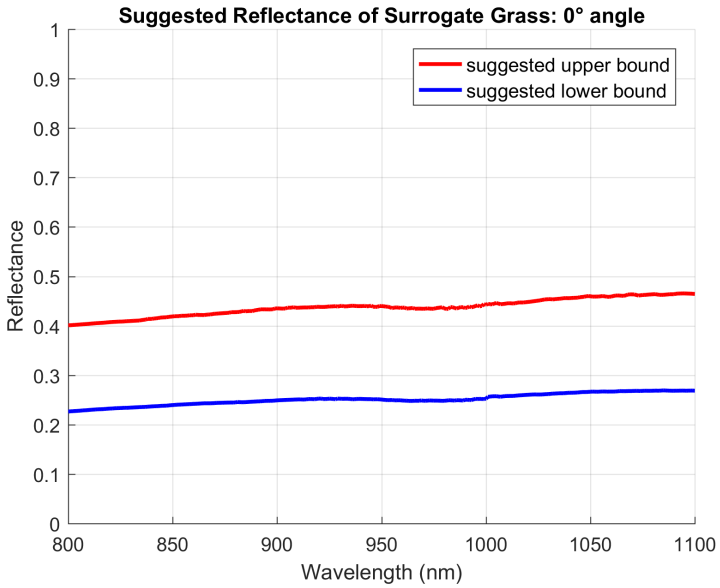

Fig. 3.71: Suggested infrared reflectance range of surrogate grass for 0° LIDAR view angle

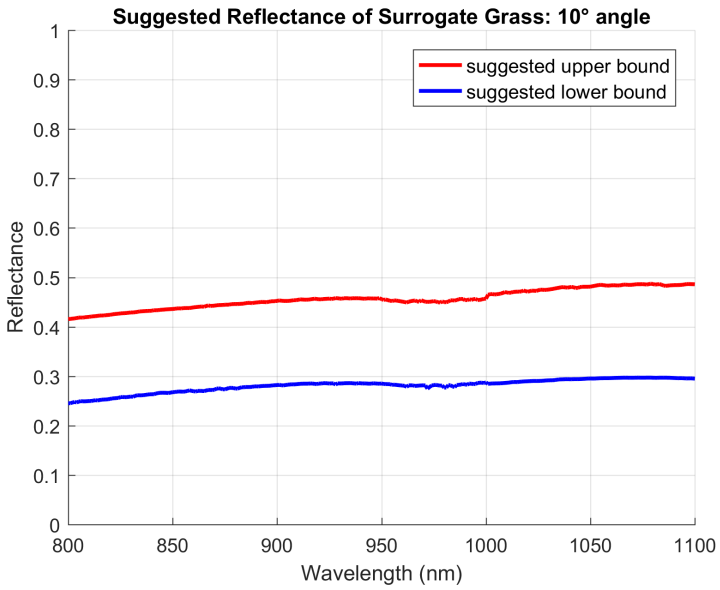

Fig. 3.72: Suggested infrared reflectance range of surrogate grass for 10° LIDAR view angle

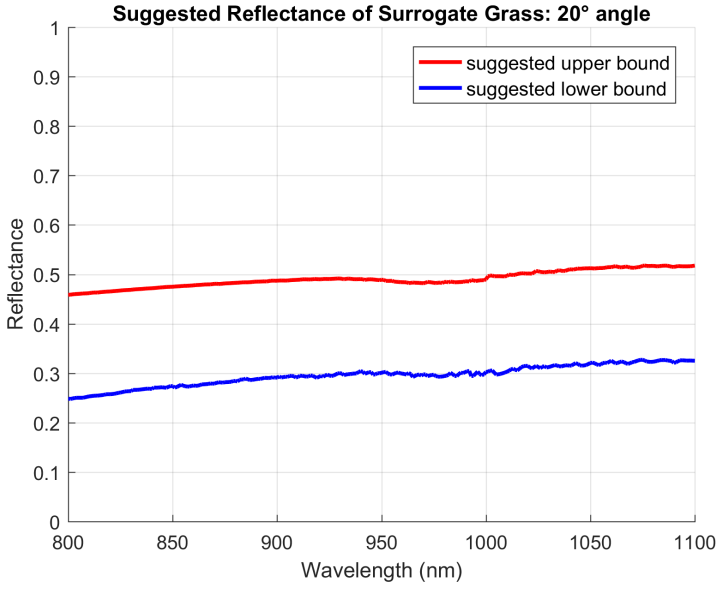

Fig. 3.73: Suggested infrared reflectance range of surrogate grass for 20° LIDAR view angle

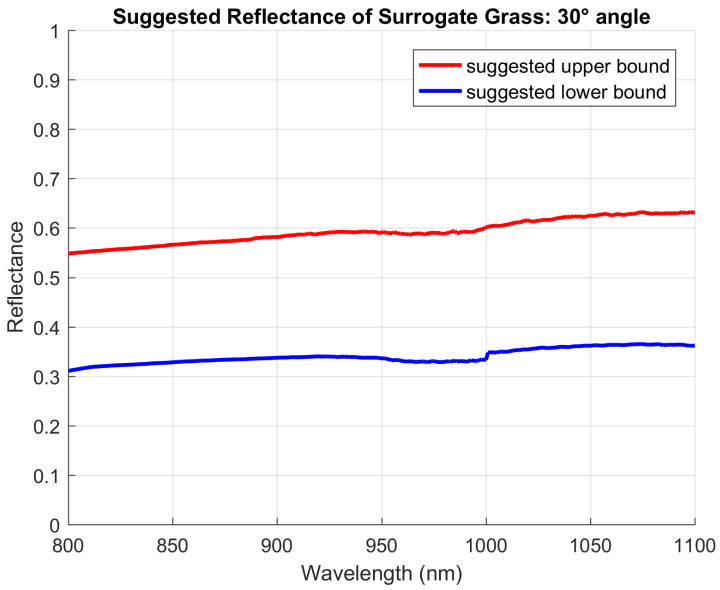

Fig. 3.74: Suggested infrared reflectance range of surrogate grass for 30° LIDAR view angle

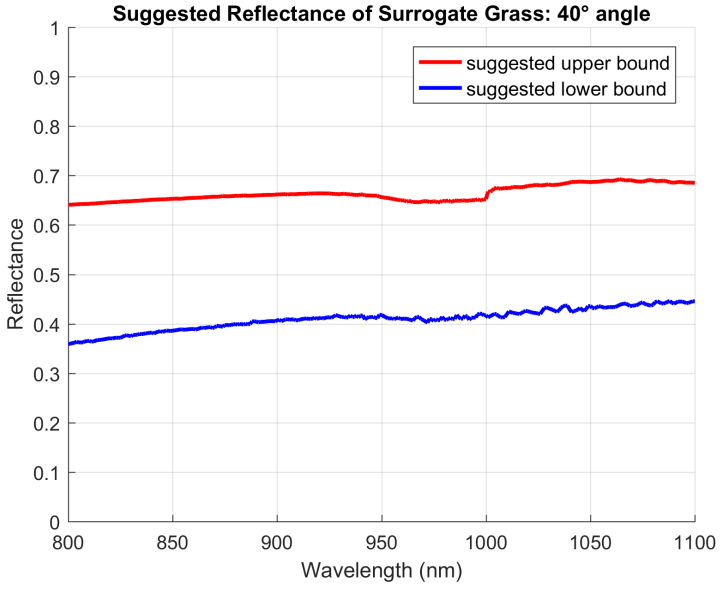

Fig. 3.75: Suggested infrared reflectance range of surrogate grass for 40° LIDAR view angle

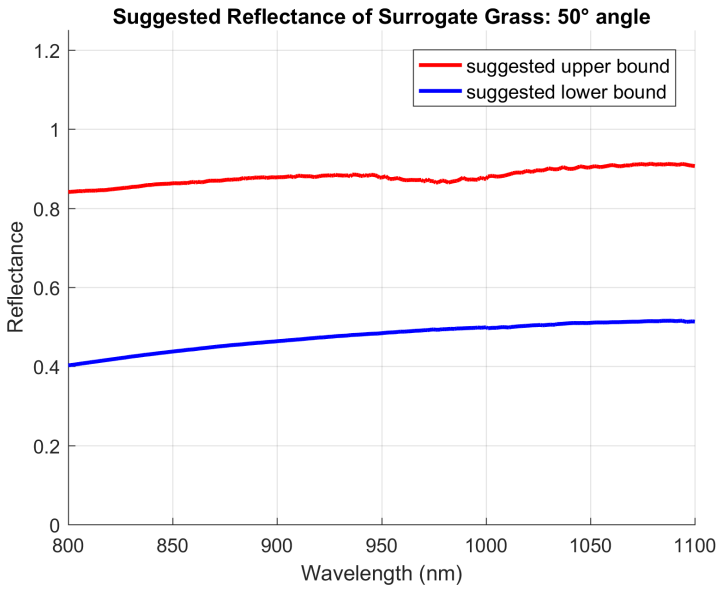

Fig. 3.76: Suggested infrared reflectance range of surrogate grass for 50° LIDAR view angle

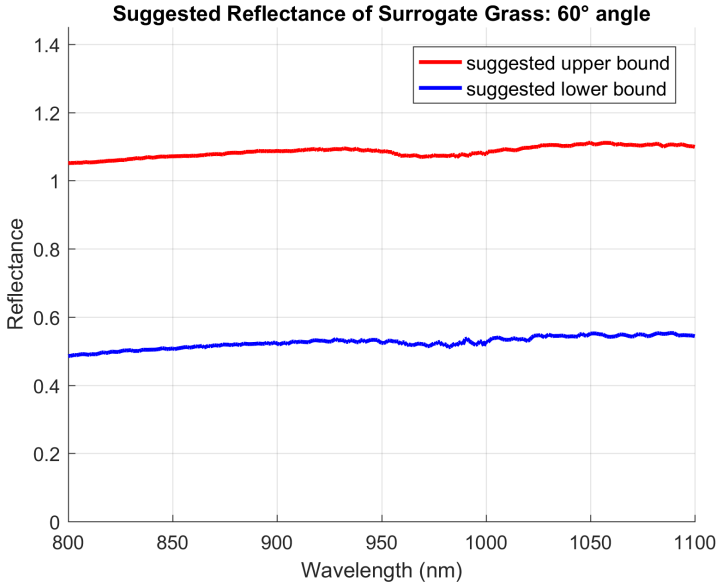

Fig. 3.77: Suggested infrared reflectance range of surrogate grass for 60° LIDAR view angle

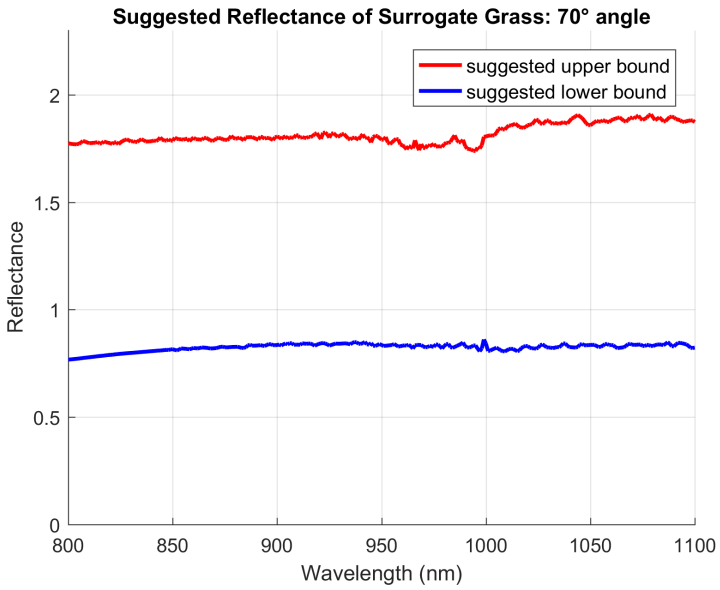

Fig. 3.78: Suggested infrared reflectance range of surrogate grass for 70° LIDAR view angle

3.5.4 Specification of Suggested IR Reflectance of Dirt for Different Angles

Patches of dirt are very commonly seen in grass. Therefore, to make surrogate grass with dirt patches, it is important to study the reflectance of dirt. In this section, the reflectance of one sample of dirt (shown in Fig. 3.79) is measured using indoor setup (approach-2) for different view angles. Based on this measurement, suggested reflectance of dirt is specified for 0-70° LIDAR view angles.

Measurement of dirt sample using approach 2 (indoor setup): The reflectance of dirt sample was measured in indoor conditions where it was possible to simulate LIDAR operation conditions – measurement angle was increased from 0° to 70° in 10° increments, and illumination angle was always kept equal to the corresponding measurement angle. A 20° phase angle was kept for ensuring even illumination of surface. Fig. 3.80 shows the reflectance of dirt for different measurement angles. It can be seen that dirt reflectance increases as measurement angle increases.

Fig. 3.79: Dirt sample

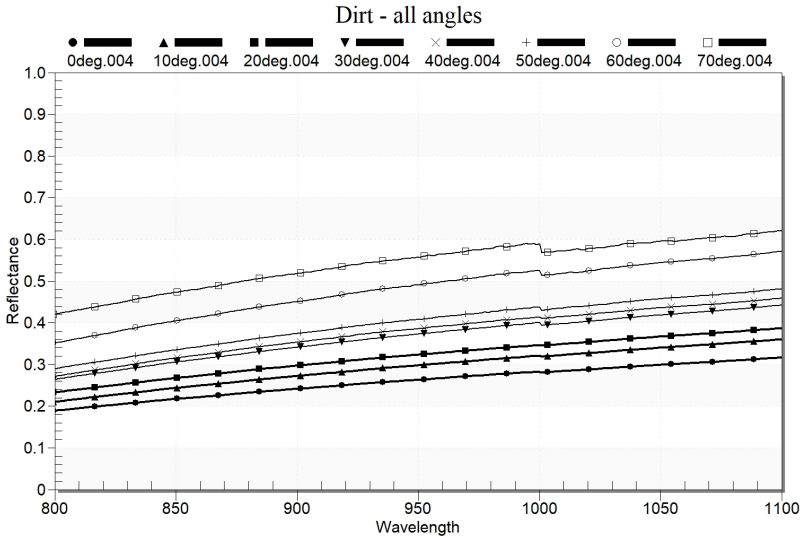

Fig. 3.80: Reflectance of dirt sample at different measurement angles, illumination angle same as corresponding measurement angle, 20° phase angle

Suggested IR reflectance of dirt for different angles: The upper and lower bounds of suggested infrared reflectance of dirt for a particular angle is achieved by giving a ±0.05 tolerance to the observed reflectance of the dirt sample at that angle. Therefore, for any particular angle, adding 0.05 to the observed dirt reflectance gives the upper bound, and subtracting 0.05 from the observed dirt reflectance gives the lower bound. Fig. 3.81 through Fig. 3.88 show the suggested IR reflectance of surrogate dirt for 0°-70° angles.

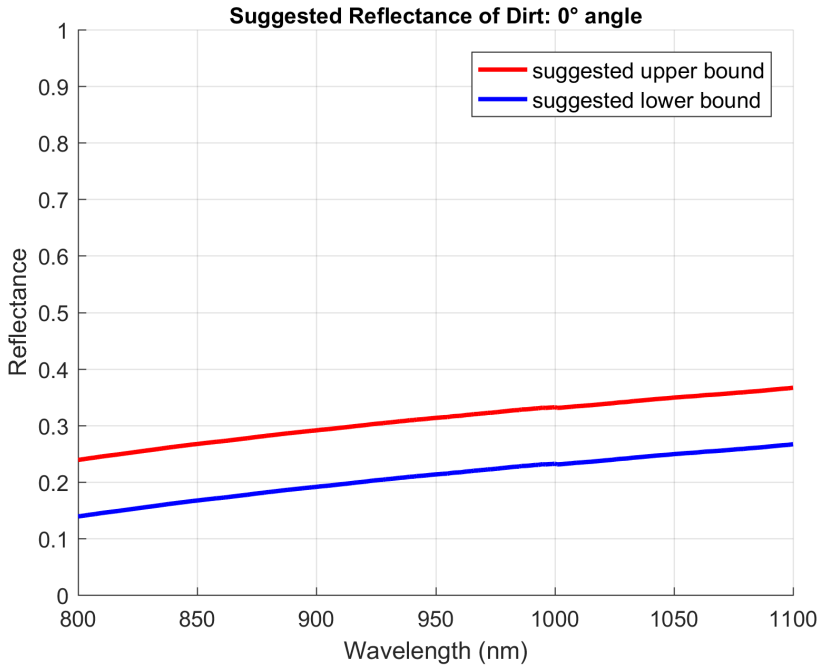

Fig. 3.81: Suggested infrared reflectance range of surrogate dirt for 0° LIDAR view angle

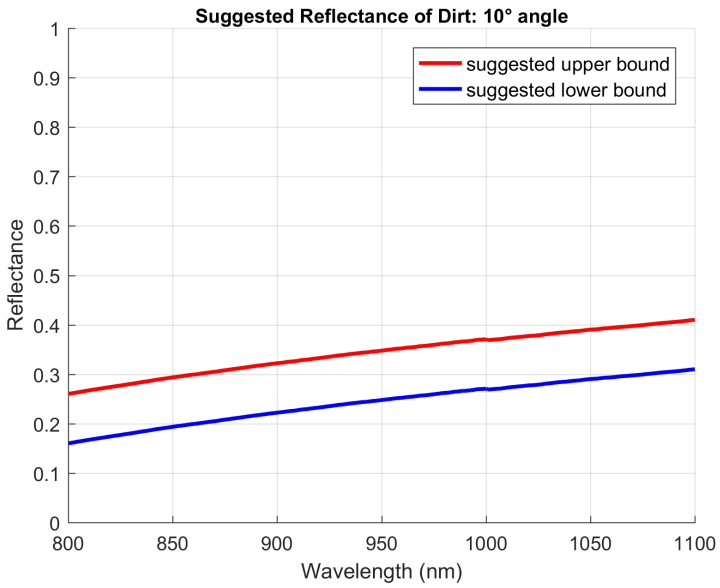

Fig. 3.82: Suggested infrared reflectance range of surrogate dirt for 10° LIDAR view angle

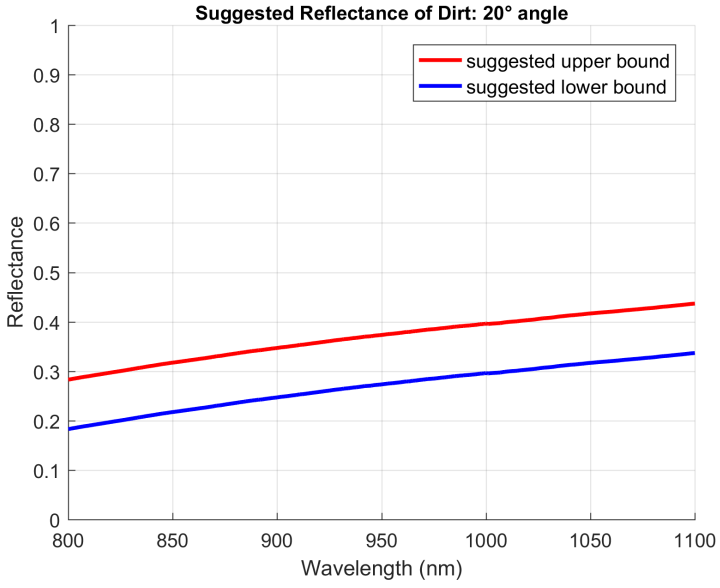

Fig. 3.83: Suggested infrared reflectance range of surrogate dirt for 20° LIDAR view angle

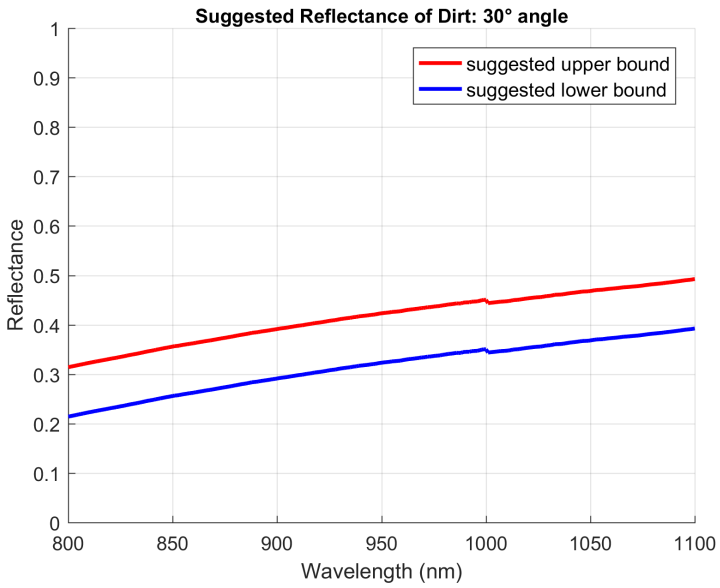

Fig. 3.84: Suggested infrared reflectance range of surrogate dirt for 30° LIDAR view angle

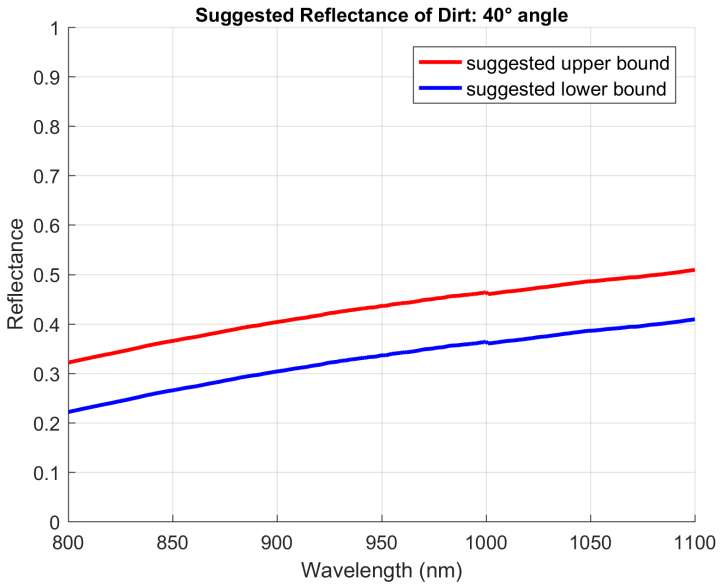

Fig. 3.85: Suggested infrared reflectance range of surrogate dirt for 40° LIDAR view angle

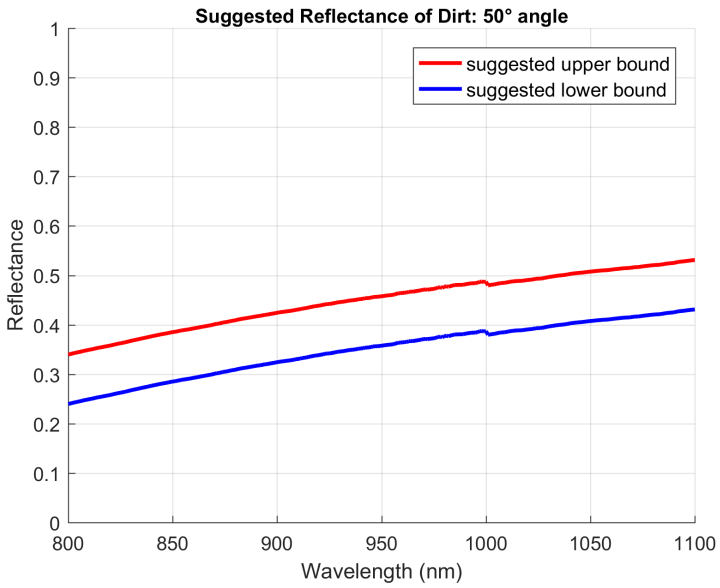

Fig. 3.86: Suggested infrared reflectance range of surrogate dirt for 50° LIDAR view angle

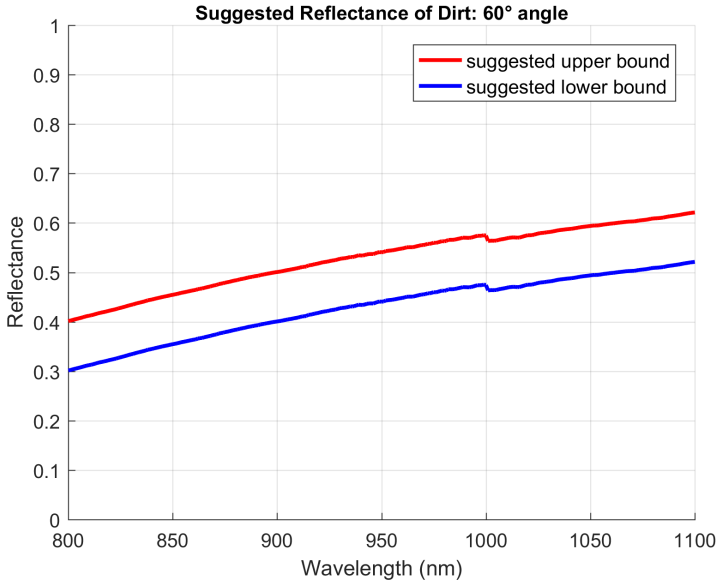

Fig. 3.87: Suggested infrared reflectance range of surrogate dirt for 60° LIDAR view angle

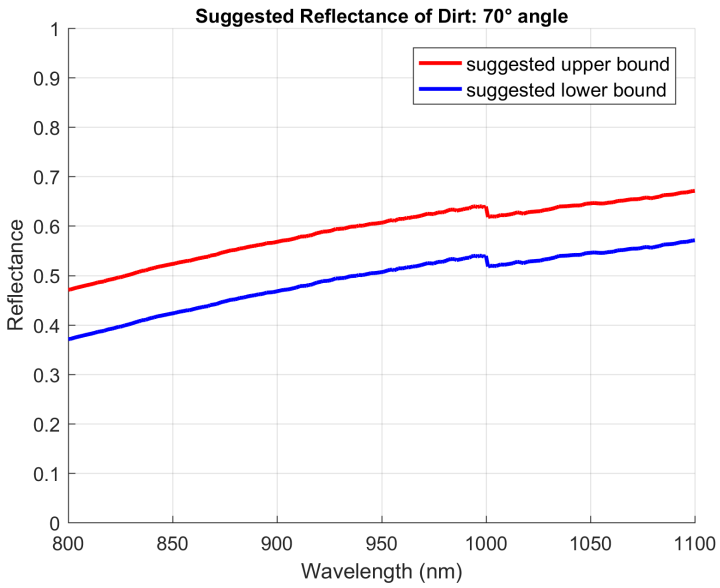

Fig. 3.88: Suggested infrared reflectance range of surrogate dirt for 70° LIDAR view angle

3.6 Summary

In this section, the approaches for measuring the reflectance of concrete, metal guardrail and grass were described. Using the indoor approach, LIDAR operation conditions can be mimicked by keeping illumination angle equal to measurement angle. Using this approach, the reflectance of real samples of concrete, metal guardrail and grass were measured from different measurement angles. Based on these measurements, the suggested IR reflectance of surrogate concrete, metal guardrail and grass for different LIDAR view angles were specified in Sections 3.3, 3.4 and 3.5 respectively.

4. MAKING SURROGATE OBJECTS WITH DESIRED INFRARED REFLECTANCE

In this section, the design of surrogate concrete skin, surrogate metal guardrail skin and surrogate grass is given. The infrared reflectance of the surrogate objects from different LIDAR view angles are compared to the reflectance requirements specified in Section 3.

The rest of the section is organized as follows. Section 4.1 gives brief description regarding surrogate objects. Sections 4.2, 4.3 and 4.4 give the description of surrogate concrete, metal guardrail and grass with satisfactory infrared reflectance for different LIDAR view angles.

4.1 Surrogate Objects

To create realistic testing conditions for evaluating the performance of road departure warning systems of cars, the test track should represent realistic driving conditions. Therefore, commonly seen roadside objects, such as concrete curbs and dividers, metal guardrails and grass should be present in the testing environment. However, using real roadside objects create several challenges. First, hard objects such as dividers and guardrails can cause severe damage to cars and human testers if the car crashes into them at high speed. Besides, such crashes will damage both the car and the roadside object itself and replacing them will be very expensive and time consuming. Additionally, real roadside objects such as grass have so much variation in terms of physical appearance and can change in appearance depending on weather and climate. Therefore, to create a standardized testing environment, roadside objects in all test tracks should have identical appearance regardless of weather conditions.

Using surrogate roadside objects provides an elegant solution to these challenges. Surrogate roadside objects should look like real roadside objects from the point of view of different sensors (camera, radar and LIDAR), and be soft, durable and reusable so that (1) they can be crashed during testing without causing non-cosmetic damage to the car being tested, the test environment or the surrogate objects themselves, (2) they can be reused even after multiple crashes.

Some basic properties of surrogate objects are given below:

1. They match the shape of the real object they are representing.
2. They match the color of the real object they represent (mainly to trick camera sensors into thinking that it is seeing the real object).
3. It looks like real object from different angles to all automotive sensors.
4. They are lightweight, soft and sturdy, so that they can be crashed without damage, and can be set up quickly after crash.

To satisfy the requirements, following approach for surrogate object design is used. For concrete dividers, concrete curbs and metal guardrails (I-beam and W-beam), the shape of the surrogate object is made using a foam frame. To satisfy the color, radar and IR requirements, the foam frame is covered by a surrogate skin.

The skin is multi-layered the radar requirements are fulfilled by controlling the contents and thickness of all layers of the skin. The LIDAR infrared requirements are fulfilled by controlling the composition of all the visible portions of the skin.

For surrogate grass, artificial turf is used as the base, and skin is created with desired paint mixtures to satisfy the camera and IR requirements.

4.2 Surrogate Concrete Skin with Desired Infrared Reflectance

As discussed in Section 4.1, the shape of the surrogate concrete divider and surrogate concrete curb is given using a foam frame. The multi-layered skin covering this frame will need to satisfy the infrared reflectance requirements specified in Section 3.3.

The skin has a base material, and the base material has coating(s) on the outermost visible side to satisfy the LIDAR requirements. To find the suitable base material, experimentation was done with clothes and polycarbonate sheets of different thickness and composition. In case of coating of outermost layer, experiment was done with paints of different colors and textures.

4.2.1 Finalized Design of the Concrete Surrogate Skin

The skin design was an iterative process which took a lot of time and required multiple redesigns. The final design uses acrylic based paint with desired color mixed with powdered cement in a suitable ratio to create a paint-cement mix. This mix was applied on the polycarbonate film to prepare the surrogate concrete skin with desired IR reflectance properties. Fig. 4.1 shows a specimen of surrogate concrete divider. The structure of the surrogate divider is made of foam, and the foam structure is covered by the prepared surrogate skin.

Fig. 4.1: Surrogate concrete divider (frame is covered by surrogate concrete skin)

4.2.2 IR Reflectance Performance of the Concrete Surrogate Skin

The reflectance for this surrogate skin was measured in indoor conditions where it was possible to simulate LIDAR operation conditions measurement angle was increased from 0° to 70° in 10° increments, and illumination angle was always kept equal to the corresponding measurement angle. A 20° phase angle was kept for ensuring even illumination of surface.

The reflectance performance of the surrogate skin at different angles is compared with the suggested IR reflectance for surrogate concrete skin (which was specified in Section 3.3), and the comparison curves are shown in Fig. 4.2 through Fig. 4.9. From the figures, it can be seen that the surrogate skin performs very well and stays within the specified suggested range for all measurement angles.

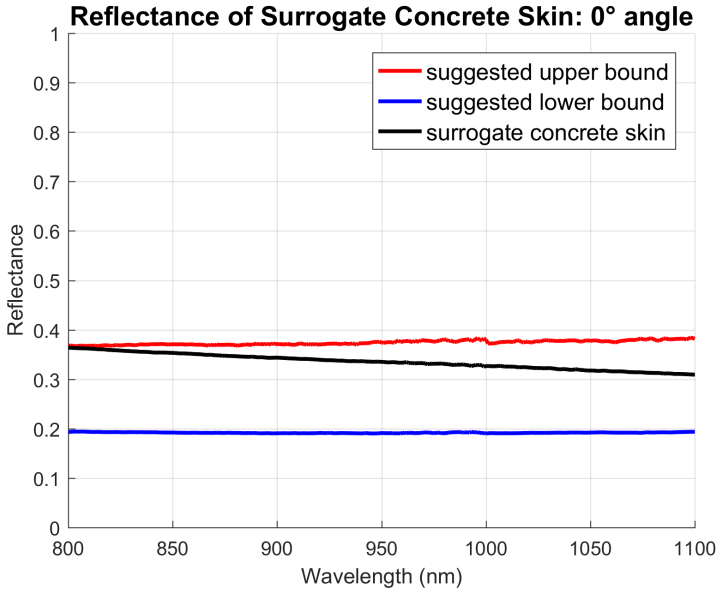

Fig. 4.2: Reflectance of concrete surrogate skin compared with the suggested range (0° measurement angle, 0° illumination angle, 20° phase angle)

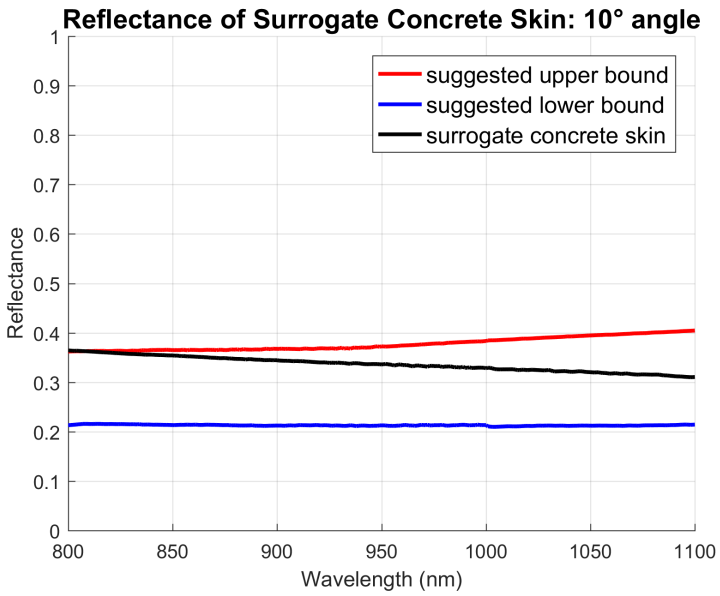

Fig. 4.3: Reflectance of concrete surrogate skin compared with the suggested range (10° measurement angle, 10° illumination angle, 20° phase angle)

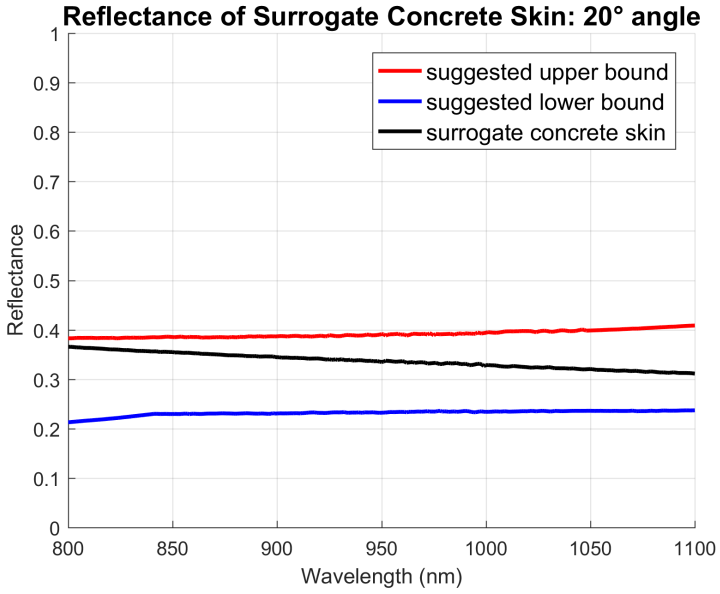

Fig. 4.4: Reflectance of concrete surrogate skin compared with the suggested range (20° measurement angle, 20° illumination angle, 20° phase angle)

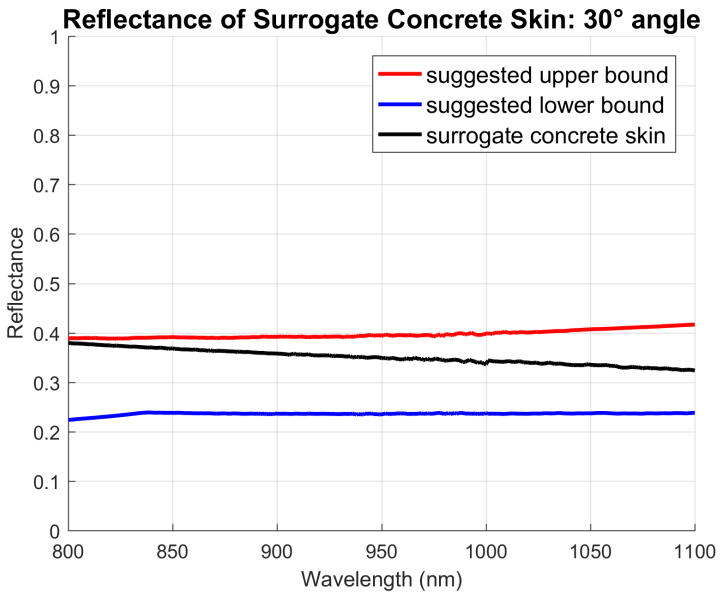

Fig. 4.5: Reflectance of concrete surrogate skin compared with the suggested range (30° measurement angle, 30° illumination angle, 20° phase angle)

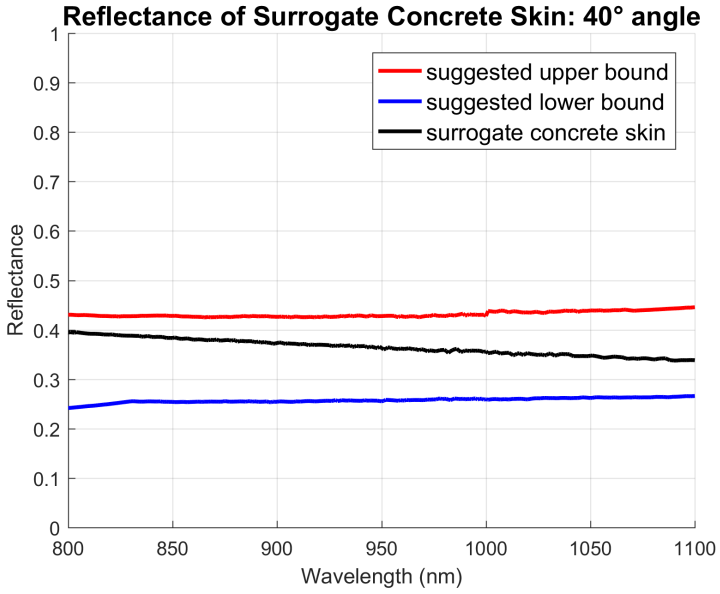

Fig. 4.6: Reflectance of concrete surrogate skin compared with the suggested range (40° measurement angle, 40° illumination angle, 20° phase angle)

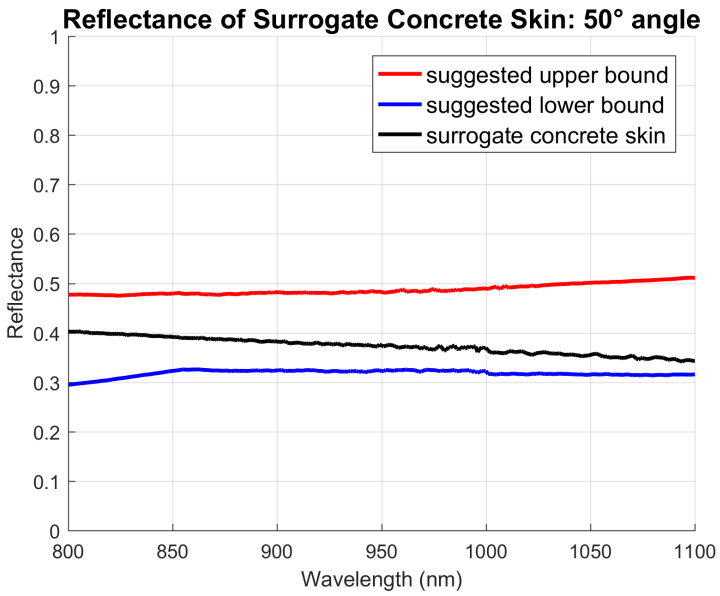

Fig. 4.7: Reflectance of concrete surrogate skin compared with the suggested range (50° measurement angle, 50° illumination angle, 20° phase angle)

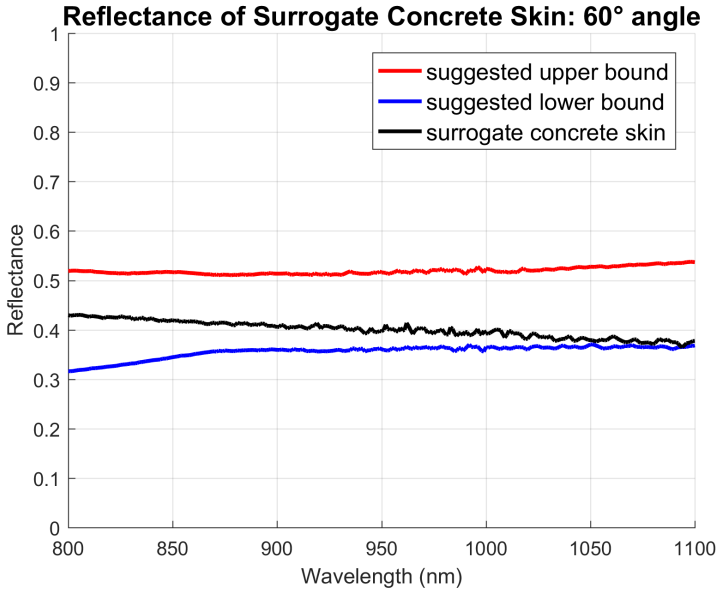

Fig. 4.8: Reflectance of concrete surrogate skin compared with the suggested range (60° measurement angle, 60° illumination angle, 20° phase angle)

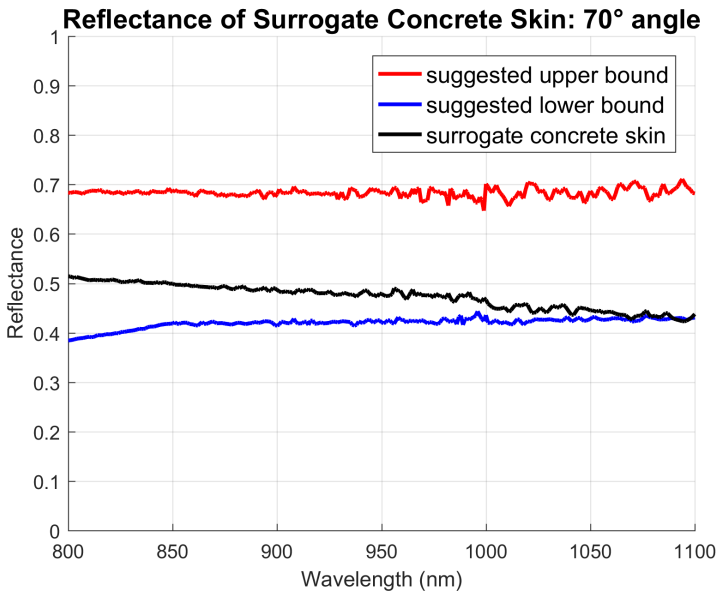

Fig. 4.9: Reflectance of concrete surrogate skin compared with the suggested range (70° measurement angle, 70° illumination angle, 20° phase angle)

Remarks

In this section, the design of a surrogate concrete skin was described, and the reflectance performance of the skin was compared to the suggested reflectance range for different measurement angles. The surrogate performs satisfactorily for 0°-70° measurement angles.

4.3 Surrogate Metal Guardrail Skin with Desired Infrared Reflectance

As discussed in Section 4.1, the shape of the surrogate metal guardrail is given using a foam frame. The multi-layered skin covering this frame will need to satisfy the suggested infrared reflectance specified in Section 3.4.

4.3.1 Finalized Design of the Metal Guardrail Surrogate Skin

The skin design was an iterative process which took a lot of time and required multiple redesigns. To prepare the surrogate metal guardrail skin, semi-transparent polycarbonate film was used as the base. A thin layer of zinc was applied on one side of the base and an aluminum layer was applied on the same side to finalize the skin. Fig. 4.10 shows a surrogate metal guardrail with the surrogate skin mounted.

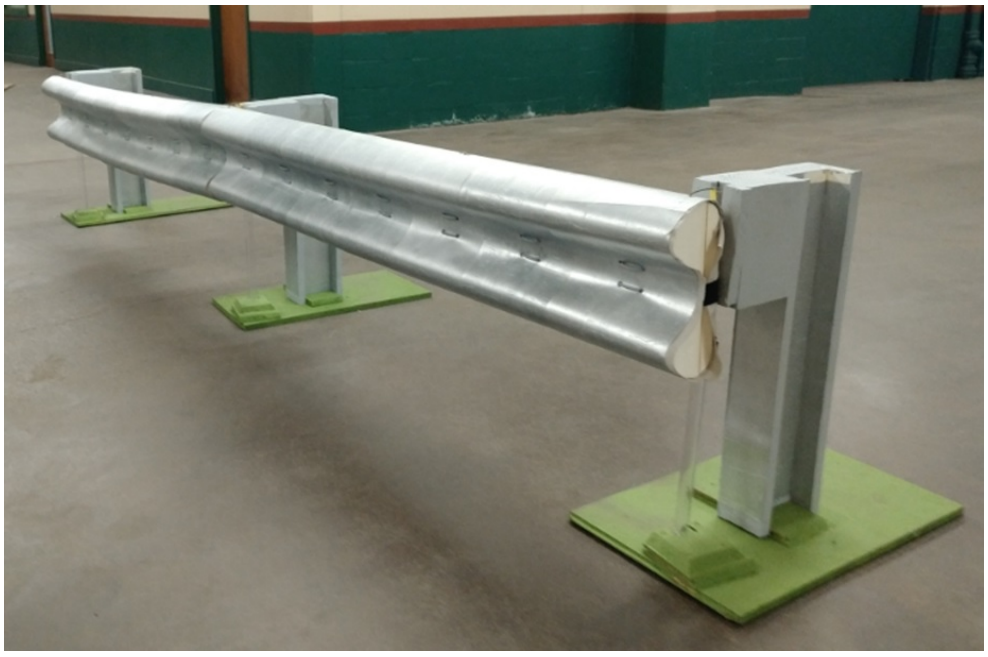

Fig. 4.10: Surrogate Metal Guardrail. The skin has been mounted on both surrogate W-beam frame and surrogate I-beam frame

4.3.2 IR Reflectance Performance of the Surrogate Metal Guardrail Skin

The reflectance for this surrogate skin was measured in indoor conditions where it was possible to simulate LIDAR operation conditions measurement angle was increased from 0° to 70° in 10° increments, and illumination angle was always kept equal to the corresponding measurement angle. A 20° phase angle was kept for ensuring even illumination of surface.

The reflectance performance of the surrogate skin at different angles is compared with the suggested IR reflectance for surrogate metal guardrail skin (which was specified in Section 3.4), and the comparison curves are shown in Fig. 4.11 through Fig. 4.18. From the figures, it can be seen that the surrogate skin performs very well for 20-70° measurement angles. For 0° and 10° measurement angles, the reflectance of the skin at certain wavelengths is higher than the suggested range. Since the requirement for road departure warning systems is to be able to detect roadside objects from far (i.e., viewing angle will be high), therefore reflectance of these low viewing angles (0-10°) is less important. For the more important 20°-70° measurement angles, reflectance follows the suggested range satisfactorily.

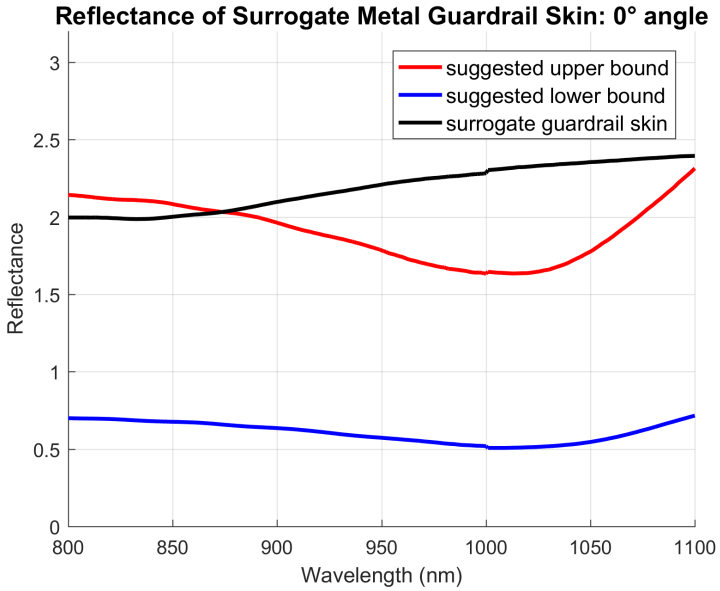

Fig. 4.11: Reflectance of surrogate metal guardrail skin compared with the suggested range (0° measurement angle, 0° illumination angle, 20° phase angle)

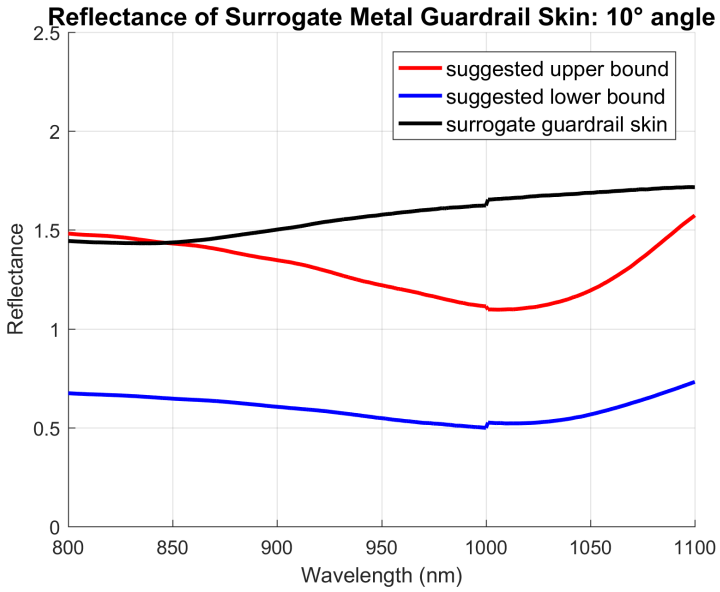

Fig. 4.12: Reflectance of surrogate metal guardrail skin compared with the suggested range (10° measurement angle, 10° illumination angle, 20° phase angle)

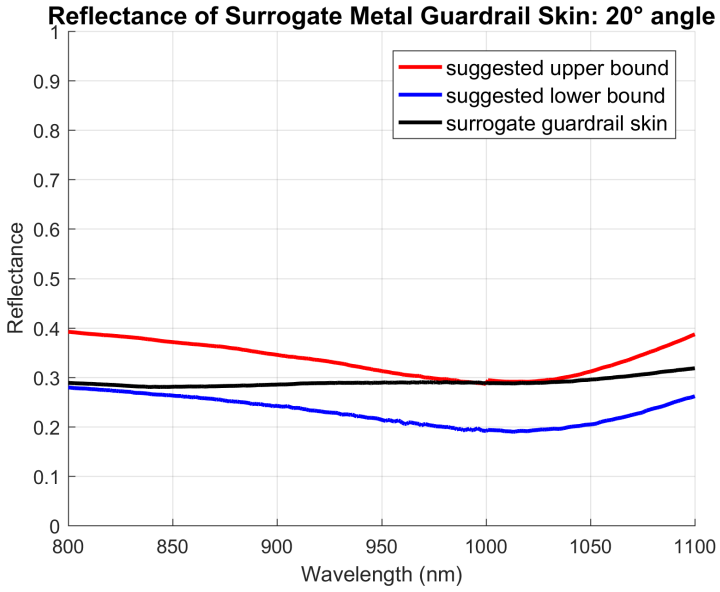

Fig. 4.13: Reflectance of surrogate metal guardrail skin compared with the suggested range (20° measurement angle, 20° illumination angle, 20° phase angle)

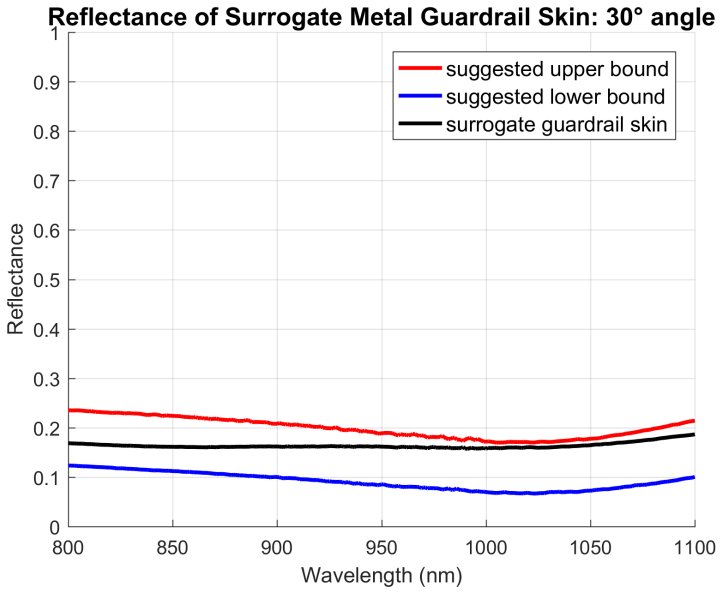

Fig. 4.14: Reflectance of surrogate metal guardrail skin compared with the suggested range (30° measurement angle, 30° illumination angle, 20° phase angle)

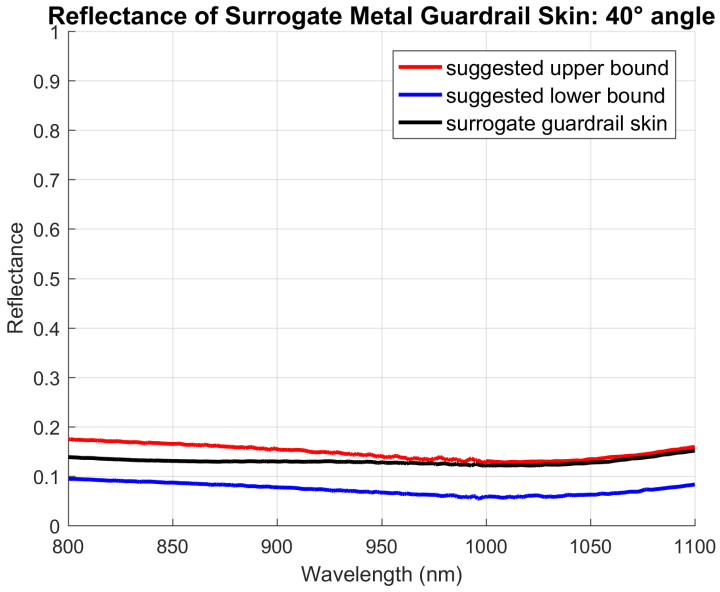

Fig. 4.15: Reflectance of surrogate metal guardrail skin compared with the suggested range (40° measurement angle, 40° illumination angle, 20° phase angle)

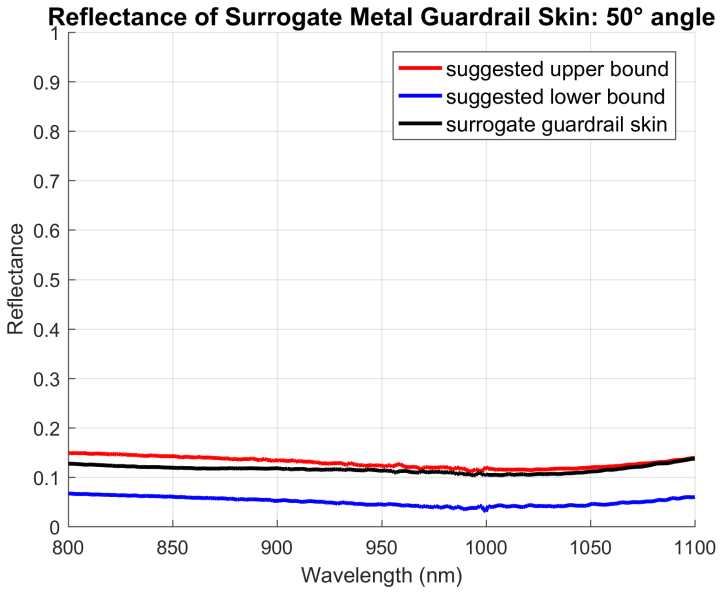

Fig. 4.16: Reflectance of surrogate metal guardrail skin compared with the suggested range (50° measurement angle, 50° illumination angle, 20° phase angle)

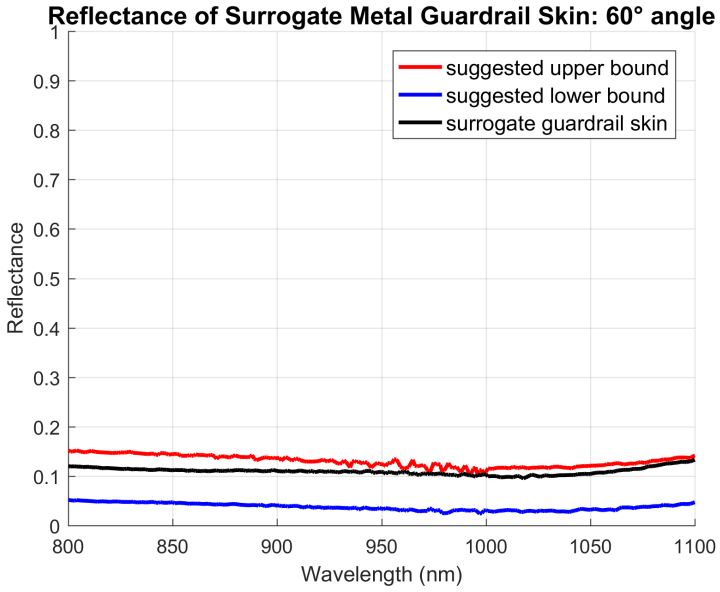

Fig. 4.17: Reflectance of surrogate metal guardrail skin compared with the suggested range (60° measurement angle, 60° illumination angle, 20° phase angle)

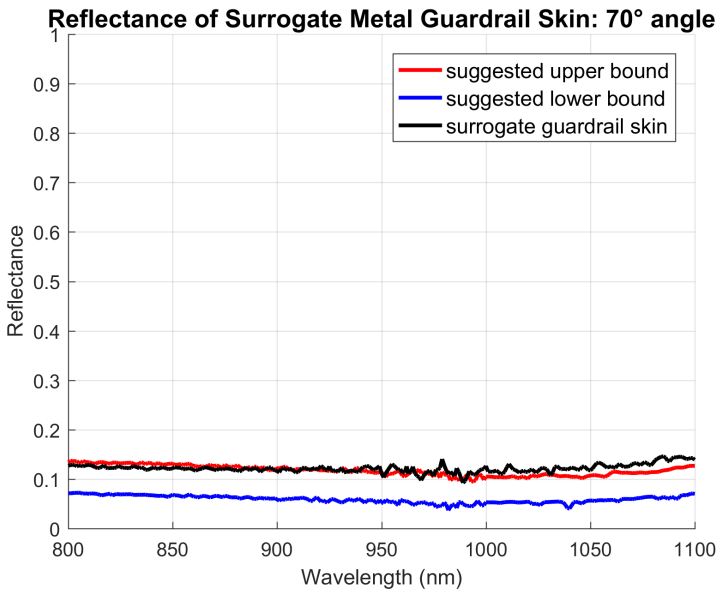

Fig. 4.18: Reflectance of surrogate metal guardrail skin compared with the suggested range (70° measurement angle, 70° illumination angle, 20° phase angle)

Remarks

In this section, the procedure to prepare a surrogate metal guardrail skin was described, and the reflectance performance of the skin was compared to the suggested metal guardrail reflectance for different measurement angles. The surrogate performs satisfactorily for 20°-70° angles.

4.4 Surrogate Grass with Desired Infrared Reflectance

As discussed in Section 4.1, the base material of the surrogate grass will be artificial turf. The desired color and IR reflectance characteristics is achieved using suitable paints. The end products will need to satisfy the suggested infrared reflectance specified in section 3.5. To find the suitable turf, experimentation was done with two types of turf. To achieve the desired color and infrared reflectance characteristics, experiment was done with paints and pigments of different colors and textures.

4.4.1 Iterative approach for making the surrogate grass

Making the surrogate grass was an iterative process and took many iterations. Some of the considerations made while preparing the surrogate grass are described below.

Type of artificial turf: At first, a high-density and a low-density artificial turf were used as the base. However, the reflectance of the high-density turf was too low from all viewing orientations and for all viewing angles. The reflectance of the low-density turf was still low from all viewing orientations and for most viewing angles but much better than the high-density artificial turf. Therefore, the high-density artificial turf was abandoned and the low-density artificial turf was selected as the base material. Attempts were made to increase the reflectance of this kind of turf by using different types of regular and high reflective coating.

Leaning orientation of turf blades with respect to viewing direction: One major difference between real grass and artificial turf is the leaning direction of blades. Grass blades lean towards different directions in a random manner, and therefore, grass has a similar appearance when viewed from different directions. On the other hand, turfs are kept tightly rolled for storage, and therefore, all turf blades lean towards a single direction. Depending on which direction the turf is facing with respect to the LIDAR, it can look very different. To analyze the effects of turf orientation, the reflectance of the low-density artificial turf was measured using the indoor setup from three orientations:

- Blades leaning *towards* probe-light setup.
- Blades leaning *away* from probe-light setup.
- Blades leaning *sideways* with respect to probe-light setup.

Fig. 4.19 shows the leaning directions of grass with respect to the measurement probe direction. Red arrows show the turf leaning direction, and blue arrows show the measurement direction.

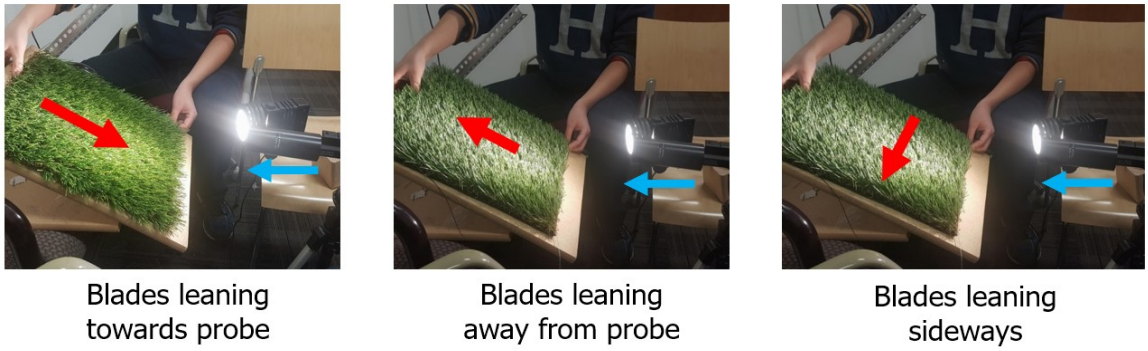

Fig. 4.19: Leaning directions of artificial turf with respect to measurement probe

Fig. 4.20 compares the reflectance of less dense turf with the suggested reflectance threshold of surrogate grass for 0°, 20°, 40° and 70° measurement angles, where the red curves denote the upper and lower threshold of suggested IR reflectance of surrogate grass.

Based on the figures, it can be seen that for 20-70° viewing angles, when blades are leaning towards probe, reflectance is lower compared to the suggested reflectance of surrogate grass for all angles. When blades are facing towards probe or sideways, for some wavelengths the reflectance is still lower than the suggested limits for surrogate grass, but overall the reflectance is much better for these two orientations. Therefore, in the test track, the turf should be facing away or sideways with respect to the vehicle's traveling direction. All surrogate efforts described in this thesis use the less dense turf, and the reflectance is measured with the turf facing away from probe.

Selection of coating to achieve desired color and reflectance characteristics: After selecting the type of turf and its orientation, experimentation was done with different paints and pigments to achieve the desired color and reflectance. Initially, several types of coatings were experimented with to bring the reflectance of low-density artificial turf to desired value. Later, high reflective pigments were used. These pigments come in powder form. These pigments can be mixed with liquid paint base and this mix is used to paint on artificial turf. Different mix of pigments and liquid paint bases were used to achieve different colors of surrogate grass with desired reflectance properties.

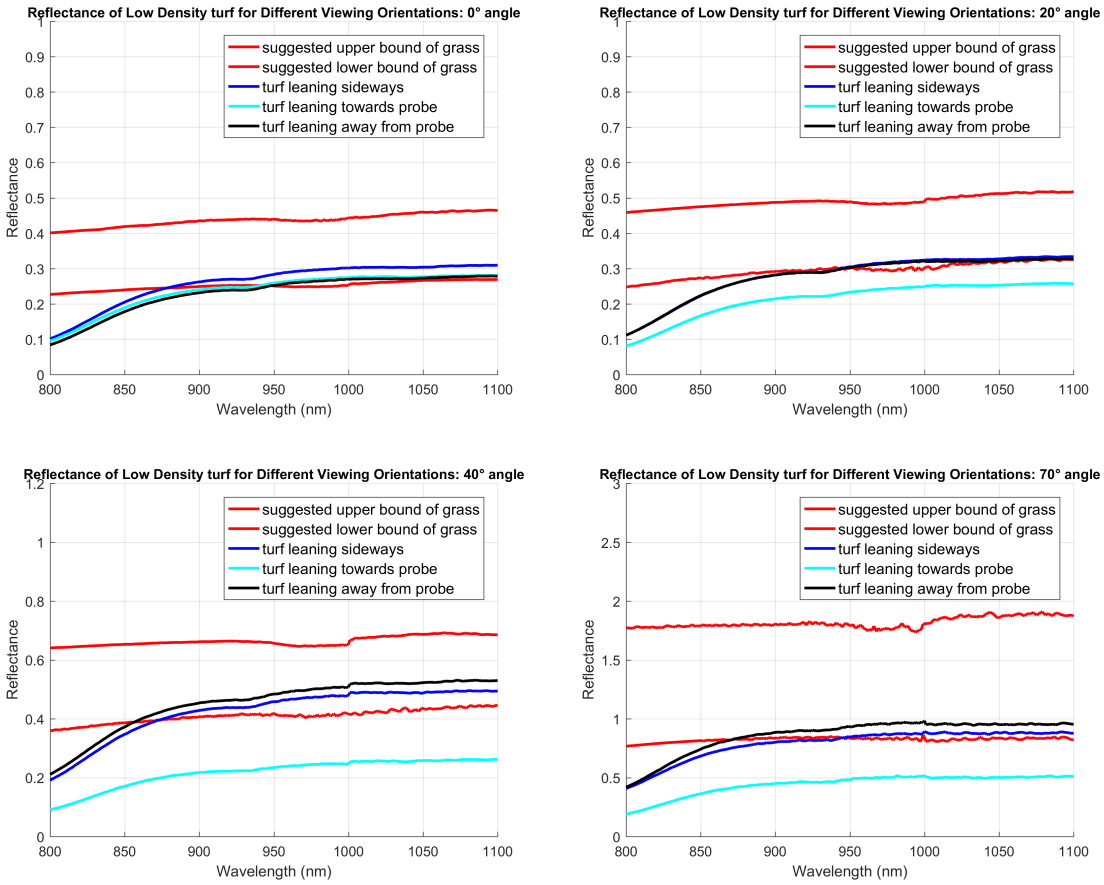

Fig. 4.20: Reflectance of low density turf measured from three viewing orientations and compared to the suggested IR reflectance of surrogate grass for 0°, 20°, 40° and 70° measurement angles. Illumination angle equal to measurement angle, 20° phase angle

4.4.2 Finalized Surrogate Grass Samples

Since the surrogate grass need to have various shade of green and yellow, different mix of high reflective pigments and liquid paint bases were applied on low-density artificial turf to prepare the finalized surrogate grass samples of different colors. Fig. 4.21 shows surrogate grass with four color shades: light green, medium green, light yellow and darker yellow.

Fig. 4.21: Four color shades of surrogate grass: (from left to right) light green, medium green, light yellow and darker yellow

4.4.3 IR Reflectance Performance of the Surrogate Grass Samples

The reflectance of all four surrogate grass samples was measured in indoor conditions where it was possible to simulate LIDAR operation conditions measurement angle was increased from 0° to 70° in 10° increments, and illumination angle was always kept equal to the corresponding measurement angle. A 20° phase angle was kept for ensuring even illumination of surface. Their performance was compared to the suggested bounds of surrogate grass for 0° to 70° angles. The comparison curves are shown in Fig. 4.22 through Fig. 4.29. From the figures, it can be seen that all four surrogate samples have satisfactory reflectance for all measurement angles, except at some wavelengths for some low viewing angles where the deviation of reflectance from the suggested bounds is less than 0.01. We consider this small amount of deviation acceptable for practical purposes.

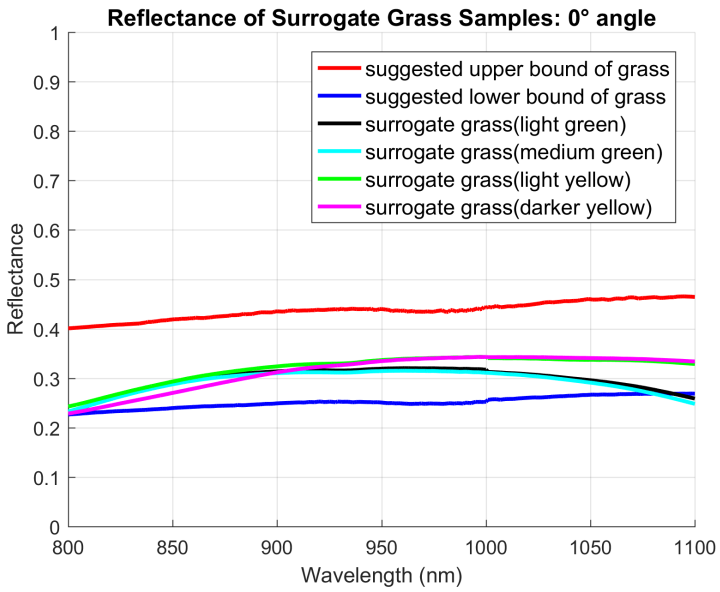

Fig. 4.22: Reflectance of all surrogate grass samples compared to the suggested range (0° measurement angle, 0° illumination angle, 20° phase angle)

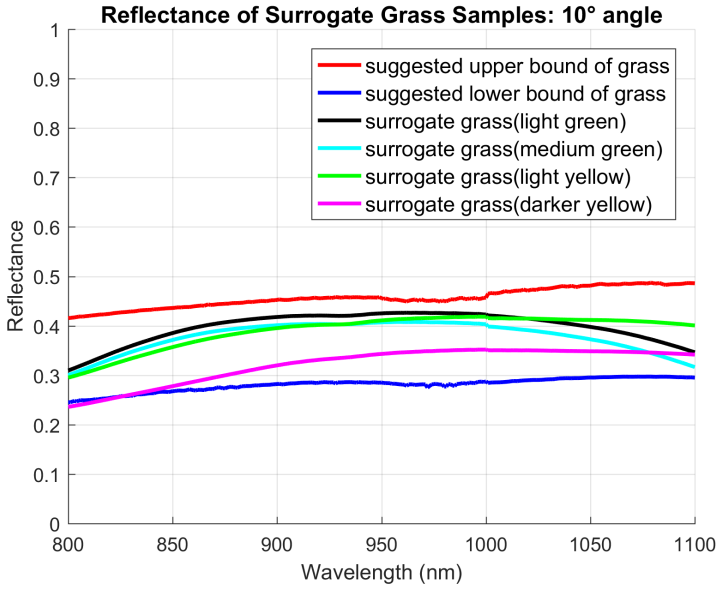

Fig. 4.23: Reflectance of all surrogate grass samples compared to the suggested range (10° measurement angle, 10° illumination angle, 20° phase angle)

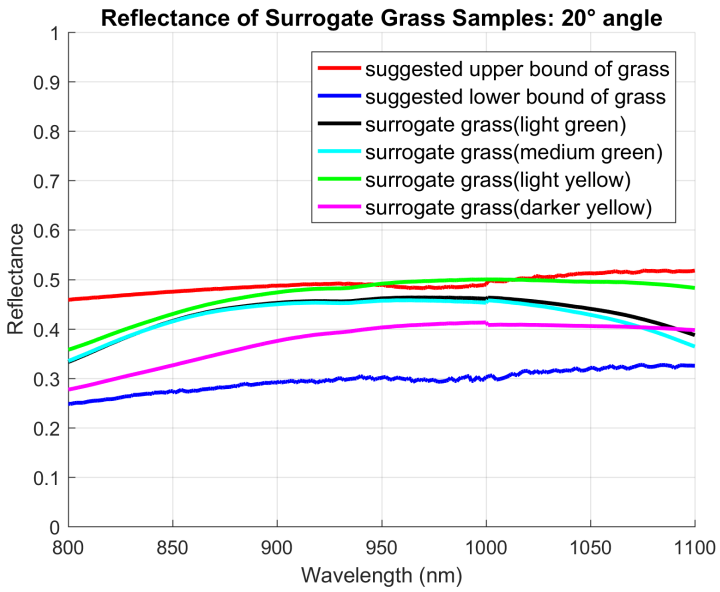

Fig. 4.24: Reflectance of all surrogate grass samples compared to the suggested range (20° measurement angle, 20° illumination angle, 20° phase angle)

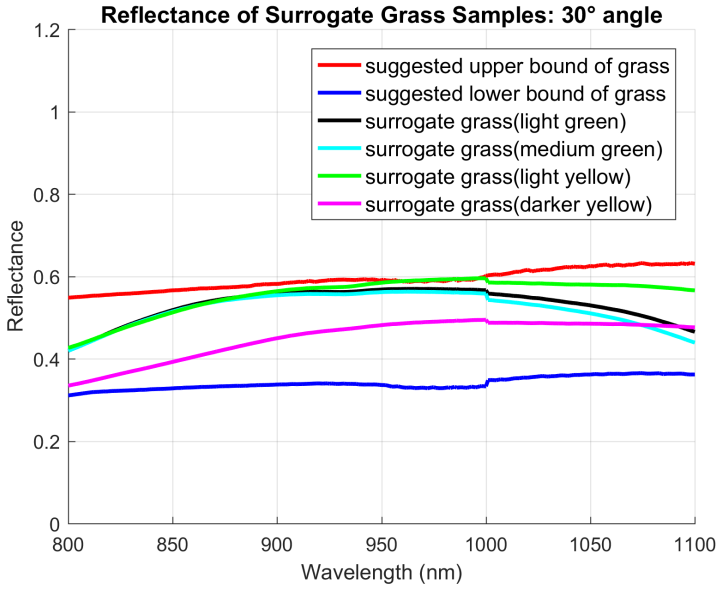

Fig. 4.25: Reflectance of all surrogate grass samples compared to the suggested range (30° measurement angle, 30° illumination angle, 20° phase angle)

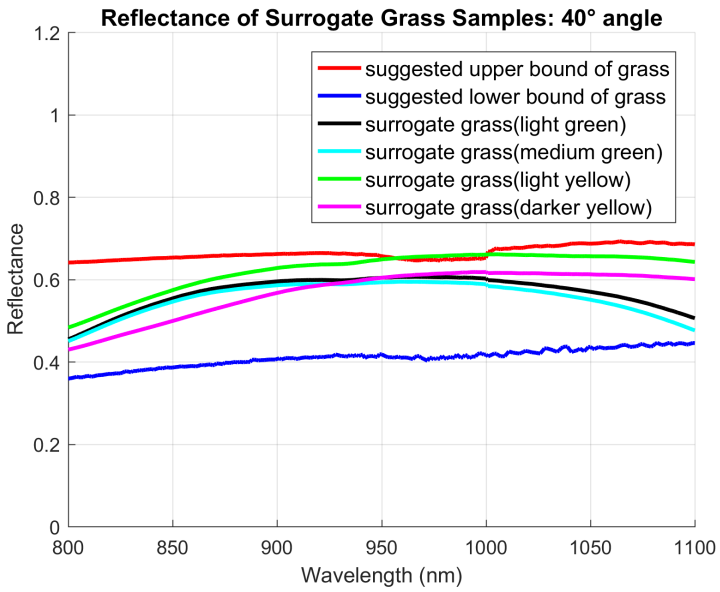

Fig. 4.26: Reflectance of all surrogate grass samples compared to the suggested range (40° measurement angle, 40° illumination angle, 20° phase angle)

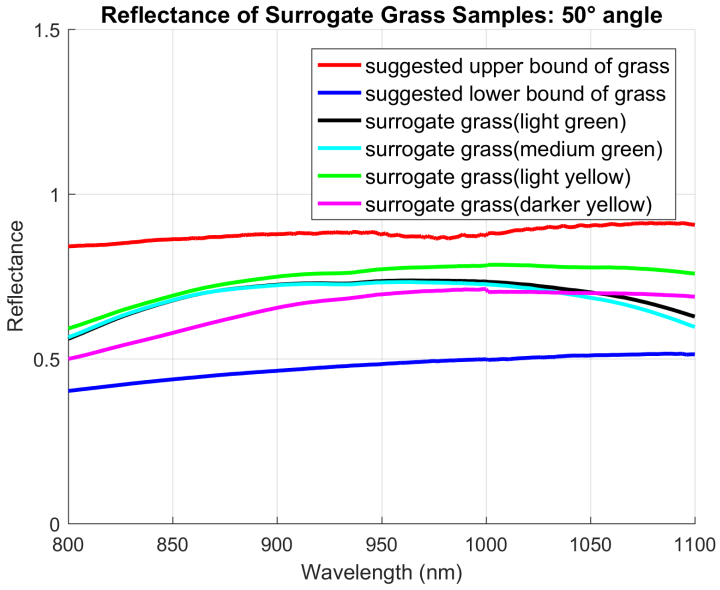

Fig. 4.27: Reflectance of all surrogate grass samples compared to the suggested range (50° measurement angle, 50° illumination angle, 20° phase angle)

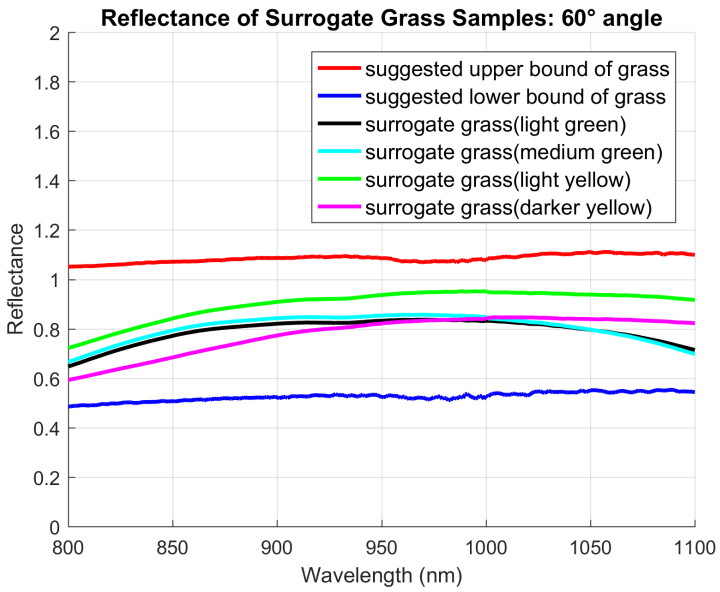

Fig. 4.28: Reflectance of all surrogate grass samples compared to the suggested range (60° measurement angle, 60° illumination angle, 20° phase angle)

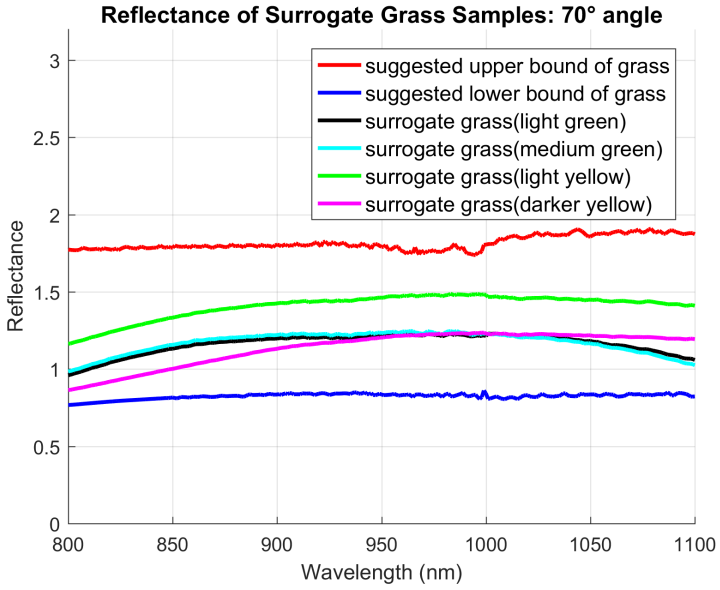

Fig. 4.29: Reflectance of all surrogate grass samples compared to the suggested range (70° measurement angle, 70° illumination angle, 20° phase angle)

4.4.4 Finalized Dirt Colored Surrogate Grass

Since the many grass road edge samples show dirt patches among grass, it is necessary to generate dirt colored patches on surrogate grass with IR reflectance similar to that of dirt. A mix of high reflective pigments and liquid paint bases were applied on low-density artificial turf to prepare a dirt colored patch of surrogate grass, which is shown in Fig. 4.30.

Fig. 4.30: Dirt colored surrogate grass

4.4.5 IR Reflectance Performance of Dirt Colored Surrogate Grass

The reflectance of the dirt colored surrogate was measured in indoor conditions where it was possible to simulate LIDAR operation conditions – measurement angle was increased from 0° to 70° in 10° increments, and illumination angle was always

kept equal to the corresponding measurement angle. A 20° phase angle was kept for ensuring even illumination of surface. Their performance was compared to the suggested bounds of surrogate dirt for 0° to 70° angles.

The comparison curves are shown in Fig. 4.31 through Fig. 4.38. For 0-30° measurement angles, the reflectance of the skin at some wavelengths is much lower than the suggested range. Since the requirement for road departure warning systems is to be able to detect roadside objects from far (i.e., viewing angle will be high), therefore reflectance of these low viewing angles is less important. For the higher angles, i.e., 40-70° measurement angles, reflectance stays within the suggested range for most of the wavelengths; and although for certain wavelengths the reflectance is still lower, the deviation is always less than 0.05, which is acceptable for practical purposes. Therefore, the dirt colored surrogate grass offers satisfactory reflectance for 40-70° measurement angles.

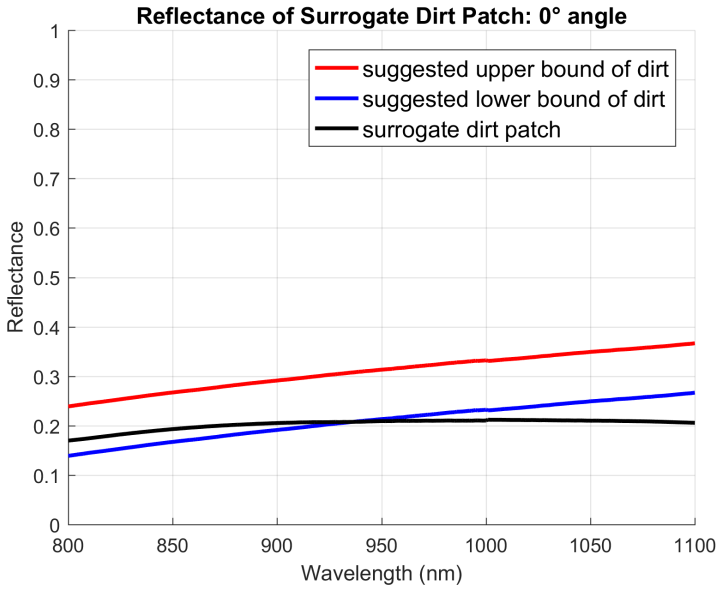

Fig. 4.31: Reflectance of dirt colored surrogate grass compared to the suggested reflectance of dirt (0° measurement angle, 0° illumination angle, 20° phase angle)

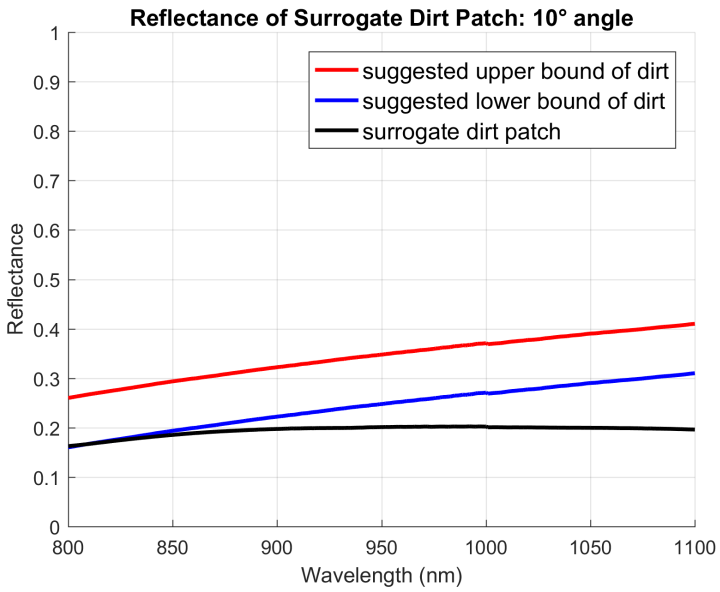

Fig. 4.32: Reflectance of dirt colored surrogate grass compared to the suggested reflectance of dirt (10° measurement angle, 10° illumination angle, 20° phase angle)

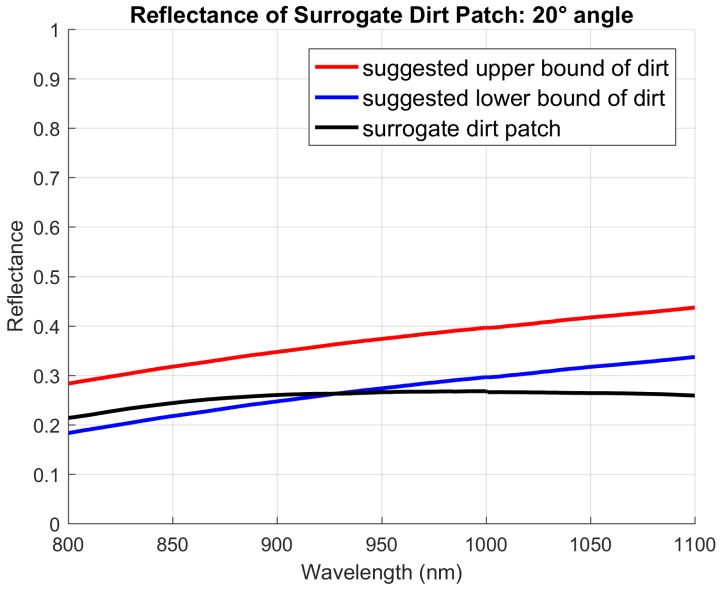

Fig. 4.33: Reflectance of dirt colored surrogate grass compared to the suggested reflectance of dirt (20° measurement angle, 20° illumination angle, 20° phase angle)

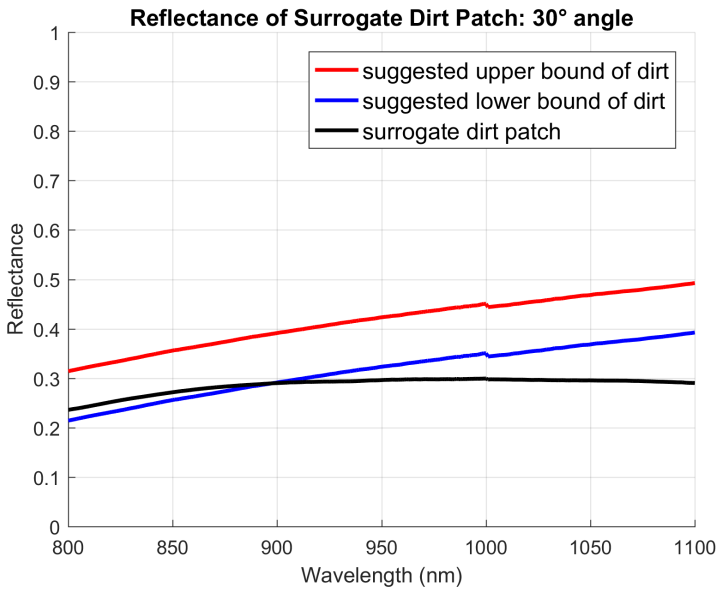

Fig. 4.34: Reflectance of dirt colored surrogate grass compared to the suggested reflectance of dirt (30° measurement angle, 30° illumination angle, 20° phase angle)

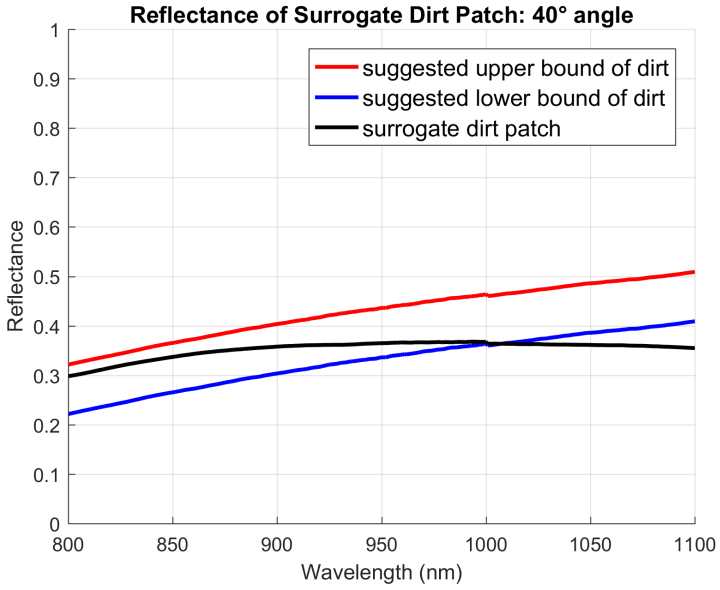

Fig. 4.35: Reflectance of dirt colored surrogate grass compared to the suggested reflectance of dirt (40° measurement angle, 40° illumination angle, 20° phase angle)

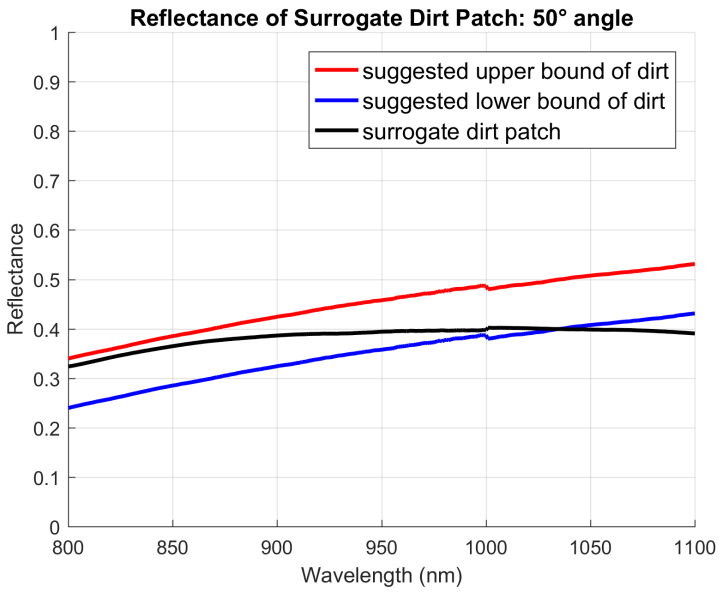

Fig. 4.36: Reflectance of dirt colored surrogate grass compared to the suggested reflectance of dirt (50° measurement angle, 50° illumination angle, 20° phase angle)

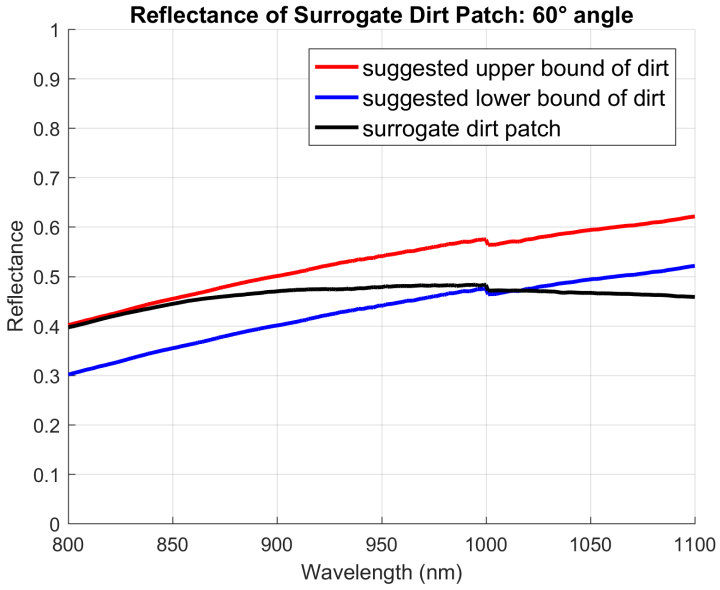

Fig. 4.37: Reflectance of dirt colored surrogate grass compared to the suggested reflectance of dirt (60° measurement angle, 60° illumination angle, 20° phase angle)

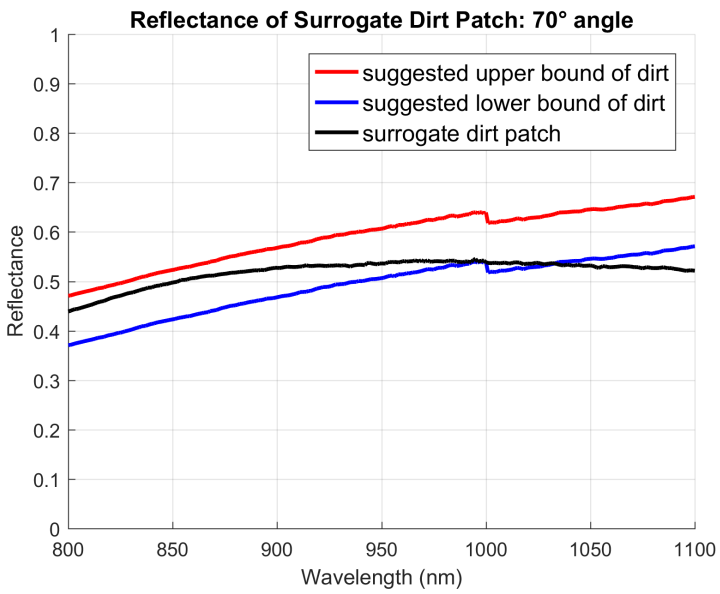

Fig. 4.38: Reflectance of dirt colored surrogate grass compared to the suggested reflectance of dirt (70° measurement angle, 70° illumination angle, 20° phase angle)

Remarks

In this section, the design of surrogate grass grass was discussed, and the reflectance performance of all samples of surrogate grass was compared to the suggested reflectance range for different measurement angles. All surrogate grass samples perform satisfactorily for 0°-70° measurement angles.

Additionally, a dirt colored surrogate grass sample was also designed, and its reflectance was compared to the suggested reflectance for surrogate dirt. The dirt colored surrogate grass sample performs well for 40°-70° measurement angles.

5. CONCLUSION AND FUTURE WORK

5.1 Conclusion

The main motivation of this thesis was to develop surrogate roadside objects that have representative characteristics of real roadside objects from the point of view of LIDARs, which commonly uses lasers in the 800-1100 nm wavelength region to detect and range targets. To this end, the first step was to study the reflectance characteristics of concrete curbs and dividers, metal guardrails and grass in the 800-1100 nm light wavelength region. An indoor setup with a spectrometer and a standard full spectrum light source was described to mimic LIDAR operation conditions. Using this setup, the reflectance of concrete, metal guardrail and grass was measured from different angles. Based on these measurements, the upper and lower bounds of infrared reflectance for 0-70° viewing angles were suggested for each of these roadside objects in Sections 3.3.3, 3.4.4 and 3.5.3 respectively. The next step was to develop surrogate objects that satisfied these specified infrared requirements. For each surrogate object, the development took many iterations. These iterative attempts led to the finalized design of surrogate objects. The reflectance performance of these surrogate objects for 0-70° viewing angles are described in section 4.

5.2 Future Work

There is further scope of research along this direction. This thesis was concerned with concrete, metal guardrail and grass. The reflectance of other roadside objects, such as traffic poles, electric poles, traffic barrels and cones can be studied to make representative surrogate objects for these. The surrogate objects developed for this thesis provide satisfactory results for 800-1100 nm wavelength lasers. Since most

widely used current generation LIDARs use lasers with 900-905 nm wavelengths, the developed surrogate objects can be used to test vehicles using the current generation of LIDARs. Right now, some research is going on a new generation of LIDARs that use 1550 nm wavelength. Future research can extend the work done in this thesis to make these surrogate objects satisfy 1550 nm LIDAR requirements.

This thesis concentrated on making surrogate objects that satisfy IR requirement for LIDAR and color requirement for camera. The research for the making these surrogate objects satisfy the radar requirements is out of scope of this thesis.

REFERENCES

REFERENCES

[1] B. Lattke, A. Eckert, and H. Feifel, "Road departure protection: A means for increasing driving safety beyond road limits," in *the 24th International Technical Conference on the Enhanced Safety of Vehicles (ESV)*, 2015, pp. 722–735.

[2] *A Compilation of Motor Vehicle Crash Data from the Fatality Analysis Reporting System and the General Estimates System*, Traffic Safety Facts, 2011.

[3] "A compilation of motor vehicle crash data from the fatality analysis reporting system and the general estimates system," Traffic Safety Facts, 2012, http://www-nrd.nhtsa.dot.gov/Pubs/812032.pdf, last date accessed: 04/02/2018.

[4] H. W. Taylor, "Taylor preventing roadway departures," U.S Department of Transportation Federal Highway Administration, https://www.fhwa.dot.gov/publications/publicroads/05jul/03.cfm, last date accessed: 04/02/2018.

[5] "Road collision types," Wikipedia, The Free Encyclopedia, https://en.wikipedia.org/wiki/Road_collision_types, last date accessed: 04/02/2018.

[6] D. I. Katzourakis, "Road-departure prevention in an emergency obstacle avoidance situation," *Transactions on Systems, Man, and Cybernetics: Systems*, vol. 44, no. 5, pp. 621–629, 2014.

[7] R. Gupta, A. Danganathan, and J. Lim, "Road departure warning system," Patent US 9 077 958 B2, 2010.

[8] R. Risack, N. Mohler, and W. Enkelmann, "A video-based lane keeping assistant," in *Intelligent Vehicles Symposium*. IEEE, 2000, pp. 356–361.

[9] T. C. Sorensen and P. D. Spudis, "The clementine missiona 10-year perspective," *Journal of Earth System Science*, vol. 114, no. 6, pp. 645–668, 2005.

[10] C. Wang and N. F. Glenn, "Integrating LIDAR intensity and elevation data for terrain characterization in a forested area," *Geoscience and Remote Sensing Letters*, vol. 6, no. 3, pp. 463–466, July 2009.

[11] A. G. Kashani, M. J. Olsen, C. E. Parrish, and N. Wilson, "A review of lidar radiometric processing: From ad hoc intensity correction to rigorous radiometric calibration," *Sensors*, vol. 15, pp. 28 099–28 128, 2015.

[12] A. Shaban, "Determination of concrete properties using hyperspectral imaging technology: A review," *Science Journal of Civil Engineering and Architecture*, pp. 1–11, 2013.

[13] R. A. Dar and H. Martin, "Imaging spectrometry of urban materials," pp. 155–181, March 2004.

[14] M. Herold, D. A. Roberts, M. E. Gardner, and P. E. Dennison, "Spectrometry for urban area remote sensing - development and analysis of a spectral library from 350 to 2400 nm," *Remote Sensing of Environment*, vol. 91, no. 3-4, pp. 304–319, 2004.

[15] J. P. Kerekes, K. Strackerjan, and C. Salvaggio, "Spectral reflectance and emissivity of man-made surfaces contaminated with environmental effects," *Optical Engineering*, vol. 47, no. 10, October 2008.

[16] M. M. Mori, T. Iwata, Y. Minami, S. Kato, and Y. Akamatsu, "Spectral analysis of building materials used in japan: The international archives of the photogrammetry," *Remote Sensing and Spatial Information Sciences*, vol. XXXVII, no. B8, 2008.

[17] J. B. Campbell, *An introduction to remote sensing*, 2nd ed. New York, USA: The Guilford Press, 1996.

[18] F. M. Danson, "Developments in the remote sensing of forest canopy structure," in *Advances on environmental remote sensing*, F. M. Danson and S. E. Plummer, Eds.

[19] M. R. Slaton, E. R. Hunt, and W. E. Smith, "Estimating near-infrared leaf reflectance from leaf structural characteristics," *American Journal of Botany*, vol. 88, no. 2, p. 278284, 2001.

[20] M. L. Adams, W. D. Philpot, and W. A. Norvell, "Yellowness index: an application of spectral second derivatives to estimate chlorosis of leaves in stressed vegetation," *International Journal of Remote Sensing*, vol. 20, no. 18, p. 36633675, 1999.

[21] E. Honkavaara, T. Hakala, J. Peltoniemi, J. Suomalainen, E. Ahokas, and L. Markelin, "Analysis of properties of reflectance reference targets for permanent radiometric test sites of high resolution airborne imaging systems," *Remote Sens.*, vol. 2, pp. 1892–1917, 2010.

[22] T. Haran and S. Chien, "Infrared reflectivity of pedestrian mannequin for autonomous emergency braking testing," in *19th International Conference on Intelligent Transportation Systems (ITSC)*. Rio de Janeiro, Brazil: IEEE, 2016, pp. 2230–2235.

[23] J. R. Schott, *Remote Sensing: The Image Chain Approach*. Oxford University Press, 1997.

[24] *FieldSpec Pro User's Guide*, http://support.asdi.com/Document/FileGet.aspx?f=600000.PDF, last date accessed: 04/02/2018.

[25] "Suncalc," https://www.suncalc.org, last date accessed: 04/02/2018.